CENTRO DE INVESTIGACION Y DE ESTUDIOS AVANZADOS DEL INSTITUTO POLITECNICO NACIONAL

Departamento de Control Automático

Control Difuso de Estructuras de Edificios Sujetas a Vibraciones Inducidas por los Sismos o el Viento

Tesis que presenta:

M. en C. Suresh Thenozhi

Para presentar el examen:
Doctor en Ciencias

En la Especialidad de
Control Automático

Director de Tesis:
Dr. Wen Yu Liu

México, D.F., **Marzo 2014**

CENTER FOR RESEARCH AND ADVANCED STUDIES OF THE NATIONAL POLYTECHNIC INSTITUTE

Department of Automatic Control

Fuzzy Control of Building Structures Subjected to Earthquake or Wind-induced Vibrations

Thesis submitted by:

Suresh Thenozhi

A thesis submitted in the partial fulfillment for the degree of
Doctor of Philosophy

In the specialization of
Automatic Control

Thesis supervisor:
Dr. Wen Yu Liu

Mexico, D.F., **March 2014**

Abstract

Protection of large civil structures and human residents from natural hazards such as earthquakes and wind is very important and extensive research has been going on in the field over the years. The purpose of this thesis was to design an active vibration control system for building structures and to perform its stability analysis.

The first part of this study focused on the estimation of velocity and position data of the building structure under seismic excitation, which is practically challenging. The majority of the control algorithms use velocity and position as their input variables. A numerical integration method which uses different filtering stages to obtain the velocity and position data from the measured acceleration signal has been proposed. The second part of the thesis focuses on the modeling and feedback control of inelastic building structures. Specifically, two types of adaptive control algorithms for the structural vibration attenuation were explored. The first controller consists of both the classic PID and fuzzy logic control techniques, where the PID is used to generate the control signal to attenuate the vibration and the adaptive fuzzy controller is used to compensate the uncertain nonlinear effects present in the system. However, its design needs some level of system knowledge. As a result, a sliding mode controller with an adaptive switching gain has been proposed, which can work with uncertain building structures. The switching gain of the sliding mode controller is tuned using the adaptive approach, without overestimating it. The discontinues switching function is fuzzified to assure a smooth operation near the sliding surface. For each controller, the adaptive tuning techniques and stability conditions were developed based on the Lyapunov stability theorem.

Within the framework of this study, a shaking table setup was established in the Automatic Control Department of CINVESTAV-IPN. The controller performance is experimentally validated based on the specific excitation and building structural characteristics, and uncertainties. An active mass damper is used to generate the force required to attenuate the vibrations. Both the earthquake and wind excitation signals were used to excite the lab prototype. In the experimental study, both the controllers provided significant vibration suppression.

Resumen

La protección de estructuras civiles debido a desastres naturales como sismos y viento es un tópico de investigación que tiene un auge importante. El propósito de esta tesis es el diseño de sistemas de control que atenúen las vibraciones de estructuras civiles, así como el análisis de su estabilidad.

La primera parte del manuscrito se enfoca en la estimación de la velocidad y de la posición de estructuras civiles. La mayoría de los algoritmos de control de estos sistemas utilizan dichas señales. Por ello se propone un método de integración numérica el cual utiliza diferentes etapas de filtrado para obtener un estimado de la velocidad y de la posición a partir de mediciones de aceleración. La segunda parte de la tesis trata el modelado y el control en lazo cerrado de estructuras inelásticas; se proponen dos algoritmos de control adaptable que permiten atenuar las vibraciones de las estructuras. El primer algoritmo combina un controlador PID clásico con una técnica de lógica difusa; el controlador PID se utiliza para generar una señal de control que atenúa las vibraciones y la técnica de lógica difusa se emplea para compensar efectos no modelados del sistema. Sin embargo, el diseño de este primer algoritmo requiere cierto conocimiento del sistema. Por ello se propone un segundo algoritmo de control que consiste en un controlador por modos deslizantes y que cuenta con una ganancia adaptable, la cual permite la compensación de la incertidumbre de la estructura. Este segundo controlador presenta una operación suave cerca de la superficie de deslizamiento. Es importante mencionar, que la estabilidad de los dos controladores se analiza mediante el método directo de Lyapunov.

Para validar los controladores propuestos se presentan resultados experimentales obtenidos con una estructura pequeña que se encuentra en el laboratorio de servicios experimentales del departamento de Control Automático del CINVESTAV-IPN. Para atenuar las vibraciones de esta estructura se emplea un amortiguador activo que consiste en una masa. Además, dicho prototipo se excita mediante señales de sismos y de viento. Los resultados experimental confirman que ambos controladores atenúan considerablemente las vibraciones del prototipo.

This thesis is dedicated to my father
for his endless love, support, and encouragement

Acknowledgments

I would like to express my gratitude to my thesis supervisor, Dr. Wen Yu Liu, for offering me the position as a PhD student and for his priceless guidance throughout my research and the beginning of my academic career.

I am also grateful to my thesis committee, Dr. Joaquín Collado, Dr. Sergio Salazar, Dr. Marco Antonio, and Dr. Moisés Bonilla, for their help and direction. In addition, I thank Mr. Jesús Meza, Mr. Gerardo Castro, and Mr. Roberto Lagunes, without whom the large-scale experiments would have been very difficult.

My heartiest love for my father, Somakumaran, who has always encouraged and supported me in chasing my dreams and my mother, Padmini, for her love and care. I cannot forget the love and support from my sister, Jyothi, and brothers, Sunil and Satish. Furthermore, I want to thank my fiancée, Asha, for her infinite patience and support during my graduate studies. I would especially like to thank my colleagues Antonio, his family, and Gadi, as well as all my friends for their inspirational discussions and entertainment.

Finally, I mention CONACyT, for financially supporting my research, and the Department of Automatic Control and the Coordination for International Relations at CINVESTAV-IPN, which has been very supportive of my research.

Contents

List of Figures

Chapter 1

Introduction

Recent advances in civil engineering technologies resulted in high-rise buildings. These buildings are sometimes vulnerable to natural hazards, which may result in financial, environmental, and human losses. This fact influenced the demand for the protection of these structures including the human occupants and non-structural components and systems from the natural and man-made hazards. One approach to mitigate this undesirable behavior is to alter the dynamic characteristics of the building with respect to a given load. This idea further developed into a new field called Structural Control, which was first presented by Yao in 1972 with a practical illustration [131]. For the past few decades, structural control is an active, vast, and growing research area among civil, mechanical, and control engineers.

Structural vibration can be generally controlled in two ways: 1) by constructing the buildings using smart materials [46]; 2) by adding controlling devices like dampers, isolators, and actuators to the building [15, 30, 127]. This thesis focuses on the latter case, where the structural dynamics are modified favorably by adding active devices. The performance of a structural control system depends on various factors including excitation type (e.g., earthquakes and winds), structural characteristics (e.g., degree of freedom, natural frequency, and structure nonlinearity), control system design (e.g., type and number of devices, placement of devices, system model, and the control algorithm), etc. [133]. In active control, the structural response under the input excitations are measured using sensors and an appro-

priate control force, calculated by a pre-assigned controller is used to drive the actuators for suppressing the unwanted structure vibrations.

Due to the popularity and importance of structural control, a number of textbooks [23, 67] and review papers have been presented. A brief review was presented by Housner *et al.* [46] in 1997, which discusses the passive, active, semi-active, and hybrid control systems and explores the potential of control theory in structural vibration control. It explains different types of control devices and sensors used in structural control. This review paper concludes with some recommendations for future research. A recent survey on active, semi-active, and hybrid control devices and some control strategies for smart structures was presented in [34, 35]. Some reviews were carried out with particular emphasis on active control [29, 59, 78, 101, 129], on semi-active control [106], and on control devices [102, 104, 107]. This shows that a significant progress has been made on most aspects of the structural control in the past few decades.

While there is no doubt about the advances, there still exist some areas which need more exploration. During the seismic excitation the reference where the displacement and velocity sensors are attached will also move, as a result the absolute value of the above parameters cannot be sensed. Alternatively, accelerometers can provide inexpensive and reliable measurement of the acceleration at strategic points on the structure. Most of the controllers use the displacement and velocity as its input variable, which are not easy to obtain from the acceleration signal with simple integration. Application of the state observers is impossible if the system parameters are unknown. Similarly, parameter uncertainties can be a problem for some control designs. There are different techniques available for identifying building parameters [55]. But these parameters may change under different load conditions. However, these control laws would be applicable to real buildings if they could be made adaptive and robust towards the system uncertainties.

The active devices have the ability to add force onto the building structure. If the controller generates unstable dynamics, it can cause damages to the building. So it is important to study the stability of the controller. Only a few structural controllers such as H_∞ and sliding mode controller consider the stability in their design, whereas the other control

strategies do not. Furthermore, there is a lack of experimental verification of these control algorithms. Some other areas that demand attention are the time-delay present in the actuator mechanism, actuator saturation, and the optimal placement of sensors and actuators. The implementation of a controller will be challenging if these issues were not resolved. The motivation of this thesis is to push forward the performance and capabilities of the structural vibration control system by acknowledging the aforementioned issues.

1.1 Objectives

Acceleration signals are the most reliable sources especially during the seismic events. Obtaining velocity and displacement from the measured acceleration signal is practically a challenging task. The primary objective of this thesis work is to develop a numerical integrator for estimating the velocity and displacement from the measured acceleration signal. The performance of the numerical integrator needs to be evaluated experimentally.

The structural control system must sense the structure response continually and react to any vibration caused by the external excitations. Many kinds of controllers were employed to attenuate the structural vibrations caused by the earthquake and wind loads. Based on the measured response the designed controller must be able to control the actuator mechanism, so that the structural vibration is reduced. The aim is to perform output regulation, where the system states such as the position and the velocity are kept as close to zero as possible. A proper controller design will maximize the effectiveness of the vibration attenuation. Stability is an important aspect in control design. The instability of the controller will result in improper operation of the system, and possibly significant damage to the building and may injure the occupants. Another challenge about the buildings are their parameter uncertainty. In that case, it will be reasonable to design a controller, which demands least structural information. Collectively, the second objective is to design a high-performing controller for the vibration attenuation, which needs to be stable and robust. The performance of the proposed controllers should be verified under both the wind and seismic loadings.

Based on the above discussions, the objectives of this thesis can be enlisted as follows:

- Design a numerical integrator for estimating the velocity and position from the measured acceleration signal.
- Design a high-performing controller, which demands least structural information.
- Theoretically demonstrate the stability of the proposed controllers.
- Experimentally verify the performance of the proposed algorithms.

1.2 Contributions and Significance

The first contribution of this thesis work is the numerical integrator for estimating the position and velocity. Accelerometers are used to measure the floor accelerations, which is then integrated to obtain the velocity and position. The low-frequency noises present in the measured acceleration signals will cause drifting while integration. The proposed numerical integrator consists of different filtering stages, which removes these noise from the acceleration signal. It has very few parameters that need tuning, which makes its design and implementation quite simple. The integrator is used in the vibration control experiments and found to be effective. This integrator can also be useful in structural health monitoring systems.

The second contribution is the control algorithm, which consist of two different designs. In the first case, the classic PID (Proportional-Integral-Derivative) and fuzzy logic controller has been combined to handle the uncertainties present in the buildings. PID controller is simple and can handle the system uncertainties and the fuzzy logic can be used to compensate the system nonlinearities. Due to the parallel structural design, the proposed controller possesses the advantages of both the PID and fuzzy techniques. A method for tuning the fuzzy weights, to reduce the regulation error, and the conditions for choosing stable PID gains has been developed. Both these tuning techniques are derived using Lyapunov theorem, to ensure the overall system stability.

In the previous control design, the tuning of PID gains requires some level of system knowledge. In the second case a new controller was proposed, which does not need the system

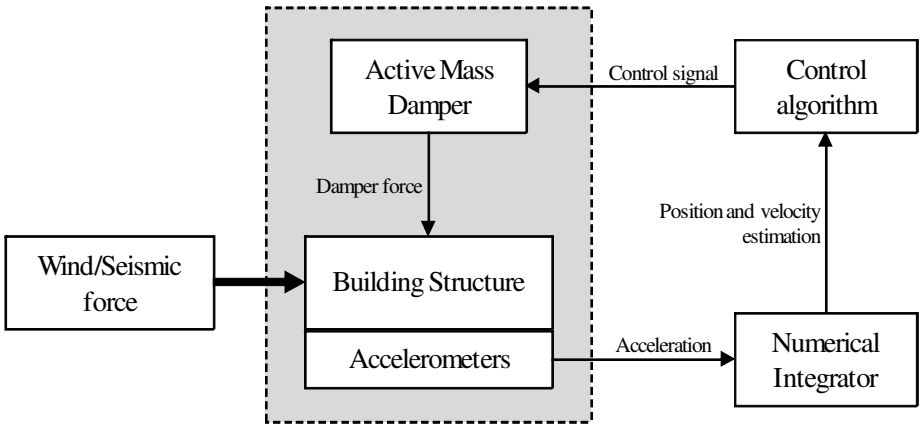

Figure 1.1: Active vibration control of building structures.

parameters or uncertainty bounds in its design. The classic sliding mode technique using adaptation and fuzzy logic techniques (AFSMC) has been extended. The proposed adaptive controller determines the unknown switching gain on-line and can reduce the structural vibrations effectively. This extends the ability of these controllers in applying to uncertain building structures.

The significance of the presented work is the ability to handle structure uncertainty using the on-line adaptation scheme. Most importantly, the closed-loop stability of proposed methodologies were demonstrated theoretically. Furthermore, the performance of the controllers has been verified experimentally under both seismic and wind excitations.

An additional contribution of this thesis is the state-of-the-art review [111], which presents an overview of the research literature contributions towards the structural vibration control field. A reduced version of the review is presented in Chapter 2. An active vibration control system for building structures is depicted in Figure 1.1. The structural system uses accelerometers for measurement and Active Mass Damper (AMD) for generating the force required to suppress the vibrations. The building velocity and position was estimated from the acceleration measurements as discussed in Chapter 3. Based on the estimated velocity and position, the proposed controllers generate an appropriate control signal. This signal

will control the AMD movement for reducing the vibration. In Chapter 4, an adaptive type Fuzzy PD/PID controllers were used to attenuate the vibration caused by the earthquake and Chapter 5 deals with vibrations caused by the wind excitation using the AFSMC. Finally, Chapter 6 summarizes the thesis, iterates contributions to the field of structural vibration control and discusses the successes of the presented approaches.

1.3 Publications

Most contributions described in this thesis have appeared in various publications. Below are the list of publications:

1.3.1 International journals

1. Suresh Thenozhi, Wen Yu, Asdrúbal López Chau, Xiaoou Li, "Structural Health Monitoring of Tall Buildings with Numerical Integrator and Convex-Concave Hull Classification", *Mathematical Problems in Engineering*, doi:10.1155/2012/212369, 2012.

2. Suresh Thenozhi, Wen Yu, Rubén Garrido, "A Novel Numerical Integrator for Velocity and Position Estimation", *Transactions of the Institute of Measurement and Control*, Vol.35, No.6, pp. 824-833, 2013.

3. Suresh Thenozhi, Wen Yu, "Advances in Modeling and Vibration Control of Building Structures", *Annual Reviews in Control*, Vol.37, No.2, pp. 346-364, 2013.

4. Suresh Thenozhi, Wen Yu, "Active Vibration Control of Building Structures using Fuzzy Proportional-Derivative/Proportional-Integral-Derivative Control", *Journal of Vibration and Control*, doi:10.1177/1077546313509127, 2013.

5. Suresh Thenozhi, Wen Yu, "Stability Analysis of Active Vibration Control of Building Structures with PD/PID Control", *Engineering Structures*. (Under review)

6. Suresh Thenozhi, Wen Yu, "Sliding Mode Control of Wind-Induced Vibration using Fuzzy Sliding Surface and Gain Adaptation", *International Journal of Systems Science*. (Under review)

1.3.2 International conferences

1. Suresh Thenozhi, Wen Yu, Rubén Garrido, "A Novel Numerical Integrator for Structural Control and Monitoring", *2012 IEEE International Conference on Information Reuse and Integration (IEEE IRI 2012)*, Las Vegas, USA, pp. 680-686, 2012.

2. Suresh Thenozhi, Wen Yu, Rubén Garrido, "A Novel Numerical Integrator for Structural Health Monitoring", *IEEE 5th International Symposium on Resilient Control Systems (ISRCS 2012)*, Salt Lake City, USA, pp. 92-97, 2012.

3. Suresh Thenozhi, Wen Yu, "Fuzzy Sliding Surface Control of Wind-Induced Vibration", *2014 IEEE International Conference on Fuzzy Systems (FUZZ-IEEE 2014)*, Beijing, China, July 7-13, 2014.

4. Wen Yu, Suresh Thenozhi, Xiaoou Li, "Stable PID Vibration Control of Building Structures", *19th IFAC World Congress (IFAC 2014)*, Cape Town, South Africa, 24-29 August, 2014

Chapter 2

Structural Vibration Control

This chapter provides an overview of building structure modeling and control. It focuses on different types of control devices and control strategies used in structural control systems. This chapter also discusses system identification techniques and some important implementation issues, like the time-delay in the system, state estimation, and optimal placement of the sensors and control devices. A detailed version of this chapter can be found in [111].

2.1 Modeling of Building Structures

Structural control concerns mainly with the protection of buildings from strong winds and seismic loads. In order to control a structure effectively, it is important to have the knowledge about its dynamics. A mathematical model of the structure determines whether a controller is able to produce the desired dynamics in the building structure within a stable region [37, 136]. The close relationship between the control algorithm design and the mathematical model is discussed in [46].

2.1.1 Excitations

In order to derive a dynamic model of a building structure, it is important to know the behavior and impact of the excitations on the buildings, such as strong wind and seismic forces. An earthquake is the result of a sudden release of energy in the Earth crust that creates seismic waves. If the frequency of the motion of the ground is close to the natural frequency of the building, resonance occurs. As a result, the floors may move rigorously in different directions causing interstory drift, the relative translational displacement between two consecutive floors. If the building drift value or deformation exceeds its critical point, the building damages severely. The force exerted by the earthquake on the structure can be represented as

$$f = -m\ddot{x}_g \tag{2.1}$$

where m is the building mass and $\ddot{x}_g$ is the ground acceleration caused by the earthquake.

In the case of high-rise flexible buildings, strong winds cause sickness or psychological responses like anxiety to the occupants and also may damage the fragile items. When the vibrations of taller buildings due to the high wind exceed a limit of $0.15\,\mathrm{m/s^2}$, humans may feel uncomfortable [104]. As a result, the main objective of structural control is to reduce the acceleration response of buildings to a comfortable level.

It is worth to note that the main difference between the effects of earthquake and wind forces on a structure is that, the earthquake causes internally generated inertial force due to the building mass vibration, whereas wind acts in the form of externally applied pressure, see Figure 2.1 (a). Moreover, the frequency range of both the earthquake and wind forces are different to each other. The wind force usually has lower frequency spectrum than that of the earthquake, see Figure 2.1 (b). As a result, the high-rise and low-rise buildings are effected more by the wind and earthquake forces, respectively.

2.1.2 Building structure

A Single-Degree-of-Freedom (SDOF) structure can be modeled using three components: the mass component m, the damping component c, and the stiffness component k [26], which

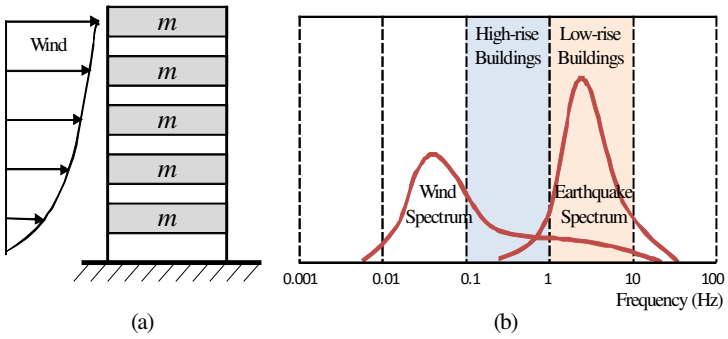

Figure 2.1: (a) Wind excitation (b) Frequency spectrum of excitations.

is shown in Figure 2.2. The stiffness component k can be modeled as either a linear or a nonlinear component, in other words elastic or inelastic, respectively [78]. Usually the mass is considered as a constant, which is concentrated at each floor. When an external force f is applied to a structure, it produces change in its displacement $x(t)$, velocity $\dot{x}(t)$, and acceleration $\ddot{x}(t)$.

The structure displacement under seismic excitation can be referred in three ways: a) absolute or total displacement $x_a(t)$, b) ground displacement $x_g(t)$, and c) relative displacement $x(t)$ between the mass and the ground. The relationship between these three displacements is

$$x_a(t) = x_g(t) + x(t) \tag{2.2}$$

Thus the equation of motion governing the relative displacement $x(t)$ of the linear structure subjected to ground acceleration $\ddot{x}_g(t)$ is

$$m\ddot{x}(t) + c\dot{x}(t) + kx(t) = -m\ddot{x}_g(t) \tag{2.3}$$

The above equation can be written down in terms of its modal parameters, which will be useful in modal analysis. Dividing (2.3) by m gives [26]

$$\ddot{x}(t) + 2\zeta\omega_n\dot{x}(t) + \omega_n^2 x(t) = -\ddot{x}_g(t) \tag{2.4}$$

where $\omega_n = \sqrt{\frac{k}{m}}$ is the natural frequency and $\zeta = \frac{c}{2m\omega_n}$ is the damping ratio.

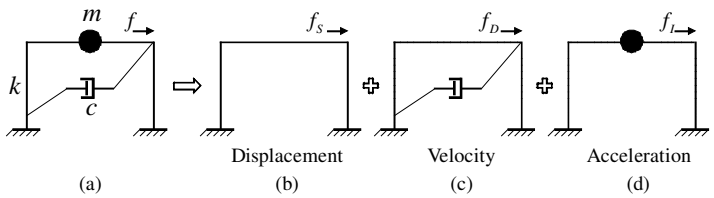

Figure 2.2: (a) Structure; (b) Stiffness component; (c) Damping component; (d) Mass component.

For the n-Degree-of-Freedom (n-DOF) case, (2.3) becomes

$$M\ddot{x}(t) + C\dot{x}(t) + Kx(t) = -M\theta\ddot{x}_g(t) \tag{2.5}$$

where M, C, and $K \in \Re^{n\times n}$ are the mass, damping, and stiffness matrices respectively, $\ddot{x}(t)$, $\dot{x}(t)$, and $x(t) \in \Re^n$ are the relative acceleration, velocity, and displacement vectors respectively, and $\theta \in \Re^n$ denotes the influence of the excitation force.

The material nonlinearity can be expressed using the stiffness matrix. Thus, the equation of motion of a nonlinear structure subjected to ground acceleration $\ddot{x}_g(t)$ is

$$m\ddot{x}(t) + c\dot{x}(t) + f_s(x, \dot{x}) = -m\ddot{x}_g(t) \tag{2.6}$$

If the structural elements have plastic or multilinear elastic or hyper-elastic behavior, then the structural stiffness will change at different load levels. This time varying behavior of the stiffness is termed as hysteresis phenomenon, which is amplified under large deformations [94]. The hysteresis can be described using different models like the Bouc-Wen model [50, 103, 118], the Hysteron [60], the Chua-Stromsmoe [27], and the Preisach models [17, 77]. The nonlinear force $f_s(x, \dot{x}) \in \Re$ of a single stiffness element in (2.6) can be modeled using Bouc-Wen model as

$$f_s(x, \dot{x}) = \tilde{\alpha}kx + (1 - \tilde{\alpha})k\tilde{\eta}f_r \tag{2.7}$$

In the above expression, f_r introduces the nonlinearity, which satisfies the following condition.

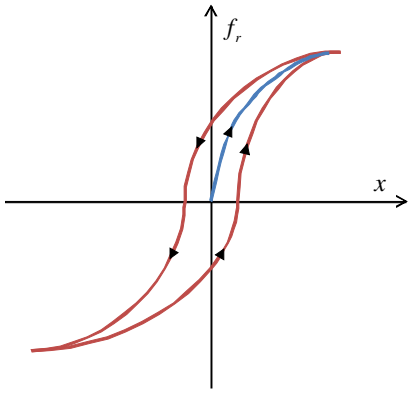

Figure 2.3: Hysteresis loop of Bouc-Wen model.

$$\dot{f}_r = \tilde{\eta}^{-1}\left[\tilde{\delta}\dot{x} - \tilde{\nu}(\tilde{\beta}|\dot{x}||f_r|^{\tilde{n}-1}f_r + \tilde{\gamma}\dot{x}|f_r|^{\tilde{n}})\right] \tag{2.8}$$

where f_r is the nonlinear restoring force, $\tilde{\delta}, \tilde{\beta}, \tilde{\gamma}, \tilde{\nu}, \tilde{\eta}$ and $\tilde{n}$ are the parameters, which controls the shape of the hysteresis loops and system degradation. The variables $\tilde{\delta}, \tilde{\alpha}, \tilde{\eta}$ and k control the initial tangent stiffness. The Bouc-Wen model has hysteresis property. Its input displacement and the output force is shown in Figure 2.3. The dynamic properties of the Bouc-Wen model has been analyzed in [50].

In the case of closed-loop control systems, its input and output variables may respond to a few nonlinearities. From the control point of view, it is crucial to investigate the effects of the nonlinearities. on the structural dynamics.

The Bouc-Wen model represented in (2.7) and (2.8) is said to be bounded input-bounded output (BIBO) stability, if and only if the set Ω_{bw} with initial conditions $f_r(0)$ is non-empty. The set Ω_{bw} is defined as: $f_r(0) \in \Re$ such that f_s is bounded for all $\mathcal{C}^1$ input signal, and $x(t)$ with fixed values of parameters $\tilde{\delta}, \tilde{\beta}, \tilde{\gamma}$, and $\tilde{n}$, f_{r0} and f_{r1} are defined as

$$f_{r0} = \sqrt[\tilde{n}]{\frac{\tilde{\delta}}{\tilde{\beta}+\tilde{\gamma}}},\ f_{r1} = \sqrt[\tilde{n}]{\frac{\tilde{\delta}}{\tilde{\gamma}-\tilde{\beta}}}$$

For any bounded input signal $x(t)$, the corresponding hysteresis output f_s is also bounded.

On the other hand if $f_r(0) \in \Omega_{bw} = \emptyset$, then the model output f_s is unbounded. Table 2.1 shows how the parameter $\tilde{\delta}, \tilde{\beta}, \tilde{\gamma}$, affect the stability property of the Bouc-Wen model.

Table 2.1: Stability of Bouc-Wen model with different $\tilde{\delta}, \tilde{\beta}, \tilde{\gamma}$

Case	Conditions	Ω_{bw}	Upper bound on $\lvert f_r(t)\rvert$
1	$\tilde{\delta} > 0, \tilde{\beta} + \tilde{\gamma} > 0$ and $\tilde{\beta} - \tilde{\gamma} \geq 0$	$\Re$	$\max\left(\lvert f_r(0)\rvert, f_{r0}\right)$
2	$\tilde{\delta} > 0, \tilde{\beta} - \tilde{\gamma} < 0$ and $\tilde{\beta} \geq 0$	$[-f_{r1}, f_{r1}]$	$\max\left(\lvert f_r(0)\rvert, f_{r0}\right)$
3	$\tilde{\delta} < 0, \tilde{\beta} - \tilde{\gamma} > 0$ and $\tilde{\beta} + \tilde{\gamma} \geq 0$	$\Re$	$\max\left(\lvert f_r(0)\rvert, f_{r1}\right)$
4	$\tilde{\delta} < 0, \tilde{\beta} + \tilde{\gamma} < 0$ and $\tilde{\beta} \geq 0$	$[-f_{r0}, f_{r0}]$	$\max\left(\lvert f_r(0)\rvert, f_{r1}\right)$
5	$\tilde{\delta} = 0, \tilde{\beta} + \tilde{\gamma} > 0$ and $\tilde{\beta} - \tilde{\gamma} \geq 0$	$\Re$	$\lvert f_r(0)\rvert$
6	All other conditions	$\emptyset$	Unbounded

Passivity is the property stating that the system storage energy is always lesser than its supply energy. On the other hand, the active systems generate energy. In [50], it is shown that the Bouc-Wen model is passive with respect to its storage energy. Case 1 in Table 2.1 describes the physical system sufficiently well and preserves both the BIBO stability and passivity properties.

The nonlinear differential equation (2.8) is continuos dependence on time. It is locally Lipschitz. For the case $\tilde{n} > 1$, we can conclude that (2.8) has a unique solution on a time interval $[0, t_0]$. This property will be used later during the stability analysis.

In the case of n-DOF structures, the nonlinear model can be modified as

$$M\ddot{x}(t) + C\dot{x}(t) + F_s(x, \dot{x}) = -M\theta\ddot{x}_g(t) \tag{2.9}$$

where $F_s(x, \dot{x}) \in \Re^n$ is the nonlinear stiffness force vector.

2.1.3 Control devices

The structural vibration control is aimed to prevent structural damages using vibration control devices. Various control devices have been developed to ensure the safety of the building structure, even when excessive vibration amplitudes occur due to earthquake or wind excitations. The control devices are actuators, isolators, and dampers, which are used

to attenuate the unwanted vibrations in a structure. Many active and passive devices have been used as vibration control devices. The most commonly utilized control devices are discussed below.

Passive devices

A passive control device does not require an external power source for its operation and utilizes the motion of the structure to develop the control forces. These devices are normally termed as energy dissipation devices, which are installed on structures to absorb a significant amount of the seismic or wind induced energy. The energy is dissipated by producing a relative motion within the control device with respect to the structure motion [107].

Vibration absorber systems such as Tuned Mass Damper (TMD) has been widely used for vibration control in mechanical systems. Basically, a TMD is a device consisting of a mass attached to a building structure such that it oscillates at the same frequency of the structure, but with a phase-shift. The mass is usually attached to the building through a spring-dashpot system and energy is dissipated by the dashpot as relative motion develops between the mass and structure [61]. Tuned Liquid Column Damper (TLCD) dissipates energy similar to that of TMD, where the secondary mass is replaced with a liquid column, which results in a highly nonlinear response. They dissipate energy by passing the liquid through the orifices.

Other passive dampers are [46, 102]: metallic yield dampers which dissipate the energy through the inelastic deformation of metals, friction dampers which utilize the mechanism of solid friction, develops between two solid bodies sliding relative to one another, to provide the desired energy dissipation, viscoelastic dampers that dissipates the energy through the shear deformation, and viscous fluid damper works based on the concept of sticky consistency between the solid and liquid.

Passive dampers are very simple and they do not add energy to the structure, hence it cannot make the structure unstable. Most of the passive dampers can be tuned only to a particular structural frequency and damping characteristics. Sometimes, these tuned values will not match with the input excitation and the corresponding structure response.

For example; 1) nonlinearities. in the structure cause variations in its natural frequencies and mode shapes during large excitation, 2) a structure with a Multiple-Degree-of-Freedom (MDOF) moves in many frequencies during the seismic events. As the passive dampers cannot adapt to these structure dynamics, it cannot always assure a successful vibration suppression [34]. This is the major disadvantage of the passive dampers, which can be overcome either by using multiple passive dampers, each tuned to different frequencies (e.g., doubly-TMD, Multiple-TMD) or by adding an active control to it.

Active devices

The concept of active control has started in early 1970's and the full-scale application was performed in 1989 [104]. An active control system can be defined as a system that typically requires a large power source for the operation of electrohydraulic or electromechanical (servo motor) actuator, which increases the structural damping or stiffness. The active control system mainly comprises of three units; 1) a sensing unit, 2) a control unit, 3) an actuation unit [107]. The sensors measure both the input excitation and structural output responses. Using these measurements, the control algorithm will generate a control signal required to effectively attenuate the structural vibrations. Based on this control signal, the actuators placed in desired locations of the structure generate a secondary vibrational response, which reduces the overall structure response [99]. Depending on the size of the building structure, the power requirements of these actuators vary from kilowatts to several megawatts [100]. Hence, an actuator capable of generating a required control force should be used. As the active devices can work with a number of vibration modes, it is a perfect choice for the MDOF structures. A number of reviews on active structural control were presented [29, 47, 59, 101, 129].

There are many active control devices designed for structural control applications. A recent survey on active control devices is presented in [34]. An AMD or Active Tuned Mass Damper (ATMD) is created by adding an active control mechanism into the classic TMD. This system utilizes a moving mass without a spring and dashpot to generate a force required for attenuating the vibrations. ATMD control devices were first introduced in [19]. These

devices are mainly used to reduce structural vibrations under strong winds and moderate earthquake.

Active tendons are pre-stressed cables, where its stress is controlled using actuators for suppressing the vibration [34]. At low excitations, the active control system can be switched-off, then the tendons will resist the structural deformation in passive mode. At higher excitations, active mode is switched-on to reach the required tension in tendons.

A comparison study between active and passive control systems was carried out in [133]. It is shown that for SDOF structure both the active and passive control systems performed similarly, whereas in the case of structure with MDOF the active control system showed high performance.

The active control devices found to be very effective in reducing the structural response due to high magnitude earthquakes. However, there are some challenges left to the engineers, such as how to eliminate the high power requirements, how to reduce the cost and maintenance etc. These challenges resulted in the development of semi-active and hybrid control devices [37].

Semi-active devices

A semi-active control system typically requires a small external power source for its operation and utilizes the motion of the structure to develop control force, where the magnitude of the force can be adjusted by an external power source [107]. It uses the advantages of both active and passive devices. The semi-active devices for structural control application were first proposed by Hrovat, Barak, and Rabins in 1983 [48].

The benefits of the semi-active devices over active devices are their less power requirements. These devices can even be powered using a battery that is more important during the seismic events, when the main power source to the building may fail. Semi-active devices cannot add mechanical energy into the controlled structural system, but has properties that can be controlled to optimally reduce the response of the system. Therefore, in contrast to active control devices, semi-active control devices do not have the potential to destabilize (in BIBO sense) the structural system [37]. A detailed review of semi-active control systems

is provided in [104, 106, 107, 124].

Like passive friction dampers, these semi-active frictional control devices dissipate energy through friction caused by the sliding between two surfaces. For this damper, a pneumatic actuator is provided in order to adjust the clamping force [81]. In contrast with the passive friction dampers, the semi-active friction dampers can easily adapt the friction coefficient to varying excitations from weak to strong earthquakes.

The semi-active fluid viscous damper consists of a hydraulic cylinder, which is separated using a piston head. The cylinder is filled with a viscous fluid, which can pass through the small orifices. An external valve which connects the two sides of the cylinder is used to control the device operation. The semi-active stiffness control device modifies the system dynamics by changing the structural stiffness [107].

Semi-active controllable fluid dampers are one of the most commonly used semi-active control device. For these devices, the piston is the only moving part, which makes them more reliable. These devices have some special fluid, where its property is modified by applying external energy field. The electric and magnetic fields are mainly used to control these devices, which is so called as Electro Rheological (ER) and Magneto Rheological (MR) dampers, respectively [102].

ER damper [107] : ER dampers consist of liquid with micron sized dielectric particles within a hydraulic cylinder. When an electric field is applied, these particles will polarize due to the aligning, thus offers more resistance to flow resulting a solid behavior. This property is used to modify the dynamics of the structure to which it is attached.

MR damper [107] : The construction and functioning of MR dampers are analogous to that of ER dampers, except the fact that instead of the electric field, magnetic field is used for controlling the magnetically polarizable fluid. MR dampers have many advantages over ER dampers, which made them more popular in structural control applications. These devices are able to have a much more yield stress than ER with less input power. Moreover, these devices are less sensitive to impurities.

Different modeling techniques are available to express the behavior of these devices, such as; Bingham model, Bingham viscoplastic model, Gamota and Filisko model, Bouc-Wen

model, modified Bouc-Wen model, etc. [105].

Base isolators

Base isolators are flexible isolation devices, placed between the building structure and the foundation for reducing seismic wave propagation into the structure. The addition of this device will increase the flexibility of the structure, hence the structural time period. For that reason, isolators reduce the propagation of high-frequency signal from ground to the structure, which makes it suitable for implementing in small and middle-rise building structures [23].

Base isolation is well known passive control technique. But active [18] and semi-active [52] control schemes were also proposed. Another class of base isolation devices is the Hybrid Base Isolation (HBI), made by combining the passive base isolator with the active or semi-active base isolator/control [104]. Sometimes, the seismic activity in the building is reduced by placing isolators between the substructure columns, not in the base, hence called seismic isolators.

Hybrid devices

Hybrid actuators combine robustness of the passive device and high performance of the active devices. Due to the inclusion of multiple control devices, the hybrid system overcomes the limitations and restrictions seen in the single control devices like passive, active, and semi-active devices. The hybrid systems are further classified into two classes: HBI and Hybrid Mass Damper (HMD) [104].

HMD can be formed by combining the passive devices like TMD along with some active devices like AMD. The capability of the TMD is increased by adding a controlling actuator to it, which increases the system robustness in changing the structure dynamics. These HMDs are found to be cost effective in terms of the energy requirement for their operation, when compared with active control systems [104]. The full-scale implementation of active structural control systems in Japan, USA, Taiwan, and China are enlisted in [102], which

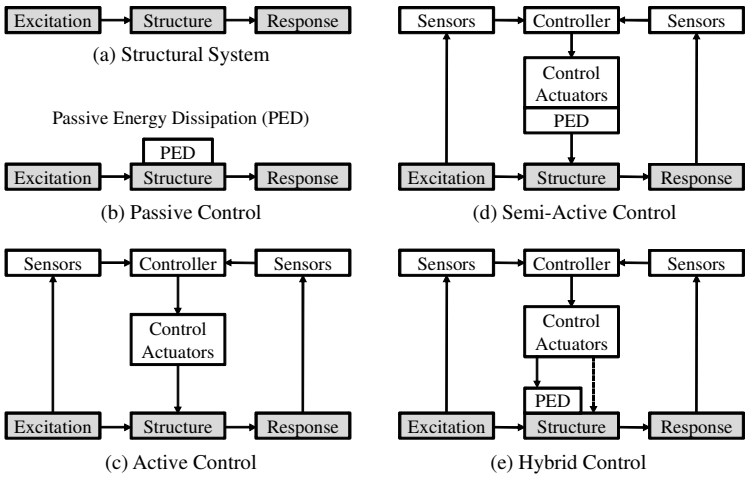

Figure 2.4: Control schemes.

indicates that the HMD is a commonly employed vibration control device.

The implementation of the above mentioned devices will result in different control schemes, which are summarized in Figure 2.4 and typical installations of control devices are shown in Figure 2.5. A brief state-of-the-art review about the structural control devices can be found in [102]. The simplicity of the passive systems made them more common in seismic control applications. The active systems including the semi-active and hybrid systems generates a control force based on the measurements of the structural responses. Due to this ability of measuring the structural response it can be designed to accommodate a variety of disturbances, which makes them to perform better than the passive systems.

2.1.4 Structure-control device systems

Control devices are used to control the dynamics of the structure to a desired response. Therefore, the dynamic model of a structure will change once a control device is installed on it. That is, it is expected that the installation of a control device will modify the structure parameters like its natural frequency, thereby changing the system model [136]. Consider

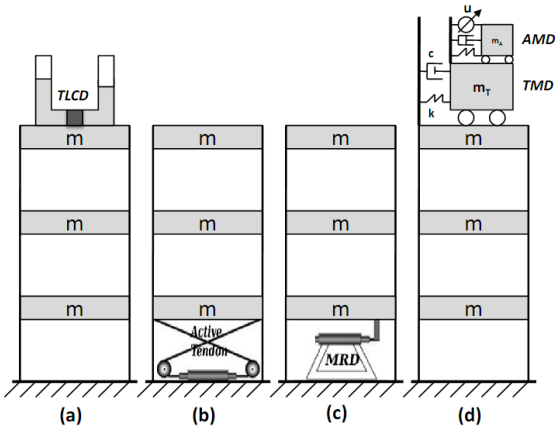

Figure 2.5: Typical implementation of control devices on structures.

a passive damper added to a structure represented in (2.3), then the system model can be rewritten as [102]

$$m\ddot{x}(t) + c\dot{x}(t) + kx(t) + \Pi(x) = -(m + m_d)\ddot{x}_g(t) \tag{2.10}$$

where m_d is the mass of the damper and $\Pi(x)$ represents the force corresponding to the damper, used to modify the structure response for reducing vibrations. The same formulation can be done in the case of active control devices, where (2.3) can be rewritten as follows:

$$m\ddot{x}(t) + c\dot{x}(t) + kx(t) = -mu(t) - m\ddot{x}_g(t) \tag{2.11}$$

If the control force is selected as per the relationship given below

$$u(t) = \frac{\Pi(x)}{m} \tag{2.12}$$

then (2.11) becomes

$$m\ddot{x}(t) + c\dot{x}(t) + kx(t) + \Pi(x) = -m\ddot{x}_g(t) \tag{2.13}$$

In contrast to the passive control method, here the control function $\Pi(x)$ is derived as a control law.

The motion equation of a structural system with n-DOF and o control devices subjected to an earthquake excitation can be expressed as

$$M\ddot{x}(t) + C\dot{x}(t) + Kx(t) = \Upsilon u(t) - M\theta\ddot{x}_g(t) \tag{2.14}$$

where $u(t) \in \Re^n$ is the control force vector and $\Upsilon \in \Re^{n\times o}$ is the location matrix of the control devices. Equation (2.14) becomes nonlinear if the control force is generated using a nonlinear device, such as MR damper or by using a nonlinear control algorithm, such as intelligent control.

2.2 Estimation and Sensing of Structure Parameters

2.2.1 System identification

In order to identify the parameters of the civil structures, the dynamic response is studied from its input and output data, and the parameters are estimated using some sort of identification techniques. The inputs are the excitation forces like the earthquake and wind loads, and the outputs are the displacements, velocities, and accelerations corresponding to the input excitation. In practice, it is very difficult to derive an exact system model, so the original problem is to obtain parameters, such that the estimated model responses closely match the output of the building dynamic behaviors. There exists different methods for identification of both linear and nonlinear systems [72].

For the purpose of system identification, the structural system can be represented in many ways, such as Ordinary Differential Equation (ODE), transfer functions, state-space models, and Auto Regressive Moving Average with exogenous input (ARMAX) models [51]. Consider a state-space variable $z = \left[x^T,\ \dot{x}^T\right]^T \in \Re^{2n}$, then the system described in (2.14) can be represented in state-space form as

$$\dot{z}(t) = Az(t) + Bu(t) + E\ddot{x}_g(t) \tag{2.15}$$

$$y(t) = Hz(t) + Du(t) \tag{2.16}$$

where $A \in \Re^{2n\times 2n}$, $B \in \Re^{2n\times n}$ and $E \in \Re^{2n}$.

$$A = \begin{bmatrix} 0 & I_n \\ -M^{-1}K & -M^{-1}C \end{bmatrix}$$
$$B = \begin{bmatrix} 0 \\ M^{-1}\Upsilon \end{bmatrix}, \quad E = \begin{bmatrix} 0 \\ -\theta \end{bmatrix}$$

Here the matrices H and D and their dimensions change according to the design demands.

System identification can be broadly classified into parametric and non-parametric identification. In parametric identification, the system parameters like the mass, stiffness, and damping are estimated [136]. Most commonly used algorithms are least squares method, maximum likelihood method, extended Kalman filter, and variations of them [51]. Non-parametric identification determines a system model from the measured data, which is a mathematical function that can approximate the input-output representations sufficiently well [75]. This method is suitable for the systems with infinite number of parameters. Artificial Neural Network (ANN) is one of the popular non-parametric identification method [49]. Some other known methods are wavelet networks, splines, and neuro-fuzzy models [55].

Identification can also be classified into time-domain and frequency-domain, where the identification takes the form of time series and frequency response functions or spectra, respectively [51, 55]. System identification can be performed either using on-line or off-line techniques. In off-line identification, all the data including the initial states must be available before starting the identification process. For example, in the case of building parameter identification, the excitation and the corresponding structure response are recorded and later used for identification. Whereas, the on-line identification is done immediately after each input-output data is measured. In other words, the on-line identification is performed parallel to the experiment, that is during the structural motion due to seismic or wind loads.

A brief review about the identification of nonlinear dynamic structures is presented by Kerschen *et al.* [55] in 2006. The fundamentals and methods of identification for linear and nonlinear structural dynamic systems are reviewed in [51].

2.2.2 Sensors

In order to control the structural dynamics it is necessary to measure the system states directly using a sensor or indirectly by using a state observer. There are different sensors available to measure the displacement, velocity, and acceleration [46]. Among these sensors the accelerometer is the commonly used sensor, especially for the seismic vibration control applications. But the estimation of the position and velocity from acceleration signal is a challenging task. Some structural control applications use the Kalman filter as the observer for estimating the velocity and displacement [41, 133]. These observers are not practical if the building parameters; mass, stiffness and damping are not available. Chapter 3 describes various techniques for estimating the building position and velocity.

2.3 Control of Building Structures

The objective of structural control system is to reduce the vibration and to enhance the lateral integrity of the building due to earthquakes or large winds, through an external control force [56]. In active control system, it is essential to design one controller in order to send an appropriate control signal to the control devices so that it can effectively reduce the structural vibrations. The control strategy should be simple, robust, fault tolerant, need not be an optimal, and of course must be realizable [108].

2.3.1 Linear control of building structures

H_2/H_∞ control

H_∞ technique is one of the widely used linear control scheme in structural vibration control. This technique can guarantee the robust performance and insensitivity with respect to the disturbances and parametric variations, which makes them suitable for the MIMO type structural control systems [113].

A modified H_∞ controllers, for example, pole-placement H_∞ control is presented in [85]. In this work, instead of changing the structure stiffness, a target damping ratio is considered.

Normally, the H_∞ design results in a higher order system, which will make the implementation more difficult. So it may be necessary to reduce its order, which can be done by performing balanced truncation [95]. The truncation has two classes; direct method and indirect method. The balanced truncation assures very few information losses about the system, which is achieved by truncating only less controllable and observable states. It is shown that the performance of the reduced low order system is nearly same as the performance of the actual higher order controller.

A H_∞ based structural controller using Takagi-Sugeno Fuzzy model was proposed in [21, 22]. Time-delay is an important factor to be considered while designing a control system. A H_∞ controller is presented in [31], which considers time-delay in control input u. The proposed algorithm determines the feedback control gain with a random search capability of GA and solving a set of LMIs. The effectiveness of the proposed algorithm is proved through simulation of a system with larger input time-delay.

Optimal control

Optimal control algorithms are based on the minimization of a quadratic performance index termed as cost function, while maintaining a desired system state and minimizing the control effort [78]. The most basic and commonly used optimal controller is the Linear Quadratic Regulator (LQR). For structural control applications, the acceptable range of structure displacement and acceleration are considered as the cost function that is to be minimized.

An energy based LQR is proposed in [6], where the controller gain matrix is obtained by considering the energy of the structure. A modified LQR is proposed in [30], which is formed by adding an integral and a feed-forward control to the classic LQR. A state feedback gain and an integral gain are used to reduce the steady-state error. A feed-forward control is included to suppress the structural responses and to reduce the effect of earthquakes. A structural vibration control utilizing a filtered LQ control is presented in [96]. Since all the structural state variables are not observable, a sub-optimal control is used, where the system states are reduced using low-pass filters. A LQR based on GA is presented [53], where the GA is used for choosing the weighting matrix.

Sometime, states of the structures are obtained indirectly using some observers like Kalman filters. The addition of a Kalman filter to a LQR control strategy leads to what is termed as Linear Quadratic Gaussian (LQG) [136]. In other words, LQG is formed by combining the linear quadratic estimator with LQR. These LQG are generally used for the systems with Gaussian white noise [35].

2.3.2 Intelligent control of building structures

Neural Network control

In recent years, the structural control systems based on NN are very popular, because of its massively parallel nature, ability to learn, and its potential in providing solutions to the foregoing unsolved problems. They provide a general framework for modeling and control of nonlinear systems such as building structures.

In the middle of 90's, very few structural control applications have been reported based on NN. Reference [119] presented a NN based active control of a SDOF system that can become nonlinear and inelastic. One inverse mapping NN and one emulator NN are used in the design. The difference between the actual overall structural response and response due to the control force only, is used as the input to the inverse mapping NN. The emulator NN predicts the response of the structural system to the applied control force. Using this response, a control force with a phase-shift is generated to nullify the excitation.

A Back-Propagation (BP) based ANN for the active control of SDOF structure is proposed by Tang [108]. This control strategy does not need the information of the external excitation in advance and the control force needed for the next sampling time is completely determined from the currently available information. The ANN with five neuron elements (displacement, velocity, and load of the preceding time step and displacement and velocity of the current time step) is used, which will perform two sequential calculations in every sampling interval; (a) calculate the load (b) based on the calculated load, the control force needed for the next time interval is calculated. A multi-layer NN controller with a single hidden layer is presented in [24].

Probabilistic Neural Networks (PNN) are feed-forward networks built with three layers. They are derived from Bayes decision networks that estimates the probability density function for each class based on the training samples. The PNN trains immediately but execution time is slow and it requires a large amount of memory space. A new method to prepare the training pattern and to calculate PNN output (control force) quickly is proposed in [57]. The training patterns are uniformly distributed at the lattice point in state-space, so that the position of invoked input can be known. This type of network is called as Lattice Probabilistic Neural Network (LPNN). The calculation time is reduced by considering only the adjacent patterns. Here the distance between the input pattern (response of structure) and training patterns (lattice type) for LPNN are calculated, which is then converted as the weights.

An active type NN controller using one Counter-Propagation Network (CPN) is presented in [73], which is an unsupervised learning type NN, so that the control force is generated without any target control forces. Another intelligent control technique using a NN is proposed for seismic protection of offshore structures [58].

The ability of the nets to perform nonlinear mappings between the inputs and outputs, and to adapt its parameters so as to minimize an error criterion, make the use of ANN particularly well suited for the identification of both linear and nonlinear dynamic systems. The NN for system identification in structural control applications were presented in [20, 22, 70, 109, 121]. A NN is designed to approximate the nonlinear structural system and the corresponding stability conditions are derived [22]. A state-feedback controller for the NN is designed using a Linear Differential Inclusion (LDI) state-space representation, which is useful in the stability analysis. Using NN, the system in (2.15) is approximated as a LDI representation with less modeling errors.

An intelligent structural control system with improved BP-NN is proposed in [70], which is used to predict the inverse model of the MR damper and for eliminating time-delay in the system. The system has two controllers; the first one modifies the actual structural model, which was off-line trained before and the second controller causes error emendation by means of on-line feedback. A multi-layer NN for structural identification and prediction

of the earthquake input is presented in [109].

Fuzzy logic control

Like NN, Fuzzy logic is also a model free approach for system identification and control. The FLC design involves; the selection of the input, output variables, and data manipulation method, membership function, and rule base design. Due to its simplicity, nonlinear mapping capability, and robustness, the FLC has been used in many structural control applications [8, 25, 43, 83, 84, 90, 97, 110, 126, 127].

A FLC is designed [43] for a 15-story structure with two type of actuators, one mounted on the first floor and the other actuator (ATMD) on the fifteenth floor. The proposed FLC uses the position error and their derivatives as the input variable to produce the control forces for each actuator. The rule base is formed using seven fuzzy variables. The controller uses Mamdani method for fuzzification and Centroid method for defuzzification. A simulation using Kocaeli earthquake signal is carried out to prove the improvement in the performance of the FLC. A similar type of FLC is presented in [7], for the active control of wind excited tall buildings using ATMD. Another FLC for MDOF is proposed [132], that uses the same architecture, which is further modified into MDOF using weighted displacement and weighted velocity. In order to get the maximum displacement and velocity values, a high magnitude earthquake signal is used to excite the building structure. As all the floors do not have control devices, a weighting value is assigned to each floor, which will be large if the control device is closer to that particular floor. Finally, a force factor is calculated based on the weighting value of each floor.

A Fuzzy based on-off controller is designed to control the structural vibration using a semi-active TLCD [126]. The optimal control gain vector is obtained using LQR strategy. The control force will act opposite to the direction of the liquid velocity. The regulation of the control force is done by varying the coefficient of headloss with the semi-active control rule.

A fuzzy supervisory control method is presented in [83], which has a fuzzy supervisor in the higher level and three sub-controllers in the lower level. First, the sub-controllers

are designed based on the LQR strategy, where the three sub-controllers are derived from three different weight matrices. The fuzzy-supervisor tunes these sub-controllers according to the structure's current behavior. A similar work is done in [84], where the sub-controller is designed using an optimal controller in the modal space. The matrix in the Riccati equation is calculated using the natural frequencies of the dominant modes and a corresponding gain matrix is determined. Another FLC for active control of structure using modal space is presented in [25], which uses a Kalman filter as an observer for the modal state estimation and a low-pass filter for eliminating the spillover problem.

Instead of using a mathematical model, a black-box based controller is proposed in [28]. Here the force-velocity characteristics of the MR damper corresponding to different voltages are obtained experimentally, which are used to calculate the desired control force. The effect of the damper position and capacity on the control response is also studied.

An alternative to the conventional FLC using an algebraic method is proposed in [32]. Here the hedge algebra is used to model the linguistic domains and variables and their semantic structure is obtained. Instead of performing fuzzification and defuzzification, more simple methods are adopted, termed as semantization and desemantization, respectively. The hedge algebra based fuzzy system is a new topic, which was first applied to fuzzy control in 2008. Compared to the classic FLC, this method is simple, effective, and can be easily interpreted.

Some structural vibration controllers were designed, where the FLC is combined with the GA [8, 88, 97, 127]. The GA is known for its optimization capabilities. The GA is used here to optimize different parameters in the FLC like its rule base and membership function.

Genetic algorithm

GA is an iterative and stochastic process that proceeds by creating successive generation of offsprings from parents by performing the operations like selection, crossover, and mutation. The above operation is performed based on the fitness value (termed as cost function in optimization problems) assigned to each individual. After these operations, the parents are replaced by the offsprings, which is continued till an optimal solution for the problem is

attained [36].

The structural control problem consists of different objectives to be optimized, which can be formulated using multi-objective optimization algorithms like GA. In [82], a preference-based optimum design using GA for an active control of structure is proposed, where the structure and control system is treated as a combined system. Here the structural sizing variables, locations of actuators, and the elements of the feedback gain matrix are considered as the design variables and the cost of structural members, required control efforts, and dynamic responses due to earthquakes are considered as the objective functions to be minimized. An active control of structures under wind excitations using a multi-level optimal design based on GA is proposed [65]. The proposed Multi-Level Genetic Algorithm (MLGA) considers the number and position of the actuators and control algorithm as multiple optimization problems. In [64], a GA is used to tune the mass, damping, and stiffness of the MRF absorber.

The disadvantage of the GA is that, it requires long computational time if the number of variables involved in the computation increases. A modified GA strategy is proposed in [86] to improve the computational time efficiency, which uses the Search Space Reduction Method (SSRM) using a Modified GA based on Migration and Artificial Selection (MGA-MAS) strategy. In order to improve the computational performance, the algorithm utilizes some novel ideas including nonlinear cyclic mutation, tagging, and reduced data input.

2.3.3 Time-delay

One of the main challenges in structural control system is the time-delay, which may occur in different stages of the systems like in data acquisition, data processing, sophisticated control algorithms, control device, or the sum of these effects [31]. Among these delays, the delay in control force caused by large mechanical control devices will affect the properties of the building structure models. The inclusion of time-delay in the controller design provides a more realistic model for the structural vibration control applications. These delays may cause instability in closed-loop systems [3, 4, 29, 136]. A state-of-the-art review on the fixed

time-delay effects in actively controlled civil engineering structures is presented in [4], which discusses the effect of time-delays on the stability and performance of the system. The controlled system will become unstable, if the time-delay is greater than a value termed as critical time-delay. The stability analysis method and critical time-delay calculation for a n-DOF system under single and multiple actuator cases were also discussed. A review on time-delay compensation methods is presented in [5].

2.3.4 Sensor and actuator placement

The optimal placement is concerned with placement of the sensing and controlling devices in preselected regions in order to closely perform the measurement and control operation of the structural vibration optimally. The actuator and sensor play an important role in deciding the system's controllability and observability, respectively. So it is important to perform an optimal placement of the sensors and actuators such that the controllability and observability properties of all or selected modes are maximized. Due to the above mentioned reasons and importance, a number of studies have been carried out about the optimal placements of devices [11, 40, 44, 45, 69, 71, 80]. A literature survey on the optimal placement of control devices can be found in [35].

2.4 Summary

In this chapter, vibration control of structures under both the earthquake and wind excitations are considered. It addresses the developments in control of building structures and tries to include all possible technical aspects of structural control systems. The research in this field is still growing with new type of control devices and their configurations, and with new control strategies. The emphasis is given to current developments in control strategies in the last two decades, which shows significant improvements. The other commonly seen controllers are the standard PID and sliding mode controllers, which will be discussed in detail in Chapter 4 and Chapter 5, respectively.

Chapter 3

Position and Velocity Estimation

3.1 Introduction

It has been reported that more than 90% of various practical control systems use PID type control [13], which employs position and velocity measurements. In some applications such as structural vibration control, relative positions and velocities are not easily measured directly because they require fixed reference positions in a building, which is difficult during seismic events. On the other hand, it is very easy to obtain acceleration signal from an accelerometer.

Accelerometers are very popular sensors in machinery and building health monitoring, structural vibration control, transport, and even personal electronic devices, because the structure of the accelerometer is very simple and it does not need any relative reference point. In fact, most of acceleration and tilt measurements use accelerometers. A comparison study on the performance of position, velocity, and acceleration sensors can be found in [15, 46, 122]. In order to design a PID or a state-space based control via accelerometers, velocity and position estimations are needed. Observers like Kalman filters are popular methods to estimate the velocity and position from an acceleration signal [41, 123]. These approaches work well when the measurements are corrupted by Gaussian noise. However, they need prior knowledge of the plant's parameters, for instance the mass, damping, and stiffness of the building structure.

Integration is the most direct method to obtain the velocity and position from acceleration. Since the measured acceleration signal from an accelerometer contains offset and low-frequency noise, it is not appropriate to integrate the acceleration signal directly. Numerical integrators can be designed in the time-domain [39, 89, 112] and in the frequency-domain [120]. However, it is difficult to use frequency-domain techniques for on-line integration [92].

The drift is the major problem in numerical integration, which is caused by unknown initial condition and the offset of the accelerometer. An ideal integrator amplifies direct current (DC) signals. To avoid drift during the integration it must be removed. Since the behavior of a first order low-pass filter is similar to the behavior of an ideal integrator, the former may replace the latter in some instance. In order to remove the low-frequency offsets, a high-pass filter can be used [39]. The drift can also be canceled out by a feedback method. An advantage of their integrator is that its estimation error converges to zero exponentially. However, the main problem of these numerical integrators is that they have to use large time constants to avoid the drift. The behavior of a filter with a large time constant is far from an ideal integrator, which will result a reduced integration accuracy. In [92], the drift caused by unknown initial conditions is eliminated via a frequency domain transformation. A Butterworth type filter is used as a numerical integrator in [76].

The baseline correction is an alternative method to avoid drift during integration. In [128], a polynomial baseline correction was applied to cancel out the offset. The polynomial curve is fitted using the Least-Square method. The low-frequency components in the accelerometer were estimated and removed off-line. In [112], a calibration technique and an initial velocity estimation were used to remove the integration error in double integrators. In [89], a weighted residual parabolic integration is proposed, where the position is assumed to be a fourth-order polynomial function of the acceleration. The main problem of these baseline correction integrators is that the low-frequency noise has to be removed by a special window-filter, which has to be designed only for a particular input acceleration signal. Due to this reason it cannot be useful for on-line estimation, where the input signal frequency is unknown.

This chapter addresses all the critical sources of offsets and noise that can cause drift

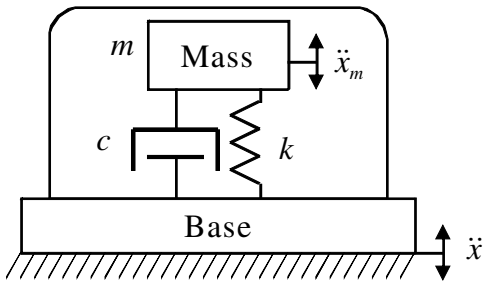

Figure 3.1: Mechanical model of an accelerometer.

during the integration and a mathematical model for the accelerometer output signal is provided. An Offset Cancellation Filter (OCF) is proposed, which removes the DC components present in the accelerometer output. In order to avoid the drift caused by low-frequency noise signals, a special high-pass filter is designed. A frequency-domain method is used to estimate the low-frequency noise components present in the accelerometer output. The high-pass filter is designed off-line according to these noise components. Since the OCF reduces the number of high-pass filtering stages, the resulting phase error has been reduced. The proposed numerical integrator combines the OCF and a high-pass filter. It is successfully applied on a linear servo actuator and on a shake table. The real-time experimental results validates the proposed method.

3.2 Numerical Integrator for Accelerometers

The accelerometer can be regarded as a single-degree-of-freedom (SDOF) mechanical system [68]. It is often modeled by a simple mass m, called proof-mass, attached to a spring of stiffness k, and a dashpot with damping coefficient c, see Figure 3.1. The inertial force acting on the proof-mass is given by

$$F = m(\ddot{x}(t) + \ddot{x}_m(t)) \tag{3.1}$$

where $\ddot{x}(t)$ is the acceleration acting on the accelerometer and $\ddot{x}_m(t)$ is the relative acceleration of the proof-mass with respect to the base.

The dynamics of an accelerometer subjected to an acceleration $\ddot{x}(t)$ using Newton's second law is given by

$$m\ddot{x}_m(t) + c\dot{x}_m(t) + kx_m(t) = -m\ddot{x}(t) \tag{3.2}$$

The deflection due to the acceleration is sensed and converted into an equivalent electrical signal. This conversion can be represented using a constant gain termed as the accelerometer gain, k_a,

$$\ddot{x}_m(t) + 2\zeta\omega_n\dot{x}_m(t) + \omega_n^2 x_m(t) = k_a\ddot{x}(t) \tag{3.3}$$

However, the accelerometer measures the input acceleration with a slight change in its amplitude defined by its gain k_a and phase, which are normally negligible [26].

Other than the input acceleration, the accelerometer output signal $a(t)$ contains offset and noise. An accelerometer has a bias, named $0g$-offset, which is measured under the absence of motion or gravity ($0g$). The $0g$-offset is normally equal to the half of its power supply ($V_{dd}/2$). This offset may vary from one sensor to another. The main causes of this variation are the sensing material, temperature, supply voltage deviation, mechanical stress and trim errors [38]. The knowledge of this offset error can be useful in removing the bias from the acceleration signal effectively.

The accelerometer output signal can be represented as [68, 137]

$$a(t) = k_a\ddot{x}(t) + w(t) + \varphi \tag{3.4}$$

where $w(t)$ is the noise and disturbance effects on the measurement, and φ denotes the $0g$-offset.

Mathematically, the velocity $\dot{x}(t)$ and position $x(t)$ are calculated by integrating the

acceleration $\ddot{x}(t)$

$$\begin{aligned} \dot{x}(t) &= \int_0^t \ddot{x}(\tau)d\tau + \dot{x}(0) \\ x(t) &= \int_0^t \int_0^\tau \ddot{x}(\tau)d\tau dt + \dot{x}(0)t + x(0) \end{aligned} \tag{3.5}$$

where $\dot{x}(0)$ and $x(0)$ is the initial velocity and position, respectively.

In discrete-time, the numerical integration is performed to get an approximation by applying the numerical interpolation,

$$\int_{t_0}^{t_n} \ddot{x}(t)dt \approx \sum_{i=1}^{n} \left[\frac{\ddot{x}(i-1) + \ddot{x}(i)}{2}\right] \Delta t \tag{3.6}$$

There exist several types of numerical integration techniques in the time-domain and in the frequency-domain. Trapezium rule, Simpson's rule, Tick's rule [120], and Rectangular rule [112] are popular time-domain integration techniques. Fourier transformation is a frequency-domain method, which is a better tool for dealing with non-periodic functions. In the frequency-domain the Fourier Transform $\mathcal{F}$ of acceleration $H_{\ddot{x}}(\omega)$ is [120]

$$H_{\ddot{x}}(\omega) = \mathcal{F}\{\ddot{x}(t)\} = \int_{-\infty}^{\infty} \ddot{x}(t)e^{-i\omega t}dt \tag{3.7}$$

The velocity and position are obtained by dividing $H_{\ddot{x}}(\omega)$ by $i\omega$ and $(i\omega)^2$, respectively. These are then converted back to the time-domain by using the inverse Fourier Transform. However, this method does not have a good low-frequency characteristics, for example the leakage problem.

3.3 Novel Numerical Integrator

Time integration of the acceleration is a straightforward solution for estimating the velocity and position. However, there are four problems affecting the performance of numerical integrators:

1) *Bias:* The behavior of a numerical integrator is similar to a low-pass filter. It amplifies the low-frequency components, reduces the magnitude of high-frequency signals, and causes a phase error. Therefore, any bias in the acceleration measurement results in integration drift. Ambient temperature change is another major offset source. A low resolution analog-to-digital converter (ADC) also adds a offset when the acceleration is slow compared with the quantization level of the analog to digital conversion [16].

2) *Noise:* There are different sources of noise in the accelerometer, which is generally modeled as white noise. Integrating these noisy signals result a large error in the velocity and position estimations. The root mean square (RMS) of the position estimation error $e_x(t)$ of the acceleration signal with a bias $\bar{\varphi}$ can be approximated as [112]

$$\mathrm{RMS}\{e_x(t)\} = \frac{1}{2}\bar{\varphi}t^2 \tag{3.8}$$

which grows at the rate of t^2, where t is the time.

3) *Aliasing:* It is caused when digitizing an analog signal with a constant sampling frequency, because the frequency components above the Nyquist rate in ADC are folded back into the frequency of interest. When ADC produces aliasing, the output signal in (3.4) can be represented as follows:

$$a(t) = k_a\ddot{x}(t) + \ddot{x}_s(t) + w(t) + \varphi \tag{3.9}$$

where $\ddot{x}_s(t)$ is the aliasing component due to sampling. Aliasing phenomena can cause low-frequency errors and is amplified during the integration process [33]. This error can be minimized by using an anti-aliasing filter between the accelerometer and data acquisition unit. Another method is to use a large and constant sampling rate.

4) *Integration technique:* The numerical integration methods like the Trapezium rule, Simpson's rule, and Tick's rule do not have good properties at low frequencies. It is also shown that the Simpson's and Tick's rules are unstable at high frequencies [120].

The motivation for the present work lies in these considerations and we propose a strategy to overcome all the problems mentioned above. To achieve this, different signal processing techniques have been applied. Among the four problems mentioned above, the first one

(due to the presence of bias) is more critical. We propose a new offset cancellation filter, which can remove the offset from the acceleration output. This filter is basically a numerical algorithm, which will remove the constant and slowly varying signals from the measured. The design procedure of this filter is discussed in the Subsection 3.3.1.

The most straightforward way to remove noise is to use a filter. Here we use a low-pass filter at the output of the accelerometer to remove any high-frequency noise signals. A Sallen-Key high-pass filter is proposed that accomplishes two jobs; 1) to attenuate the low-frequency noise, 2) to avoid drifting at the integration output by providing damping. Here the filter order and cutoff frequency is selected in such a way that the frequency of interest has minor effects by the filtering. This filter design is explained in the Subsection 3.3.2.

The useful frequency of the building structure lies in the low-frequency spectrum. Based on the observations from [120], the methods like Trapezium rule, Simpson's rule, and Tick's rule should not be used for integrating low-frequency signals like the structural acceleration. Dormand-Prince is a popular method, where the solution is computed using a higher order formula, which results in an accurate and stable result. Here we use this scheme for performing the integration operation.

The final problem is concerned with the data acquisition hardware. An anti-aliasing filter is used between the accelerometer and data acquisition unit for minimizing the aliasing effect. Moreover, we use a high-resolution ADC for the analog to digital conversion and the sampling is done at a high rate using a dedicated clock source. More details on hardware components are provided in Experiments section.

3.3.1 Offset cancellation filter

The offset voltage present in the accelerometer is one of the main cause of integration drift. Figure 3.2 shows drifting of the integrated signal in the presence of offset. Here a constant bias of $0.05m/s^2$ is added to a $1m/s^2$ acceleration signal and integrated two times. Compared to the first integrated signal the second integrated signal drifts very fast. It evidently indicates

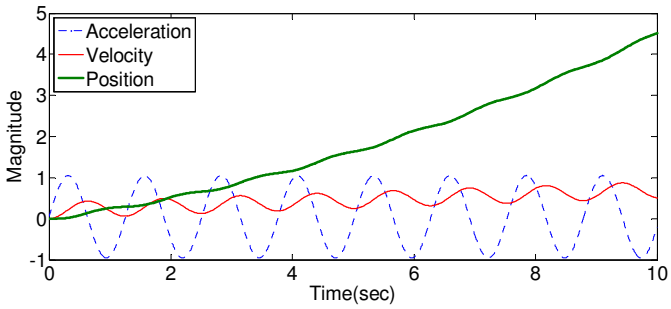

Figure 3.2: Integration in the presence of offset.

that, if there exists any bias in the acceleration signal the resulting position estimation using double integration will drift rapidly with time.

In [128], polynomial baselines have been used for removing the offset present in the estimations, which is given by

$$\begin{aligned} p(t) &= a_1 t^4 + a_2 t^3 + a_3 t^2 + a_4 t \\ \dot{p}(t) &= 4a_1 t^3 + 3a_2 t^2 + 2a_3 t \\ \ddot{p}(t) &= 12a_1 t^2 + 6a_2 t + 2a_3 \end{aligned} \tag{3.10}$$

where $p(t), \dot{p}(t)$, and $\ddot{p}(t)$ are the baselines for position, velocity, and acceleration, respectively. Once the above baselines are determined they are then subtracted from the estimations to remove the offset. The acceleration data is measured first and the corresponding polynomial coefficients $(a_1 - a_4)$ are calculated off-line using the least-square curve fitting method. For that reason, this method cannot be applied for on-line estimation. On the other hand, this scheme gives a good estimation for the off-line data.

The offset cancellation is also called offset calibration, where the $0g$-offset voltage under $0g$-motion is removed from the accelerometer output [38]. Many practical applications use an electronic voltage compensator for removing this offset. Since this offset changes with time, this circuit needs frequent calibration, which may be difficult in some applications. Another option is to use a high-pass filter in order to remove the low-frequency DC components. The major drawback of this approach is that the high-pass filter introduces a phase error in the

cutoff frequency range.

The proposed approach uses a numerical filter to remove the offset. The advantage of this method is that it does not add any phase error to the output. The ideal integrator generates unbounded output signal, if its input signal contains pure DC components. Since the OCF is able to remove the DC components completely, an ideal integrator can be used for the integration operation.

The initial condition for the acceleration is assumed to be zero; $\ddot{x}(0) = 0$ so that

$$a(0) = \varphi \tag{3.11}$$

If $a(t)$ in (3.9) is delayed for one sample time (δ_d), it becomes

$$a(t - \delta_d) = k_a \ddot{x}(t - \delta_d) + \ddot{x}_s(t - \delta_d) + w(t - \delta_d) + \varphi \tag{3.12}$$

Consider a variable $\epsilon(t)$

$$\epsilon(t) = a(t) - a(t - \delta_d) \quad ; \epsilon(0) = 0 \tag{3.13}$$

Now the offset-free acceleration $\ddot{\hat{x}}(t)$ can be found as

$$\ddot{\hat{x}}(t) = \sum_{i=0}^{n} \epsilon(t - i) \quad ; \ddot{\hat{x}}(0) = 0 \tag{3.14}$$

$$= k_a \ddot{x}(t) + \ddot{x}_s(t) + w(t) \tag{3.15}$$

It is clear that the above algorithm can remove the pure DC component (φ) completely. Here it is assumed that the acceleration signal is unknown but bounded, i.e.

$$|a(t)| \leq \bar{a} \quad \forall t \geq 0 \tag{3.16}$$

where $\bar{a}$ is a finite, positive constant. Therefore, the $\ddot{\hat{x}}(t)$ is also bounded.

If the offset changes slowly with time, then it is represented as $\varphi(t)$. Since the offset frequency is close to 0 Hz, we use the following two ways to reduce the effect of $\varphi(t)$ in the estimation.

1) The scheme is to identify the slowly changing signal close to 0 Hz and to remove it from the acceleration signal. If the offset is changing slowly, the resulting rate of change of acceleration signal $a(t)$, from one sample data to the next sample will be very small, i.e. small $\epsilon(t)$. This small $\epsilon(t)$ is identified and removed from the acceleration signal to nullify the slowly changing $\varphi(t)$ as shown below.

$$\epsilon(t) = \begin{array}{ll} 0 & \text{if } \epsilon(t) < \epsilon_{\min} \\ \epsilon(t) & \text{if } \epsilon(t) \geq \epsilon_{\min} \end{array} \tag{3.17}$$

where $\epsilon_{\min}$ is the smallest value of $\epsilon(t)$ to be removed. Due to the above scheme, we can write $\left|\ddot{\hat{x}}(t)\right| \leq |a(t)|$, which shows that boundness is still preserved. For example, consider an offset changing very slowly at a constant rate of υ with time, so that $\varphi(t) = \varphi + \upsilon t$. In this case, the offset can be removed by choosing $\epsilon_{\min} \geq \upsilon$. The change in the offset is due to different causes like the temperature changes. As the rate of change of offset is different from one accelerometer to the another, the $\epsilon_{\min}$ will also differs.

2) The OCF reset is performed such that the slowly varying offset is cancelled out more effectively. The reset should be done in the absence of motion. Once the reset is carried out the initial acceleration $a(0)$ corresponds to the new offset, which will be removed by the OCF. Simply speaking, the OCF removes very slowly changing signals from the acceleration signal.

In [39], a low-pass filter and a high-pass filter is used for removing the effect of the offset. Instead of using an ideal integrator a low-pass filter is used as follows:

$$L(s) = \frac{1}{s + \tau^{-1}} \tag{3.18}$$

By increasing the filter time constant τ, the output offset can be reduced, but doing that will add phase error to the signal. Here the offset is removed using the proposed OCF and then the ideal integrator can be used without making it unstable. Moreover, the OCF reduces the offset without adding any phase error.

In practice, the term $a(0) \neq 0$, which can be represented as

$$a(0) = \varphi + \vartheta \tag{3.19}$$

where $\vartheta \ll \varphi$ is from the noise $w(t)$ and other noise sources. Then, the output of the OCF is

$$\ddot{\hat{x}}(t) = k_a \ddot{x}(t) + \ddot{x}_s(t) + w(t) + \vartheta \tag{3.20}$$

The term ϑ is removed by using a second order high-pass filter as discussed in the section below.

3.3.2 High-pass filtering for drift attenuation

The OCF removes the DC components efficiently. However, it cannot deal with other low-frequency noises, which also cause drift in the integrator. To remove the low-frequency components in (3.9), we use a second order high-pass filter. The transfer function of a second-order unity-gain Sallen-Key high-pass filter is

$$G(s) = \frac{s^2}{s^2 + 2\tau^{-1}s + \tau^{-2}} \tag{3.21}$$

where τ is estimated using the Fast Fourier Transform (FFT). The cutoff frequency (f_c) of the filter is

$$f_c = \frac{1}{2\pi\tau} \tag{3.22}$$

The FFT gives the frequency distribution of the accelerometer output signal under $0g$-motion. The cutoff frequency of the filter (3.21) is calculated based on the noise distribution. The high-pass filter design is performed off-line. During design, the effect of the filter on the low-frequency information should be considered. The cutoff frequency should be selected in such a way that it would not attenuate the low-frequency information data. It will be a good practice to use low-noise accelerometers, so that the filter cutoff frequency can be kept low. Once the filter is designed it can deal with the acceleration signals above its cutoff frequency, so that a wide range of building structure frequencies, which makes them capable of performing on-line estimation.

The scheme of the proposed numerical integrator is shown in Figure 3.3. Initially, the high-frequency noise present in the accelerometer output signal is attenuated using a low-

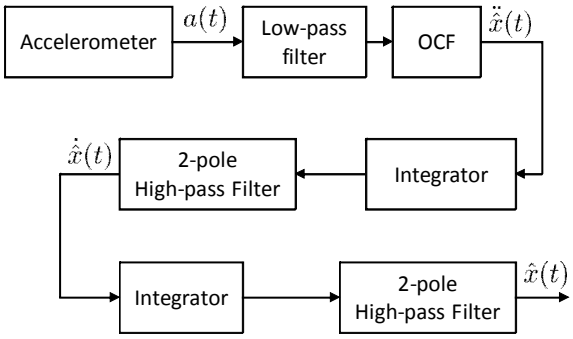

Figure 3.3: Scheme of the proposed numerical integrator.

pass filter. This filtered acceleration signal is passed through the OCF for removing the offset as explained in (3.12)-(3.17). This signal is integrated to get velocity estimation and then given to a high-pass filter for removing the low-frequency noise. The integrator and high-pass filter is cascaded, which gives

$$G(s) = \frac{s}{s^2 + 2\tau^{-1}s + \tau^{-2}} \tag{3.23}$$

Then the velocity estimation $\dot{\hat{x}}(t)$ can be expressed as

$$\dot{\hat{x}}(t) = \mathcal{L}^{-1}\left[G(s)\left(\mathcal{L}\left[\ddot{\hat{x}}(t)\right]\right)\right] \tag{3.24}$$

where $\mathcal{L}$ is the Laplace transform operator. A zero initial condition is considered for both position and velocity, which is reasonable in the case of building structure in the absence of any excitation. Similarly, the position estimation $\hat{x}(t)$ is obtained as

$$\hat{x}(t) = \mathcal{L}^{-1}\left[G(s)\left(\mathcal{L}\left[\dot{\hat{x}}(t)\right]\right)\right] \tag{3.25}$$

The anti-aliasing filter and oversampling technique is used to minimize the aliasing effects. Sometimes, the noise and information signal frequencies may be in the same band. In that case it will be difficult to remove these noise signals.

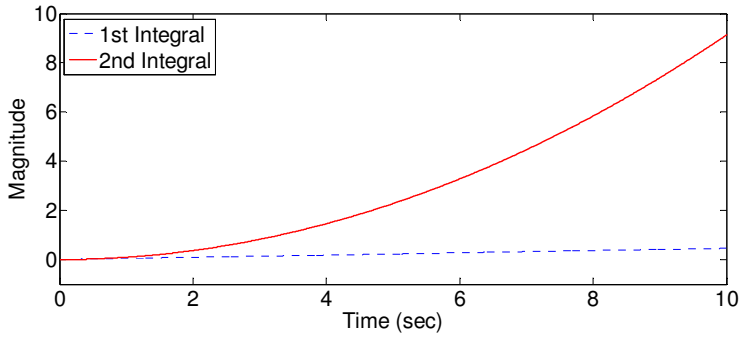

Figure 3.4: Drift in the integration output.

3.4 Experimental Results

A linear servo actuator mechanism and a shaking table are used here to evaluate the velocity and position estimations. The accelerometer is Summit Instruments 13203B. The $0g$-offset of the accelerometer is 2.44 V and the temperature drift is $3.2mg/\,^{\circ}\mathrm{C}$. The built-in temperature sensor in the accelerometer is utilized for compensating this temperature effect. The accelerometer output in $0g$-motion is integrated and the output drift is shown in Figure 3.4.

ServoToGo Model II data acquisition card is employed to acquire the acceleration signal. The data acquisition card uses a 13-bit ADC. The acceleration signal is recorded at a sampling rate of 1 ms. In order to assure a constant sampling interval, a dedicated clock source is used for the data acquisition card. This will help in reducing the low-frequency noise in the acquired acceleration signal. The Dormand-Prince method is chosen for the integration.

The Fourier spectrum of the accelerometer $0g$-motion output signal is plotted using FFT, see Figure 3.5. From the plot it is clear that the accelerometer has a measurement noise close to 0 Hz. The high-pass filter is designed ($f_c = 0.16$ Hz; $\tau = 1$) to attenuate these noise signals. As the natural frequency of the mechanical structure is 7.7 Hz, the above filter does not affect this frequency. A low-pass filter is used in the accelerometer output for attenuating the signals above 30 Hz. As the position sensor is available for both experiments, we use the measured position data to compare that with the position estimation obtained using the

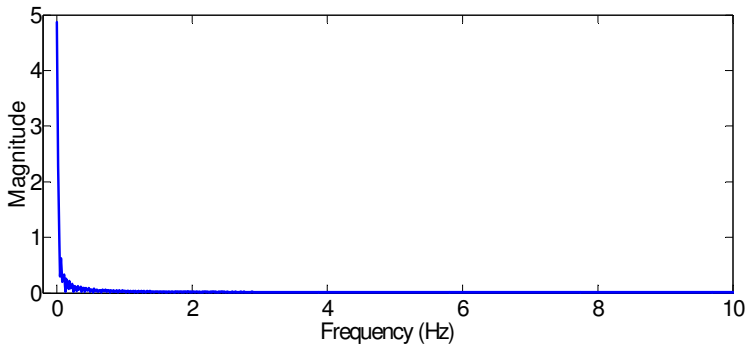

Figure 3.5: Fourier spectra of the acceleration signal for zero motion.

numerical integrator.

3.4.1 Linear servo actuator

Once the parameters of the proposed numerical integrator are calculated, the experiments were carried out to evaluate the velocity and position estimation. The linear servo mechanism (STB1108, Copley Controls Corp.) is driven using a digital servo drive (Accelnet Micro Panel, Copley Controls Corp). The servo-tube comes with an integrated position sensor with a resolution of 8 μm, which is used here as the reference for verifying the estimated position. The servo mechanism is actuated using basic sinusoidal signals and the corresponding acceleration is measured with the accelerometer. The accelerometer is mounted on the actuator, where its sensitive axis is placed parallel to the direction of actuator motion, see Figure 3.6.

A 4 Hz sinusoidal signal, a signal composed with 6 Hz, 7 Hz, and 8 Hz and a signal composed with 2 Hz, 4 Hz, 6 Hz, and 8 Hz is used here to excite the linear actuator. The acceleration of the actuator is measured using the accelerometer and fed to the OCF ($\epsilon_{\min} = 0.001$) for removing the offset. Figure 3.7 shows the Fourier spectra of both the measured and filtered acceleration signals. We can see that the low-frequency noise signals are removed. This filtered acceleration signal is then fed to the proposed integrator for estimating the velocity and position. The position estimations for a 4 Hz sine wave, signal composed with

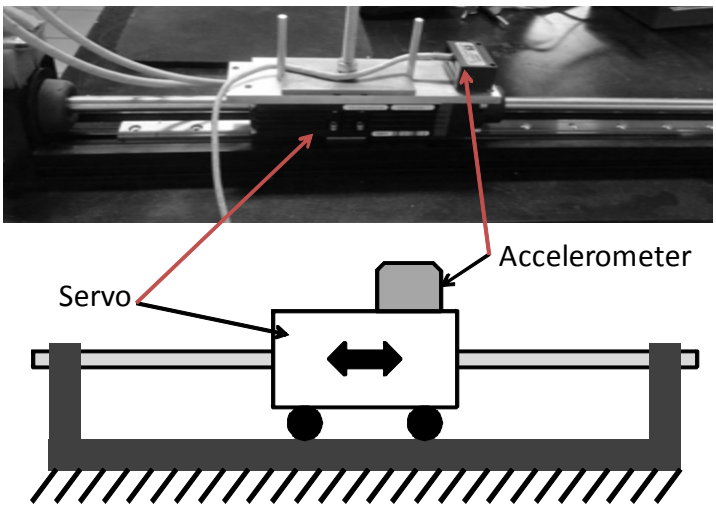

Figure 3.6: Linear servo mechanism.

6 Hz, 7 Hz, and 8 Hz, and signal composed with 2 Hz, 4 Hz, 6 Hz, and 8 Hz are shown in Figure 3.8, Figure 3.9 and Figure 3.10, respectively.

The effect of the proposed numerical integrator on the input signal frequency characteristics is studied by plotting its Fourier spectra. A sinusoidal signal composed with 6 Hz, 7 Hz, and 8 Hz is used here to excite the linear actuator. The FFT diagram of the measured and estimated position is generated, see Figure 3.11. As one can see from the figure that the frequency information is not affected, except in the low-frequency range. This low-frequency error is caused due to the presence of bias and noise in the accelerometer output.

3.4.2 Shaking table

A shaking table prototype is used to verify the estimation during the earthquake excitation. The prototype is actuated using the earthquake signal and the structure acceleration is measured, which is then used to estimate the structure velocity and position. A linear magnetic encoder (LM15) position sensor with a resolution of 50 μm is used here for measuring the structure position. The mechanical structure base is connected to the electrohydraulic shaker

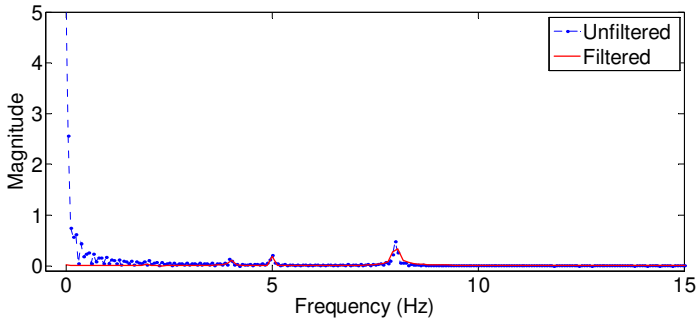

Figure 3.7: Fourier spectra of the acceleration signal before and after filtering using OCF.

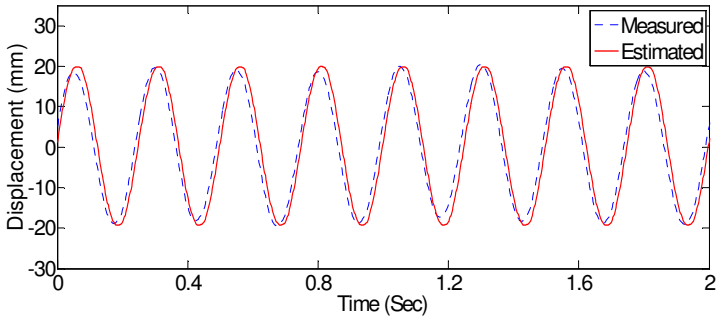

Figure 3.8: Comparison of the measured and estimated position data.

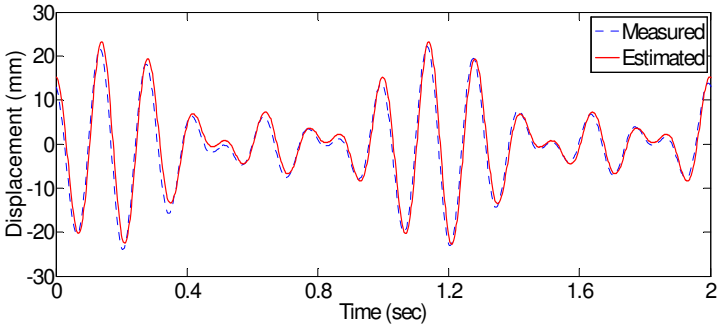

Figure 3.9: Comparison of the measured and estimated position data.

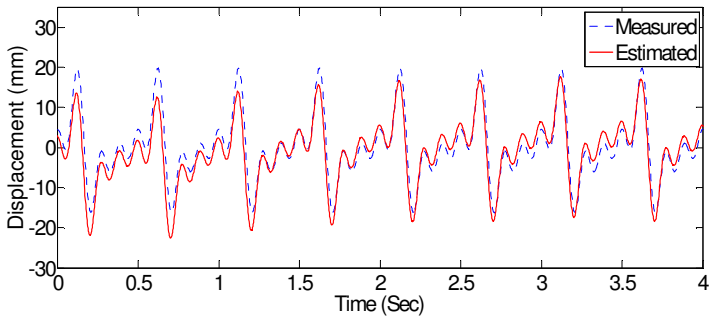

Figure 3.10: Comparison of the measured and estimated position data.

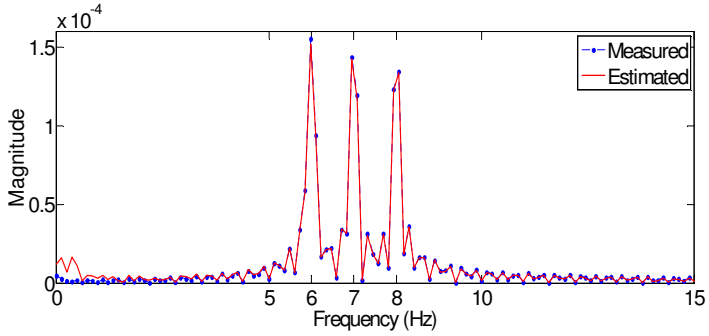

Figure 3.11: Comparison of the measured and estimated position data using Fourier spectra.

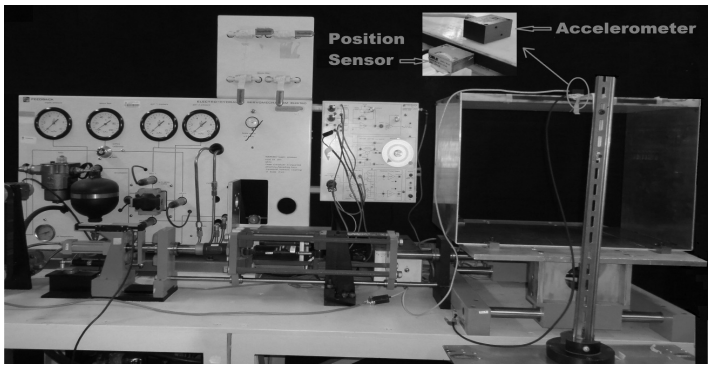

Figure 3.12: Shaking table experimental setup.

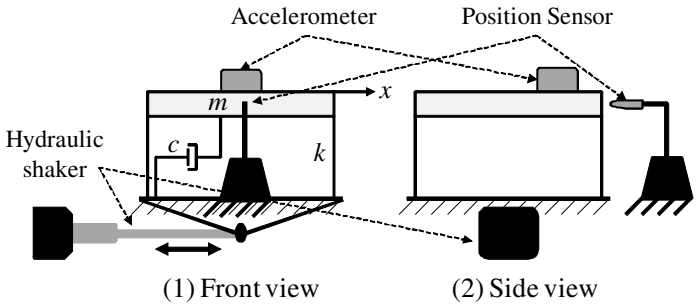

Figure 3.13: Schematic of the shaking table setup.

(FEEDBACK EHS 160), which is used to generate the earthquake signals. The experimental setups are shown in Figure 3.12 and Figure 3.13.

The natural and forced responses of the mechanical structure are evaluated. The excitation signal is generated manually by knocking the structure with a hammer to bring out its natural response. The measured acceleration signal is fed to the proposed integrator and the position is estimated, which is shown in Figure 3.14. In order to perform a comparison this figure also includes the estimation performed using the integrator proposed in [39] ($\alpha = 1$, $\beta = 0.2, K = 1$ and $\tau = 1$).

Finally, the October 17, 1989 Loma Prieta East-West earthquake signal is generated

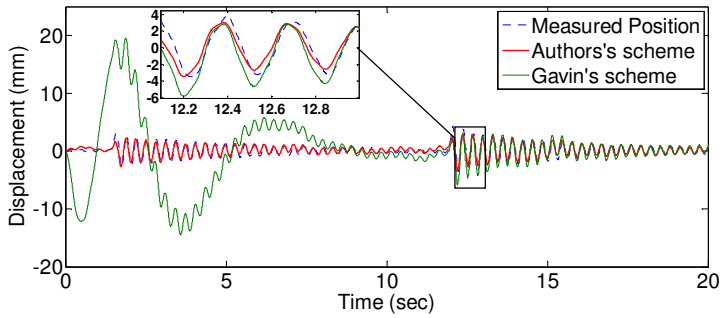

Figure 3.14: Comparison of the measured and estimated position data.

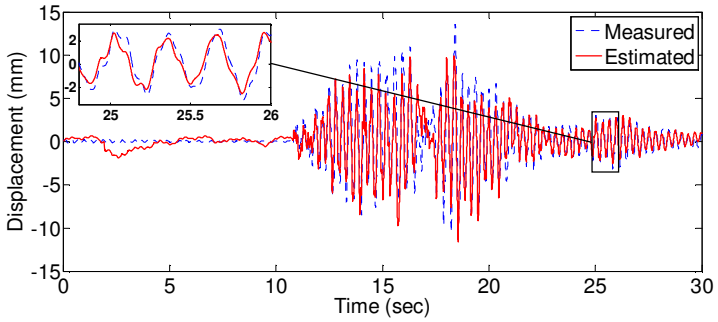

Figure 3.15: Comparison of the measured and estimated position data.

using the electrohydraulic shaker and the resulting acceleration on the mechanical structure is measured. The corresponding position estimation is shown in Figure 3.15.

From the above experiments it can be seen that the proposed integrator is able to estimate the velocity and position with a reasonable level of accuracy. Still, there exists some error between the estimated and measured position. This error is caused due to the phase error, introduced by the high-pass filter, which resulted in a small phase error. But it is found that the estimation obtained using the proposed integrator is adequate for the structural control and health monitoring applications.

In this chapter, it is assumed that the building structure natural frequencies lie between

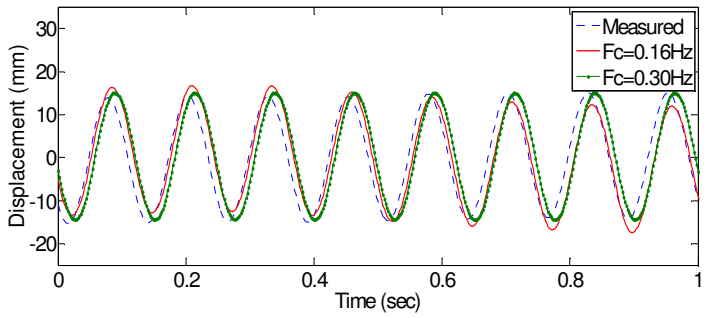

Figure 3.16: Comparison of the measured and estimated position data obtained using different high-pass filters.

1 Hz and 20 Hz. As mentioned earlier, the high-pass filter introduces phase errors in the cutoff frequency region. The resulting error is variable with the signal frequency. If the structure natural frequency is close to the high-pass filter cutoff frequency, then the estimation is affected due to the phase error introduced by the filter. The knowledge about structure natural frequency can be considered in the high-pass filter design. In Figure 3.16 the position estimation of a 8 Hz sinusoidal signal obtained using two different high-pass filters is shown. The first filter has a cutoff frequency of 0.16 Hz and the second filter has 0.3 Hz. The estimation obtained using the first filter have some low-frequency noise. This problem is solved if the second filter is used for the estimation. Moreover, this filter cutoff frequency is far from the input signal frequency.

3.5 Summary

This chapter discusses in detail the problems involved in the integration of a real-time acceleration signal. A mathematical model of different noise signals and offset in the accelerometer output has been derived and a novel numerical integrator is proposed to attenuate these undesired signals. This integrator combines the offset cancellation and high-pass filtering schemes. The common problems of numerical integrators such as; stability, on-line estima-

tion, low accuracy, and phase error have been overcome. The experimental results show that the accuracy of the drift-free integrator is improved by adding the offset cancellation filter. The estimated position and velocity is compared with other techniques and is found to be superior. This integrator can be applied to systems where the signal frequency is greater than the filter cut-off frequency.

Chapter 4

Fuzzy PID Control of Building Structures Subjected to Earthquake

4.1 Introduction

The objective of structural control is to reduce the vibrations of the buildings due to earthquake or large winds through an external control force. In active control system it is essential to design an effective control strategy, which is simple, robust, and fault tolerant. Many attempts have been made to introduce advanced controllers for the active vibration control of building structures as discussed in Chapter 2.

PID control is widely used in industrial applications. Without model knowledge, PID control may be the best controller in real-time applications [13]. The great advantages of PID control over the others are that they are simple and have clear physical meanings. Although the research in PID control algorithms is well established, their applications in structural vibration control are still not well developed. In [78], a simple proportional (P) control is applied to reduce the building displacement due to wind excitation. In [42] and [43], PD and PID controllers were used. However, the control results are not satisfactory. There are two reasons: 1) it is difficult to tune the PID gains to guarantee good performances such as the rise-time, overshoot, settling time, and steady-state error [42]; 2) in order to decrease

the regulation error of PD/PID control, the derivative gain and integration gain have to be increased. These can cause undesired transient performances, even unstability [13].

Instead of increasing PD/PID gains, a natural way is to use intelligent method to compensate the regulation error. The difference between our controller and the above intelligent method is that the main part of our controller is still classical PD/PID control. The obstacle of this kind of PD/PID controller is the theoretical difficulty in analyzing its stability. Even for linear PID, it is not easy to prove its asymptotic stability [54].

In this chapter, the well known PD/PID is extended to PD/PID control with fuzzy compensation. The stability of these novel fuzzy PD/PID control is proven. Explicit conditions for choosing PID gains are given. Unlike the other PD/PID control for the building structure, the proposed fuzzy PD/PID control does not need large derivative and integral gains. An active vibration control system for a two-story building structure equipped with an AMD is constructed for the experimental study. The experimental results are compared with the other controllers, and the effectiveness of the proposed algorithms are demonstrated.

4.2 Control of Building Structures

The n-floor structure can be expressed as

$$M\ddot{x}(t) + C\dot{x}(t) + F_s = -F_e \tag{4.1}$$

In a simplified case, the lateral force F_s can be linear with x as $F_s = Kx(t)$. However, in the case of real building structures, the stiffness component is inelastic as discussed in the second chapter. Here we consider the nonlinear stiffness represented in (2.7).

The main objective of structural control is to reduce the movement of buildings into a comfortable level. In order to attenuate the vibrations caused by the external force, an AMD is installed on the structure, see Figure 4.1. The closed-loop system with the control force $u \in \Re^n$ is defined as

$$M\ddot{x}(t) + C\dot{x}(t) + F_s + F_e = \Gamma(u - \psi) \tag{4.2}$$

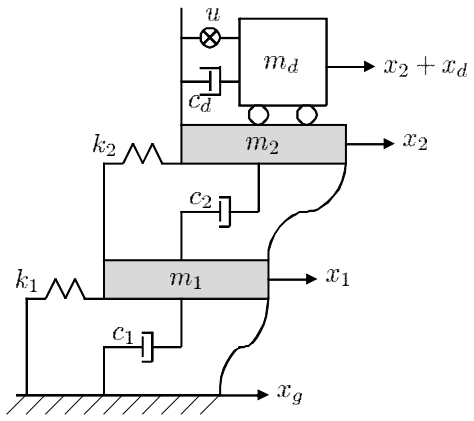

Figure 4.1: Building structure equipped with AMD.

where $\psi \in \Re^n$ is the damping and friction force of the damper and $\Gamma \in \Re^{n \times n}$ is the location matrix of the dampers, defined as follows.

$$\Gamma_{i,j} = \begin{cases} 1 & \text{if } \; i = j = v \\ 0 & \text{otherwise} \end{cases} \quad , \forall i, j \in \{1, ..., n\}, v \subseteq \{1, ..., n\}$$

where v are the floors on which the dampers are installed. In the case of a two-story building, if the damper is placed on second floor, $v = \{2\}$, $\Gamma_{2,2} = 1$. If the damper is placed on both first and second floor, then $v = \{1, 2\}$, $\Gamma_{2\times 2} = I_2$.

The damper force F_{dq}, exerted by the q-th damper on the structure is

$$F_{dq} = m_{dq}(\ddot{x}_v + \ddot{x}_{dq}) = u_q - \psi_q \tag{4.3}$$

where m_{dq} is the mass of the q-th damper, $\ddot{x}_v$ is the acceleration of the v-th floor on which the damper is installed, $\ddot{x}_{dq}$ is the acceleration of the q-th damper, u_q is the control signal to the q-th damper, and

$$\psi_q = c_{dq}\dot{x}_{dq} + \varkappa_q m_{dq} g \;\; \tanh\left[\beta_t \dot{x}_{dq}\right] \tag{4.4}$$

where c_{dq} and $\dot{x}_{dq}$ are the damping coefficient and velocity of the q-th damper respectively and the second term is the Coulomb friction represented using a hyperbolic tangent dependent

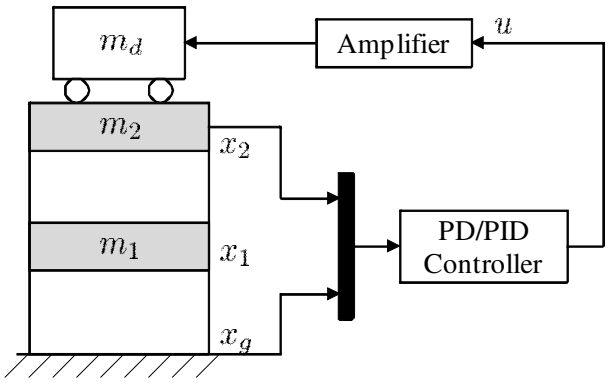

Figure 4.2: PD/PID control for a two-story building.

on β_t where $\varkappa_q$ is the friction coefficient between the q-th damper and the floor on which it is attached and g is the gravity constant [93].

Obviously, the building structures in open-loop are asymptotically stable when there is no external force, $F_e = 0$. This is also true in the case of inelastic stiffness, due to its BIBO stability and passivity properties [50]. During external excitation, the ideal active control force required for cancelling out the vibration completely is $\Gamma u = F_e$. However, it is impossible because F_e is not always measurable and is much bigger than any control device force. Hence, the objective of the active control is to maintain the vibration as small as possible by minimizing the relative movement between the structural floors. In the next section, we will discuss several stable control algorithms.

4.3 PD Controller with Fuzzy Compensation

PD control may be the simplest controller for the structural vibration control system, see Figure 4.2, which provides high robustness with respect to the system uncertainties. PD control has the following form

$$u = -K_p(x - x^d) - K_d(\dot{x} - \dot{x}^d) \tag{4.5}$$

where K_p and K_d are positive-definite constant matrices, which correspond to the proportional and derivative gains, respectively and x^d is the desired position. In active vibration control of building structures, the references are $x^d = \dot{x}^d = 0$, hence (4.5) becomes

$$\Gamma u = -K_p x - K_d \dot{x} \tag{4.6}$$

The aim of the controller design is to choose suitable gains K_p and K_d in (4.6), such that the closed-loop system is stable. Without loss of generality, we use a two-story building structure as shown in Figure 4.2. The nonlinear dynamics of the structure with control can be written as

$$M\ddot{x} + C\dot{x} + F = u \tag{4.7}$$

where

$$F = F_s(x, \dot{x}) + F_e + \psi \tag{4.8}$$

Then the building structure with the PD control (4.6) can be written as

$$M\ddot{x} + C\dot{x} + F = -K_p x - K_d \dot{x} \tag{4.9}$$

The closed-loop system (4.9) is nonlinear and the parameters of M, C, and F are unknown. It is well known that, using the PD controller the regulation error can be reduced by increasing the gain K_d. The cost of large K_d is that the transient performance becomes slow. Only when $K_d \to \infty$, the tracking error converges to zero [63]. Moreover, it is not a good idea to use a large K_d, if the system comprises high-frequency noise signals.

In this chapter, we use fuzzy compensation to estimate F such that the derivative gain K_d is not so large. A generic fuzzy model, provided by a collection of l fuzzy rules (Mamdani fuzzy model [74]) is used to approximate $\widehat{F}_q$

$$\mathrm{R}^i\text{: IF } (x \text{ is } A_{1i}) \text{ and } (\dot{x} \text{ is } A_{2i}) \text{ THEN } \widehat{F}_q \text{ is } B_i^q \tag{4.10}$$

where $\widehat{F}_q$ is the estimation of the uncertain force F.

A total of l fuzzy IF-THEN rules are used to perform the mapping from the input vector z to the output vector $\widehat{F} = \left[\widehat{F}_1 \cdots \widehat{F}_n\right]^T$. Here A_{1i}, A_{2i} and B_i^q are standard fuzzy sets. By using product inference, center-average defuzzification, and a singleton fuzzifier, the output of the fuzzy logic system can be expressed as [117]

$$\widehat{F}_q = \left(\sum_{i=1}^{l} w_{qi}\mu_{A_{1i}}\mu_{A_{2i}}\right) / \left(\sum_{i=1}^{l} \mu_{A_{1i}}\mu_{A_{2i}}\right) = \sum_{i=1}^{l} w_{qi}\sigma_i \tag{4.11}$$

where $\mu_{A_{ji}}$ are the membership functions of the fuzzy sets A_{ji}, which represents the j-th rule of the i-th input, $i = 1, ..., n$ and $j = 1, ..., l$. The Gaussian functions are chosen as the membership functions.

$$\mu_{A_{ji}} = \exp \frac{-\left(z_i - \hat{z}_{ji}\right)^2}{\rho_{ji}^2} \tag{4.12}$$

where $\hat{z}$ and ρ is the mean and variance of the Gaussian function, respectively. Weight w_{qi} is the point at which $\mu_{B_i^q} = 1$ and $\sigma_i(x, \dot{x}) = \mu_{A_{1i}}\mu_{A_{2i}} / \sum_{i=1}^{l} \mu_{A_{1i}}\mu_{A_{2i}}$. Equation (4.11) can be expressed in matrix form as

$$\widehat{F} = \widehat{W}\sigma(x, \dot{x}) \tag{4.13}$$

where $\widehat{W} = \begin{bmatrix} w_{11} & \dots & w_{1l} \\ \vdots & \ddots & \vdots \\ w_{n1} & \dots & w_{nl} \end{bmatrix}$, $\sigma(x, \dot{x}) = [\sigma_1(x, \dot{x}), ..., \sigma_l(x, \dot{x})]^T$.

The PD control with fuzzy compensation, shown in Figure 4.3 has the following form.

$$u = -K_p x - K_d \dot{x} - \widehat{W}\sigma(x, \dot{x}) \tag{4.14}$$

In order to analyze the fuzzy PD control (4.14), we define a filtered regulation error as

$$r = \dot{x} + \Lambda x \tag{4.15}$$

Then the fuzzy PD control (4.14) becomes

$$u = -K_1 r - \widehat{W}\sigma(x, \dot{x}) \tag{4.16}$$

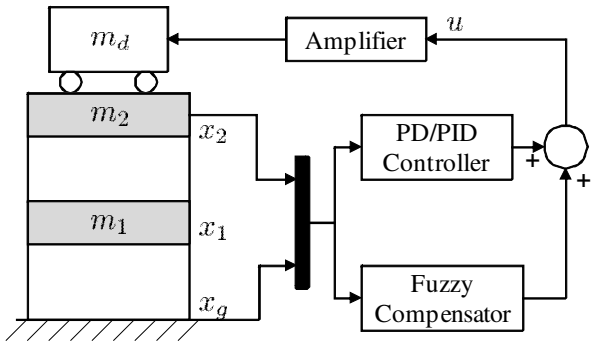

Figure 4.3: Control scheme for PD/PID controller with Fuzzy compensator.

where $K_p = K_1\Lambda$, $K_d = K_1$, and Λ is a positive definite matrix. Using (4.9), (4.15), and (4.16):

$$\begin{aligned} M\dot{r} &= M\left(\ddot{x} + \Lambda\dot{x}\right) \\ &= -C\dot{x} - F - K_1 r - \widehat{W}\sigma(x,\dot{x}) + M\Lambda\dot{x} + C\Lambda x - C\Lambda x \\ &= -K_1 r - \widehat{W}\sigma(x,\dot{x}) - Cr - F + M\Lambda\dot{x} + C\Lambda x \\ &= -K_1 r - \widehat{W}\sigma(x,\dot{x}) - Cr + (M\Lambda\dot{x} + C\Lambda x - F) \end{aligned} \tag{4.17}$$

According to the Universal approximation theorem [117], the general nonlinear smooth function F can be written as

$$M\Lambda\dot{x} + C\Lambda x - F(x,\dot{x}) = \widehat{W}\sigma(x,\dot{x}) + \phi(x,\dot{x}) \tag{4.18}$$

where $\phi(x,\dot{x})$ is the modeling error which is assumed to be bounded. The following theorem gives the stability analysis of the fuzzy PD control (4.14).

Theorem 4.1 *Consider the structural system (4.7) controlled by the fuzzy PD controller (4.16), the closed-loop system is stable, provided that the control gains satisfy*

$$K_1 > 0, \quad K_d > 0 \tag{4.19}$$

The filter regulation error converges to the residual set

$$D_r = \left\{ r \mid \|r\|^2_{K_1} \leq \bar{\mu}_1 \right\} \tag{4.20}$$

where $\mu^T\Lambda_1^{-1}\mu \leq \bar{\mu}_1$ *and* $0 < \Lambda_1 < C$.

Proof. We define the Lyapunov candidate as

$$V = \frac{1}{2} r^T M r \tag{4.21}$$

Since M and Λ are positive definite matrices, $V \geq 0$. Using (4.17) and (4.18), the derivative of (4.21) is

$$\begin{aligned} \dot{V} &= r^T M \dot{r} \\ &= r^T \left[-K_1 r - \widehat{W}\sigma(x, \dot{x}) - Cr + (M\Lambda\dot{x} + C\Lambda x - F) \right] \\ &= -r^T (K_1 + C) r + r^T \mu \end{aligned} \tag{4.22}$$

The matrix inequality: $X^T Y + Y^T X \leq X^T \Lambda X + Y^T \Lambda^{-1} Y$, is valid for any X, $Y \in \Re^{n\times m}$ and any $0 < \Lambda = \Lambda^T \in \Re^{n\times n}$. Now μ can be estimated as

$$r^T \mu \leq r^T \Lambda_1 r + \mu^T \Lambda_1^{-1} \mu$$

where Λ_1 is any positive definite matrix and we select Λ_1 as

$$C > \Lambda_1 > 0$$

So

$$\dot{V} \leq -r^T (K_1 + C - \Lambda_1) r + \mu^T \Lambda_1^{-1} \mu \tag{4.23}$$

If we choose $K_d > 0$,

$$\dot{V} \leq -r^T K_1 r + \mu \Lambda_1^{-1} \mu = -\left\| r \right\|_{K_1}^2 + \bar{\mu}_1 \tag{4.24}$$

where $K_1 > 0$. V is therefore an ISS-Lyapunov function. Using Theorem 1 from [98], the boundedness of $\mu\Lambda_1^{-1}\mu \leq \bar{\mu}_1$ implies that the filter regulation error $r = \dot{x} + \Lambda x$ is bounded, hence x is bounded. Integrating (4.24) from 0 up to T yields

$$V_T - V_0 \leq -\int_0^T r^T K_1 r dt + \bar{\mu}_1 T \tag{4.25}$$

So

$$\begin{aligned} &\textstyle\int_0^T r^T K_1 r dt \leq V_0 - V_T + \bar{\mu}_1 T \leq V_0 + \bar{\mu}_1 T \\ &\lim_{T\to\infty} \tfrac{1}{T} \textstyle\int_0^T \left\| r \right\|_{K_1}^2 dt = \bar{\mu}_1 \end{aligned} \tag{4.26}$$

■

The approximation accuracy of the fuzzy model (4.13) depends on how to design the membership functions $\mu_{A_{1i}}$, $\mu_{A_{2i}}$, and w_{qi}. In the absence of prior experience, some on-line learning algorithms can be used to obtain these.

If the premise membership functions A_{1i} and A_{2i} are given by prior knowledge, then $\sigma_i(x, \dot{x}) = \mu_{A_{1i}}\mu_{A_{2i}} / \sum_{i=1}^{l} \mu_{A_{1i}}\mu_{A_{2i}}$ is known. The objective of the fuzzy modeling is to find the center values of B_{qi} such that the regulation error r is minimized. The fuzzy PD control with automatic updating is

$$\Gamma u = -K_1 r - \widehat{W}_t \sigma(x, \dot{x}) \tag{4.27}$$

The following theorem gives a stable gradient descent algorithm for $\widehat{W}_t$.

Theorem 4.2 *If the updating law for the membership function in (4.27) is*

$$\frac{d}{dt}\widehat{W}_t = -K_w \sigma(x, \dot{x}) r^T \tag{4.28}$$

where K_w is a positive definite matrix and

$$K_1 > 0, \quad K_d > 0 \tag{4.29}$$

then the PD control law with fuzzy compensation in (4.14) can make the regulation error stable. In fact, the average regulation error r converges to

$$\limsup_{T\to\infty} \frac{1}{T} \int_0^T \|r\|_{Q_1}^2 \, dt \le \bar{\mu}_2 \tag{4.30}$$

where $Q_1 = K_1 + C - \Lambda_2$, $0 < \Lambda_2 < C$, and $\mu^T \Lambda_2^{-1} \mu \le \bar{\mu}_2$.

Proof. The Lyapunov function is

$$V = \frac{1}{2} r^T M r + \frac{1}{2} tr\left(\widetilde{W}_t^T K_w^{-1} \widetilde{W}_t\right) \tag{4.31}$$

where $\widetilde{W}_t = \widehat{W}_t - \widehat{W}$, $\frac{d}{dt}\widetilde{W}_t = \frac{d}{dt}\widehat{W}_t$. Its derivative is

$$\begin{aligned}
\dot{V} &= r^T M\dot{r} + tr\left(\widetilde{W}_t^T K_w^{-1}\tfrac{d}{dt}\widetilde{W}_t\right) \\
&= r^T\left[-K_1 r - \widehat{W}_t\sigma(x,\dot{x}) - Cr + (M\Lambda\dot{x} + C\Lambda x - F)\right] + tr\left(\widetilde{W}_t^T K_w^{-1}\tfrac{d}{dt}\widetilde{W}_t\right) \\
&= -r^T(K_1 + C)\,r + r^T\mu + r^T\widetilde{W}_t\sigma(x,\dot{x}) + tr\left(\widetilde{W}_t^T K_w^{-1}\tfrac{d}{dt}\widetilde{W}_t\right) \\
&= -r^T(K_1 + C)\,r + r^T\mu + tr\left[\widetilde{W}_t^T\left(K_w^{-1}\tfrac{d}{dt}\widetilde{W}_t + \sigma(x,\dot{x})r^T\right)\right]
\end{aligned} \tag{4.32}$$

If the updating law is (4.28)

$$\dot{V} = -r^T(K_1 + C)\,r + r^T\mu \tag{4.33}$$

The rest part is similar with the Proof of Theorem 1. ■

Compared with the fuzzy compensation (4.14), the advantage of adaptive fuzzy compensation (4.27) is that, we do not need to be concerned about the big compensation error $\phi(x,\dot{x})$ in (4.18), which results from a poor membership function selection. The gradient algorithm (4.28) ensures that the membership functions $\widehat{W}_t$ is updated such that the regulation error $r(t)$ is reduced. The above theorem also guarantees the updating algorithm is stable.

When we consider the building structure as a black-box, neither the premise nor the consequent parameters are known. Now the objective of the fuzzy compensation is to find $\widehat{W}_t$, as well as the membership functions A_{1i} and A_{2i}. Equation (4.18) becomes

$$\begin{aligned}
&\widehat{W}\sigma(x,\dot{x}) - [M\Lambda\dot{x} + C\Lambda x - F(x,\dot{x})] \\
&= \sum_{i=1}^{l}\left[w_{qi}(t) - \widehat{w}_{qi}\right] z_i^q/b_q + \sum_{i=1}^{l}\sum_{j=1}^{n}\frac{\partial}{\partial\hat{z}_{ji}^q}\left(\frac{a_q}{b_q}\right)\left[\hat{z}_{ji}(t) - \hat{z}_{ji}\right] \\
&+ \sum_{i=1}^{l}\sum_{j=1}^{n}\frac{\partial}{\partial\rho_{ji}}\left(\frac{a_q}{b_q}\right)\left[\rho_{ji}(t) - \rho_{ji}\right]
\end{aligned}$$

Define

$$a_q = \sum_{k=1}^{l} w_k\sigma_k, \quad b_q = \sum_{k=1}^{l}\sigma_k, \quad q = 1,2$$

The updating laws for the membership functions are

$$\begin{aligned}
\tfrac{d}{dt}\widehat{W}_t &= -K_w\sigma(x,\dot{x})r^T \\
\tfrac{d}{dt}\hat{z}_{ji}(t) &= -2k_c\sigma_i\tfrac{\widehat{w}_{qi}-z_i}{b_q}\tfrac{z_j-\hat{z}_{ji}}{\left[\rho_{ji}^q\right]^2}r^T \\
\tfrac{d}{dt}\rho_{ji}(t) &= -2k_\rho\sigma_i\tfrac{\widehat{w}_{qi}-z_i}{b_q}\tfrac{(z_j-\hat{z}_{ji})^2}{\left[\rho_{ji}\right]^3}r^T
\end{aligned} \tag{4.34}$$

The proof is similar with the results in [134].

4.4 PID Controller with Fuzzy Compensation

Although fuzzy compensation can decrease the regulation error of PD control, there still exits regulation error, as given in Theorem 1 and Theorem 2. From control viewpoint, this steady-state error can be removed by introducing an integral component to the PD control. The resulting PID control is given by

$$u = -K_p x - K_d\dot{x} - K_i\int_0^t x(\tau)\,d\tau \tag{4.35}$$

where $K_i > 0$ correspond to the integration gain.

In order to analyze the stability of the PID controller, (4.35) is expressed by

$$\begin{aligned}
u &= -K_p x - K_d\dot{x} - \xi \\
\dot{\xi} &= K_i x, \quad \xi(0) = 0
\end{aligned} \tag{4.36}$$

Now substituting (4.36) in (4.7), the closed-loop system can be written as

$$M\ddot{x} + C\dot{x} + F = -K_p x - K_d\dot{x} - \xi \tag{4.37}$$

In matrix form, the closed-loop system is

$$\frac{d}{dt}\begin{bmatrix}\xi\\ x\\ \dot{x}\end{bmatrix} = \begin{bmatrix} K_i x \\ \dot{x} \\ -M^{-1}\left(C\dot{x} + F + K_p x + K_d\dot{x} + \xi\right)\end{bmatrix} \tag{4.38}$$

The equilibrium of (4.38) is $\left[x^T, \dot{x}^T, \xi^T\right] = [0, 0, \xi^*]$. Since at equilibrium point $x = 0$ and $\dot{x} = 0$, the equilibrium is $\left[0, 0, F\left(0,0\right)^T\right]$. In order to move the equilibrium to origin, we define

$$\tilde{\xi} = \xi - F\left(0,0\right)$$

The final closed-loop equation becomes

$$\begin{aligned} &M\ddot{x} + C\dot{x} + F = -K_p x - K_d\dot{x} - \tilde{\xi} + F\left(0,0\right) \\ &\dot{\tilde{\xi}} = K_i x \end{aligned} \tag{4.39}$$

In order to analyze the stability of (4.39), we first give the following properties.

P1. The positive definite matrix M satisfies the following condition.

$$0 < \lambda_m(M) \leq \|M\| \leq \lambda_M(M) \leq \bar{m},\ \bar{m} > 0 \tag{4.40}$$

where $\lambda_m(M)$ and $\lambda_M(M)$ are the minimum and maximum Eigen values of the matrix M, respectively.

P2. F is Lipschitz over $\bar{x}$ and $\bar{y}$

$$\|F\left(\bar{x}\right) - F\left(\bar{y}\right)\| \leq k_F \left\|\bar{x} - \bar{y}\right\| \tag{4.41}$$

Most of uncertainties are first-order continuous functions. Since F_s, F_e, and ψ are first-order continuous ($\mathcal{C}^1$) and satisfy Lipschitz condition, **P2** can be established using (4.8). Now we calculate the lower bound of $\int F\ dx$.

$$\int_0^t F dx = \int_0^t F_s dx + \int_0^t F_e dx + \int_0^t \psi dx \tag{4.42}$$

We define the lower bound of $\int_0^t F_s dx$ is $-\bar{F}_s$ and for $\int_0^t \psi dx$ is $-\bar{\psi}$. Compared with F_s and ψ, F_e is much bigger in the case of earthquake. We define the lower bound of $\int_0^t F_e dx$ is $-\bar{F}_e$. Finally the lower bound of $\int_0^t F dx$ is

$$k_F = -\bar{F}_s - \bar{F}_e - \bar{\psi} \tag{4.43}$$

The following theorem gives the stability analysis of the PID controller (4.36).

Theorem 4.3 *Consider the structural system (4.7) controlled by the PID controller (4.36), the closed-loop system (4.39) is asymptotically stable at the equilibrium* $\left[x^T, \dot{x}^T, \tilde{\xi}^T\right]^T = 0$, *provided that the control gains satisfy*

$$\begin{aligned} &\lambda_m(K_p) \geq \tfrac{3}{2}\left[k_F + \lambda_M(C)\right] \\ &\lambda_M(K_i) \leq \beta \tfrac{\lambda_m(K_p)}{\lambda_M(M)} \\ &\lambda_m(K_d) \geq \beta\left[1 + \tfrac{\lambda_M(C)}{\lambda_M(M)}\right] - \lambda_m(C) \end{aligned} \tag{4.44}$$

where $\beta = \sqrt{\frac{\lambda_m(M)\lambda_m(K_p)}{3}}$.

Proof. Here the Lyapunov function is defined as

$$V = \frac{1}{2}\dot{x}^T M\dot{x} + \frac{1}{2}x^T K_p x + \frac{\alpha}{2}\tilde{\xi}^T K_i^{-1}\tilde{\xi} + x^T\tilde{\xi} + \alpha x^T M\dot{x} + \frac{\alpha}{2}x^T K_d x + \int_0^t F dx - k_F \tag{4.45}$$

where k_F is defined in (4.70) such that $V(0) = 0$. In order to show that $V \geq 0$, it is separated into three parts, such that $V = \sum_{i=1}^{3} V_i$

$$V_1 = \frac{1}{6}x^T K_p x + \frac{\alpha}{2}x^T K_d x + \int_0^t F dx - k_F \geq 0 \tag{4.46}$$

$$\begin{aligned} V_2 &= \tfrac{1}{6}x^T K_p x + \tfrac{\alpha}{2}\tilde{\xi}^T K_i^{-1}\tilde{\xi} + x^T\tilde{\xi} \\ &\geq \tfrac{1}{2}\tfrac{1}{6}\lambda_m(K_p)\|x\|^2 + \tfrac{\alpha\lambda_m(K_i^{-1})}{2}\left\|\tilde{\xi}\right\|^2 - \|x\|\left\|\tilde{\xi}\right\| \end{aligned} \tag{4.47}$$

When $\alpha \geq \frac{3}{\lambda_m(K_i^{-1})\lambda_m(K_p)}$,

$$V_2 \geq \frac{1}{2}\left(\sqrt{\frac{\lambda_m(K_p)}{3}}\|x\| - \sqrt{\frac{3}{\lambda_m(K_p)}}\|\xi\|\right)^2 \geq 0 \tag{4.48}$$

and

$$\begin{aligned} V_3 &= \tfrac{1}{6}x^T K_p x + \tfrac{1}{2}\dot{x}^T M\dot{x} + \alpha x^T M\dot{x} \\ \bar{y}^T A\bar{x} &\geq \|\bar{y}\|\,\|A\bar{x}\| \geq \|\bar{y}\|\,\|A\|\,\|\bar{x}\| \geq |\lambda_M(A)|\,\|\bar{y}\|\,\|\bar{x}\| \end{aligned} \tag{4.49}$$

when $\alpha \leq \frac{\sqrt{\frac{1}{3}\lambda_m(M)\lambda_m(K_p)}}{\lambda_M(M)}$

$$\begin{aligned} V_3 &\geq \tfrac{1}{2}\left(\tfrac{1}{3}\lambda_m(K_p)\|x\|^2 + \lambda_m(M)\|\dot{x}\|^2 + 2\alpha\lambda_M(M)\|x\|\,\|\dot{x}\|\right) \\ &= \tfrac{1}{2}\left(\sqrt{\tfrac{\lambda_m(K_p)}{3}}\|x\| + \sqrt{\lambda_m(M)}\|\dot{x}\|\right)^2 \geq 0 \end{aligned} \tag{4.50}$$

If

$$\sqrt{\frac{1}{3}}\lambda_m(K_i^{-1})\lambda_m^{\frac{3}{2}}(K_p)\lambda_m^{\frac{1}{2}}(M) \geq \lambda_M(M) \tag{4.51}$$

there exists

$$\frac{\sqrt{\frac{1}{3}\lambda_m(M)\lambda_m(K_p)}}{\lambda_M(M)} \geq \alpha \geq \frac{3}{\lambda_m(K_i^{-1})\lambda_m(K_p)} \tag{4.52}$$

The derivative of (4.70) is

$$\begin{aligned}\dot{V} &= \dot{x}^T M\ddot{x} + \dot{x}^T K_p x + \alpha\dot{\tilde{\xi}}^T K_i^{-1}\tilde{\xi} + \dot{x}^T\tilde{\xi} + x^T\dot{\tilde{\xi}} + \alpha\dot{x}^T M\dot{x} + \alpha x^T M\ddot{x} + \alpha\dot{x}^T K_d x + \dot{x}^T F \\ &= \dot{x}^T\left[-C\dot{x} - F - K_p x - K_d\dot{x} - \tilde{\xi} + F(0,0)\right] + \dot{x}^T K_p x + \alpha\dot{\tilde{\xi}}^T K_i^{-1}\tilde{\xi} + \dot{x}^T\tilde{\xi} + x^T\dot{\tilde{\xi}} \\ &+\alpha\dot{x}^T M\dot{x} + \alpha x^T\left[-C\dot{x} - F - K_p x - K_d\dot{x} - \tilde{\xi} + F(0,0)\right] + \alpha x^T K_d\dot{x} + \dot{x}^T F\end{aligned} \tag{4.53}$$

From (4.41)

$$\alpha x^T\left[F(0,0) - F\right] \leq \alpha k_F\|x\|^2$$

Again using the inequality: $X^TY + Y^TX \leq X^T\Lambda X + Y^T\Lambda^{-1}Y$, we can write

$$-\alpha x^T C\dot{x} \leq \alpha\lambda_M(C)\left[x^Tx + \dot{x}^T\dot{x}\right]$$

Since $\dot{\tilde{\xi}} = K_i x$, $\dot{\tilde{\xi}}^T K_i^{-1}\tilde{\xi}$ becomes $\alpha x^T\tilde{\xi}$, and $x^T\dot{\tilde{\xi}}$ becomes $x^T K_i x$, then

$$\dot{V} = -\dot{x}^T\left[C + K_d - \alpha M - \alpha\lambda_M(C)\right]\dot{x} - x^T\left[\alpha K_p - K_i - \alpha k_F - \alpha\lambda_M(C)\right]x \tag{4.54}$$

Using (4.40), (4.54) becomes,

$$\begin{aligned}\dot{V} \leq &-\dot{x}^T\left[\lambda_m(C) + \lambda_m(K_d) - \alpha\lambda_M(M) - \alpha\lambda_M(C)\right]\dot{x} \\ &-x^T\left[\alpha\lambda_m(K_p) - \lambda_M(K_i) - \alpha k_F - \alpha\lambda_M(C)\right]x\end{aligned} \tag{4.55}$$

If $\lambda_m(C)+\lambda_m(K_d) \geq \alpha\left[\lambda_M(M) + \lambda_M(C)\right]$ and $\lambda_m(K_p) \geq \frac{1}{\alpha}\lambda_M(K_i)+k_F+\lambda_M(C)$, then $\dot{V} \leq 0$, hence $\|\mathbf{x}\|$ decreases. From (4.52), $\frac{\sqrt{\frac{1}{3}\lambda_m(M)\lambda_m(K_p)}}{\lambda_M(M)} \geq \alpha \geq \frac{3}{\lambda_m(K_i^{-1})\lambda_m(K_p)}$ and $\lambda_m\left(K_i^{-1}\right) = \frac{1}{\lambda_M(K_i)}$, if

$$\begin{aligned}&\lambda_m(K_d) \geq \sqrt{\tfrac{1}{3}\lambda_m(M)\lambda_m(K_p)\left[1 + \tfrac{\lambda_M(C)}{\lambda_M(M)}\right] - \lambda_m(C)} \\ &\lambda_m(K_p) \geq \tfrac{3}{2}\left[k_F + \lambda_M(C)\right]\end{aligned} \tag{4.56}$$

then (4.44) is established.

There exists a ball Σ of radius $\kappa > 0$ centered at the origin of the state-space on which $\dot{V} \leq 0$. The origin of the closed-loop equation (4.39) is a stable equilibrium. Since the closed-loop equation is autonomous, we use La Salle's theorem. Define Ω as

$$\begin{aligned} \Omega &= \left\{ \bar{z}(t) = \left[x^T, \dot{x}^T, \tilde{\xi}^T \right]^T \in \Re^{3n} : \dot{V} = 0 \right\} \\ &= \left\{ \tilde{\xi} \in \Re^n : x = 0 \in \Re^n, \dot{x} = 0 \in \Re^n \right\} \end{aligned} \tag{4.57}$$

From (4.72), $\dot{V} = 0$ if and only if $x = \dot{x} = 0$. For a solution $\bar{z}(t)$ to belong to Ω for all $t \geq 0$, it is necessary and sufficient that $x = \dot{x} = 0$ for all $t \geq 0$. Therefore, it must also hold that $\ddot{x} = 0$ for all $t \geq 0$. We conclude that from the closed-loop system (4.39), if $\bar{z}(t) \in \Omega$ for all $t \geq 0$, then

$$\begin{aligned} &F(x, \dot{x}) = F(0,0) = \tilde{\xi} + F(0,0) \\ &\tfrac{d}{dt}\xi = 0 \end{aligned} \tag{4.58}$$

implies that $\tilde{\xi} = 0$ for all $t \geq 0$. So $\bar{z}(t) = 0$ is the only initial condition in Ω for which $\bar{z}(t) \in \Omega$ for all $t \geq 0$.

Finally, we conclude from all this that the origin of the closed-loop system (4.39) is asymptotically stable. It establishes the stability of the proposed controller, in the sense that the domain of attraction can be arbitrarily enlarged with a suitable choice of the gains. Namely, increasing K_p the basin of attraction will grow. ■

Remark 4.1 *Since the stiffness element of the building structure has hysteresis property, its output depends on both the instantaneous and the history of the deformation. The deformation before applying the force (loading) and after removing the force (unloading) is not the same, i.e, the position before the earthquake and after the vibration dies out is not the same. In the absence of external force, the SDOF inelastic structure can be represented as*

$$m\ddot{x} + c\dot{x} + f_s(x, \dot{x}) = 0 \tag{4.59}$$

The above system can be described in matrix form as

$$\frac{d}{dt} \begin{bmatrix} x \\ \dot{x} \end{bmatrix} = \begin{bmatrix} \dot{x} \\ -\frac{1}{m}\left(c\dot{x} + f_s(x, \dot{x})\right) \end{bmatrix} \tag{4.60}$$

The equilibrium of (4.60) is $\left[x^T, \dot{x}^T\right] = \left[\frac{(\tilde{\alpha}-1)}{\tilde{\alpha}}\tilde{\eta} f_r, 0\right]$*, hence the equilibrium position of the system is determined by the nonlinear term* f_r*. As a result, after the seismic event, the structural system possibly has infinite number of equilibrium positions. On the other hand, if the system represented in (4.59) is controlled using a PID controller, (as indicated in (4.38)), the integral action force the position asymptotically to zero. However, due to the possibility of variable equilibrium points (this corresponds to the term* $F(0,0)$*), we cannot conclude that the closed-loop system (4.39) is globally stable.*

It is well known that, in the absence of the uncertainties and external forces, the PD control (4.6) with any positive gains can guarantee the asymptotically stable closed-loop system. The main objective of the integral action can be regarded to cancel F. In order to decrease the integral gain, an estimated F is applied to the PID control (4.36). The PID control with an approximate force compensation $\widehat{F}$ is

$$u = -K_p x - K_d \dot{x} - \xi + \widehat{F}, \quad \dot{\xi} = K_i x \tag{4.61}$$

The above theorem can also be applied for the PID controller with an approximate F compensation (4.61). The condition for PID gains (4.44) becomes $\lambda_m(K_p) \geq \frac{3}{2}\left[\tilde{k}_F + \lambda_M(C)\right]$ and $\lambda_M(K_i) \leq \frac{3\beta}{2}\frac{\tilde{k}_F + \lambda_M(C)}{\lambda_M(M)}$, where $\tilde{k}_F \ll k_F$.

However, a big integration gain causes unacceptable transient performances and stability problems. Similar to the fuzzy PD control, a fuzzy compensator for PID control may be used. The fuzzy rules have the same form as (4.10), so the PID control with adaptive fuzzy compensation is

$$u = -K_p x - K_d \dot{x} - K_i \int_0^t x(\tau)\, d\tau - \widehat{W}_t \sigma(x, \dot{x}) \tag{4.62}$$

Hence, the closed-loop system becomes

$$M\ddot{x} + C\dot{x} + F = -K_p x - K_d \dot{x} - \xi - \widehat{W}_t \sigma(x, \dot{x}) \tag{4.63}$$

Similar to the PID, the final closed-loop equation can be written as

$$\begin{aligned} &M\ddot{x} + C\dot{x} + \widehat{W}\sigma(x, \dot{x}) + \phi(x, \dot{x}) = -K_p x - K_d \dot{x} - \tilde{\xi} - \widehat{W}_t \sigma(x, \dot{x}) + \phi(0,0) \\ &\dot{\tilde{\xi}} = K_i x \end{aligned} \tag{4.64}$$

with the equilibrium $[0, 0, \phi(0,0)]$, where $\tilde{\xi} = \xi - \phi(0,0)$ is defined to move the equilibrium point to origin.

In order to analyze the stability of (4.64), we use the following property for $\phi(x, \dot{x})$.

P3. ϕ is Lipschitz over $\bar{x}$ and $\bar{y}$.

$$\|\phi(\bar{x}) - \phi(\bar{y})\| \leq k_\phi \|\bar{x} - \bar{y}\| \tag{4.65}$$

Now we calculate the lower bound of $\int \phi \, dx$ as

$$\int_0^t \phi dx = \int_0^t F_s dx + \int_0^t F_e dx + \int_0^t \psi dx - \int_0^t \widehat{W}\sigma dx \tag{4.66}$$

Since $\sigma(\cdot)$ is a Gaussian function, $\int_0^t \widehat{W}\sigma dx = \frac{\widehat{W}}{2}\sqrt{\pi}\,\mathrm{erf}(z(t))$. Then the lower bound of $\int_0^t \phi dx$ is

$$k_\phi = k_F - \frac{1}{2}\sqrt{\pi}\widehat{W} \tag{4.67}$$

The following theorem gives the stability analysis of the PID control with adaptive fuzzy compensation (4.62).

Theorem 4.4 *Consider the structural system (4.7) controlled by the fuzzy PID controller (4.62), the closed-loop system (4.63) is asymptotically stable, i.e.* $\lim_{t\to\infty} x(t) = 0$, *if the initial condition of* $\left[x^T, \dot{x}^T, \tilde{\xi}^T\right]^T$ *is inside of* Ω *and provided that the updating law for the fuzzy compensator is*

$$\frac{d}{dt}\widehat{W}_t = -\left[K_w \sigma(x, \dot{x})(\dot{x} + \alpha x)^T\right]^T \tag{4.68}$$

where K_w *is a positive definite matrix and* $\alpha > 0$ *is a designing parameter and the control gains satisfy*

$$\begin{aligned} &\lambda_m(K_p) \geq \tfrac{3}{2}\left[k_\phi + \lambda_M(C)\right] \\ &\lambda_M(K_i) \leq \beta \tfrac{\lambda_m(K_p)}{\lambda_M(M)} \\ &\lambda_m(K_d) \geq \beta\left[1 + \tfrac{\lambda_M(C)}{\lambda_M(M)}\right] - \lambda_m(C) \end{aligned} \tag{4.69}$$

Proof. We define the Lyapunov function as

$$\begin{aligned} V = &\tfrac{1}{2}\dot{x}^T M\dot{x} + \tfrac{1}{2}x^T K_p x + \tfrac{\alpha}{2}\tilde{\xi}^T K_i^{-1}\tilde{\xi} + \tfrac{\alpha}{2}x^T K_d x \\ &+ \textstyle\int_0^t \phi dx - k_\phi + x^T\tilde{\xi} + \alpha x^T M\dot{x} + \tfrac{1}{2}tr\left(\widetilde{W}_t^T K_w^{-1}\widetilde{W}_t\right) \end{aligned} \tag{4.70}$$

In order to show that $V \geq 0$, it is separated into three parts, where the (4.46) is modified as

$$V_1 = \frac{1}{6}x^T K_p x + \frac{\alpha}{2}x^T K_d x + \int_0^t \phi dx - k_\phi + \frac{1}{2}tr\left(\widetilde{W}_t^T K_w^{-1}\widetilde{W}_t\right) \geq 0 \tag{4.71}$$

whereas the V_2 and V_3 remains the same as in (4.47) and (4.49), respectively. The derivative of (4.70) is

$$\begin{aligned}
&\dot{V} = \dot{x}^T M\ddot{x} + \dot{x}^T K_p x + \alpha\dot{\tilde{\xi}}^T K_i^{-1}\tilde{\xi} + \dot{x}^T\tilde{\xi} + x^T\dot{\tilde{\xi}} + \dot{x}^T\phi + \alpha\dot{x}^T M\dot{x} \\
&+\alpha x^T M\ddot{x} + \alpha\dot{x}^T K_d x + tr\left(\widetilde{W}_t^T K_w^{-1}\tfrac{d}{dt}\widetilde{W}_t\right) \\
&= \dot{x}^T\left[-C\dot{x} - \widetilde{W}_t\sigma(x,\dot{x}) - \phi - K_p x - K_d\dot{x} - \tilde{\xi} + \phi(0,0)\right] + \dot{x}^T K_p x + \dot{x}^T\phi \\
&+\alpha\dot{\tilde{\xi}}^T K_i^{-1}\tilde{\xi} + \dot{x}^T\tilde{\xi} + x^T\dot{\tilde{\xi}} + \alpha\dot{x}^T M\dot{x} + \alpha\dot{x}^T K_d x + tr\left(\tfrac{d}{dt}\widetilde{W}_t^T K_w^{-1}\widetilde{W}_t\right) \\
&+\alpha x^T\left[-C\dot{x} - \widetilde{W}_t\sigma(x,\dot{x}) - \phi - K_p x - K_d\dot{x} - \tilde{\xi} + \phi(0,0)\right] \\
&= \dot{x}^T\left[-C\dot{x} - \phi - K_p x - K_d\dot{x} - \tilde{\xi} + \phi(0,0)\right] + \dot{x}^T K_p x + \alpha\dot{\tilde{\xi}}^T K_i^{-1}\tilde{\xi} \\
&+\dot{x}^T\tilde{\xi} + x^T\dot{\tilde{\xi}} + \alpha\dot{x}^T M\dot{x} + \alpha x^T\left[-C\dot{x} - \phi - K_p x - K_d\dot{x} - \tilde{\xi} + \phi(0,0)\right] \\
&+\alpha x^T K_d\dot{x} + \dot{x}^T\phi - tr\left(\tfrac{d}{dt}\widetilde{W}_t^T K_w^{-1}(\dot{x} + \alpha x)^T\sigma(x,\dot{x})\right)\widetilde{W}_t
\end{aligned} \tag{4.72}$$

If the fuzzy is tuned using (4.68) then

$$\begin{aligned}
&\dot{V} = \dot{x}^T\left[-C\dot{x} - K_d\dot{x} + \phi(0,0)\right] + \alpha\dot{\tilde{\xi}}^T K_i^{-1}\tilde{\xi} + x^T\dot{\tilde{\xi}} \\
&+\alpha\dot{x}^T M\dot{x} + \alpha x^T\left[-C\dot{x} - K_p x - \tilde{\xi} + \phi(0,0) - \phi\right]
\end{aligned} \tag{4.73}$$

From (4.65)

$$\alpha x^T\left[\phi(0,0) - \phi\right] \leq \alpha k_\phi \|x\|^2$$

The rest part is similar with Proof of Theorem 4.3. ■

All the above stability proofs consider that $\Gamma_{n\times n} = I_n$. However in real applications, only few dampers will be utilized for the vibration control, which results in an under-actuated system. In this case, the location matrix Γ should be included along with the gain matrices. In this chapter, we consider only one damper which is installed on the second floor of the structure. For example, in the case of PID controller the control signal becomes,

$$\Gamma u = \begin{bmatrix} 0 & 0 \\ 0 & 1 \end{bmatrix} \left\{ - \begin{bmatrix} k_{p1} & 0 \\ 0 & k_{p2} \end{bmatrix} \begin{bmatrix} x_1 \\ x_2 \end{bmatrix} - \begin{bmatrix} k_{i1} & 0 \\ 0 & k_{i2} \end{bmatrix} \begin{bmatrix} \int_0^t x_1 d\tau \\ \int_0^t x_2 d\tau \end{bmatrix} - \begin{bmatrix} k_{d1} & 0 \\ 0 & k_{d2} \end{bmatrix} \begin{bmatrix} \dot{x}_1 \\ \dot{x}_2 \end{bmatrix} \right\} \tag{4.74}$$

$$\Gamma u = \begin{bmatrix} 0 \\ -k_{p2} x_2 - k_{i2} \int_0^t x_2 d\tau - k_{d2} \dot{x}_2 \end{bmatrix} \tag{4.75}$$

where the scalars k_{p2}, k_{i2}, and k_{d2} are the position, integral, and derivative gains, respectively. In this case, (4.44) becomes,

$$\begin{aligned} k_{p2} &\geq \tfrac{3}{2} \left[k_F + \lambda_M (C) \right] \\ k_{i2} &\leq \bar{\beta} \tfrac{\min\{k_{p2}\}}{\lambda_M(M)} \\ k_{d2} &\geq \bar{\beta} \left[1 + \tfrac{\lambda_M(C)}{\lambda_M(M)} \right] - \lambda_m(C) \end{aligned} \tag{4.76}$$

where $\bar{\beta} = \sqrt{\frac{\lambda_m(M) \min\{k_{p2}\}}{3}}$.

4.5 Experimental Results

To illustrate the theory analysis results, a two-story building prototype is constructed which is mounted on a shaking table, see Figure 4.4. The building structure is constructed of aluminum. The shaking table is actuated using the hydraulic control system (FEEDBACK EHS 160), which is used to generate earthquake signals. The AMD is a linear servo actuator (STB1108, Copley Controls Corp.), which is mounted on the second floor. The moving mass of the damper weights 5% (0.45 kg) of the total building mass. The linear servo mechanism is driven by a digital servo drive (Accelnet Micro Panel, Copley Controls Corp). ServoToGo II I/O board is used for the data acquisition purpose.

The proposed fuzzy PID control needs the structure position and velocity data. Three accelerometers (Summit Instruments 13203B) are used to measure the accelerations on the ground and each floor. The ground acceleration is then subtracted from the each floor accelerations to get the relative floor movement. The relative velocity and position data are then estimated using the numerical integrator proposed in Chapter 3.

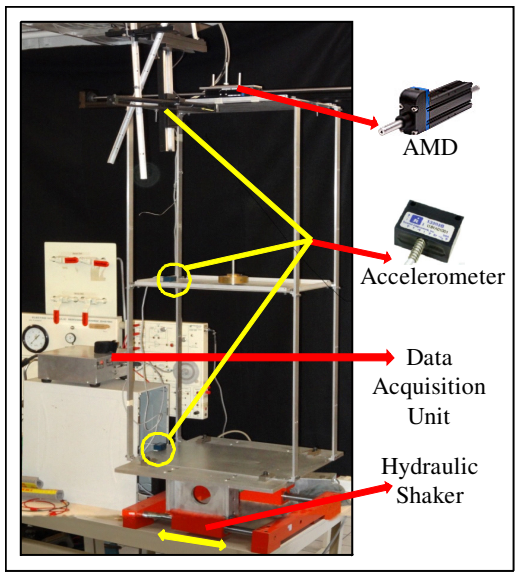

Figure 4.4: Two-story building prototype with the shaking table.

The control programs were operated in Windows XP with Matlab 6.5/Simulink. All the control actions were employed at a sampling frequency of 1.0 kHz. The control signal generated by the control algorithm was fed as voltage input to the amplifier. The current control loop is used to control the AMD operation. The amplifier converts its voltage input to a corresponding current output with a gain of 0.5. The AMD has a force constant of 6.26 N/ A or 3.13 N/ V. The masses of the structure prototype are $m_1 = 3.3\,\text{kg}$ and $m_2 = 6.1\,\text{kg}$, the damping coefficients are $c_1 = 2.5\,\text{N s/ m}$ and $c_2 = 1.4\,\text{N s/ m}$. Hence, $\lambda_M(M) = 6.1$, $\lambda_m(C) = 0.6$, and $\lambda_M(C) = 5.8$.

We compare our fuzzy PD/PID control with the standard PD/PID control and fuzzy control [43]. In order to perform a fair comparison, all the controllers except the fuzzy controller use the same proportional and derivative gains, and same integral gains in the case of PID controllers.

Now, we describe the procedure for selecting the gains for a stable operation. The theorems in this chapter give sufficient conditions for the minimal values of the proportional

and derivative gains and maximal values of the integral gains. Here the initial task is to select k_F, which is dominated by the external force F_e. In the experiment, the maximum force used to actuate the building prototype is below 300 N. Hence, we choose $k_F = 365$. Applying these values in Theorem 4.3 we get

$$\lambda_m(K_p) \geq 556,\ \lambda_M(K_i) \leq 3066,\ \lambda_m(K_d) \geq 65$$

Remark 4.2 *The PID tuning methods are different for the system with and without prior knowledge. If the system parameters are unknown, then auto-tuning techniques are employed to choose the gains either on-line or off-line. These techniques are broadly classified into direct and indirect methods [12]. In direct method, the closed-loop response of the system is observed and the controller gains are tuned directly based on the past experience and heuristic rules. In the case of indirect method, the structure parameters are identified first from the measured output, and based on these identified parameters the controller is then tuned to achieve the desired system dynamics. This chapter provides a tuning method that ensures a stable closed-loop performance. For that purpose, the structural parameters* $\lambda_M(M)$, $\lambda_m(C)$, $\lambda_M(C)$, *and* k_F, *are determined from the identified parameters*

The membership functions of the fuzzy controller in [43] are triangle functions. The position and velocity inputs to this fuzzy system are normalized, such that $x, \dot{x} \in (-1, 1)$. Several experiments showed that nine rules are sufficient to achieve a minimal regulation error.

In our fuzzy PID control, since we use adaptive law, the membership functions are Gaussian functions. Each floor position or velocity is converted into linguistic variables using three membership functions, hence $\widehat{W}^T$, $\sigma \in \Re^9$. We only use the position and velocity of the second floor, and one damper for the control operation, so $r, \widehat{F} \in \Re$. The position and velocity inputs to the adaptive fuzzy system are normalized, such that $x, \dot{x} \in (-1, 1)$. The adaptation rules (4.28) and (4.68) are chosen to be identical by selecting $\Lambda = \alpha$. From (4.52) we choose $\alpha = 6$.

In order to evaluate the performance, these controllers were implemented to control the vibration on the excited lab prototype. The control performance is evaluated in terms of their ability to reduce the relative displacement of each floor of the building. The proportional, derivative, and integral gains are further adjusted to obtain a higher attenuation. Finally, the PID controller gains are chosen as

$$k_p = 635,\ k_i = 3000,\ k_d = 65$$

and the PD controller gains are

$$k_p = 635,\ k_d = 65$$

Table 4.1 shows the mean squared error, $MSE = \frac{1}{N}\sum_{i=1}^{N} e_i^2$ of the displacement with proposed controllers, here N is the number of data samples and $e = \left(x^d - x\right) = -x$, where x is the position achieved using the controllers. The last row of the Table 4.1 gives the MSE of control signals of each controller $\left(\frac{1}{N}\sum_{i=1}^{N} u_i^2\right)$ with respect to the no control case. Figures 4.5–4.14 show the time response of the first and second floor displacements for both controlled and uncontrolled cases. The control algorithm outputs are shown in Figures 4.15–4.19.

Table 4.1: Comparison of vibration attenuation obtained using different controllers

Controller	**PD**	**PID**	**Fuzzy**	**PD+F**	**PD+F**	**No Control**
Floor-1 (x_1)	0.1669	0.1281	0.0589	0.0255	0.0246	1.0688
Floor-2 (x_2)	0.5141	0.3386	0.1434	0.0733	0.0615	3.3051
Control (u)	0.1232	0.0993	0.1124	0.1408	0.1320	0.0000

From Table 4.1 one can observe that the controllers effectively decrease the vibration. The controlled response using the PD controller is reduced significantly by providing a damping using the derivative gain. Figures 4.5 and 4.6 show the vibration attenuation achieved by adding an integral action to the above PD controller. The results demonstrate that the PID controller performs better than the PD controller. From Figures 4.7 and 4.8, it can be seen that the Fuzzy controller achieves more attenuation compared to the PD/PID control. Figures 4.9, 4.10, 4.13, and 4.14 illustrate that the structure response reduction can be

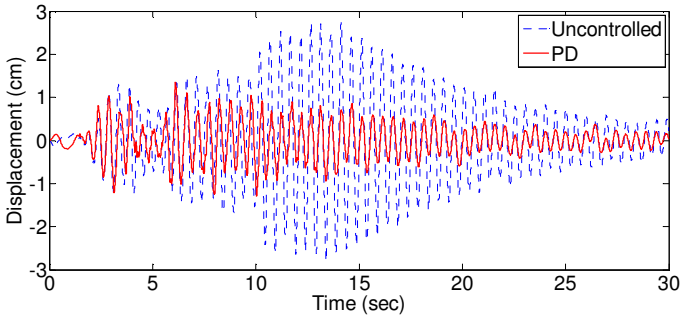

Figure 4.5: Uncontrolled and controlled displacements of the first floor using PD controller.

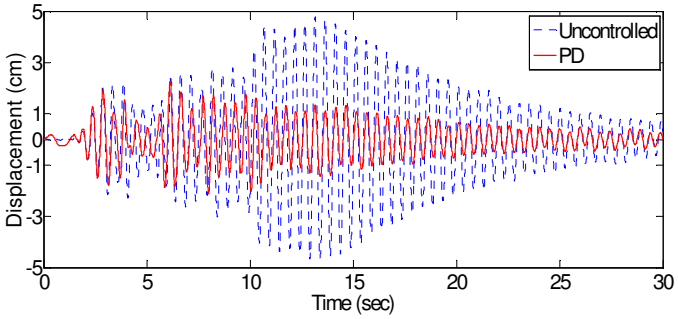

Figure 4.6: Uncontrolled and controlled displacements of the second floor using PD controller.

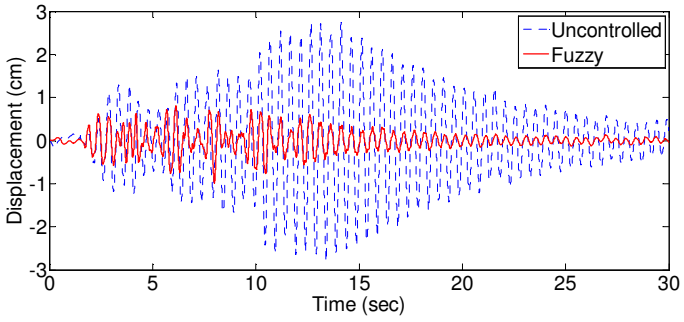

Figure 4.7: Uncontrolled and controlled displacements of the first floor using Fuzzy controller.

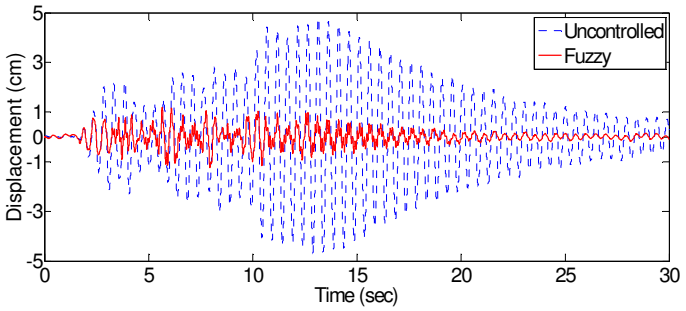

Figure 4.8: Uncontrolled and controlled displacements of the second floor using Fuzzy controller.

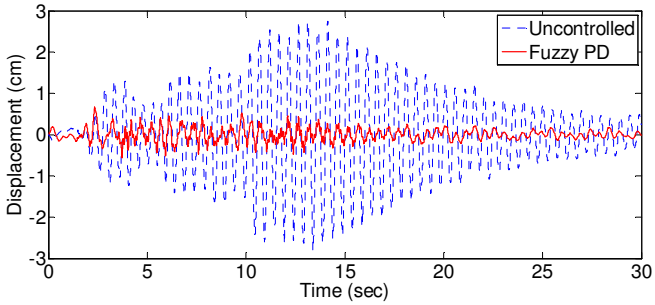

Figure 4.9: Uncontrolled and controlled displacements of the first floor using Fuzzy PD controller.

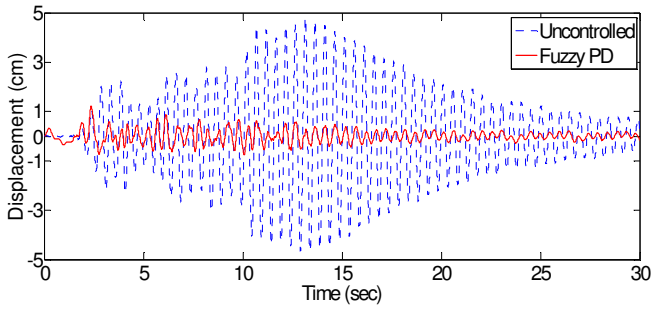

Figure 4.10: Uncontrolled and controlled displacements of the second floor using Fuzzy PD controller.

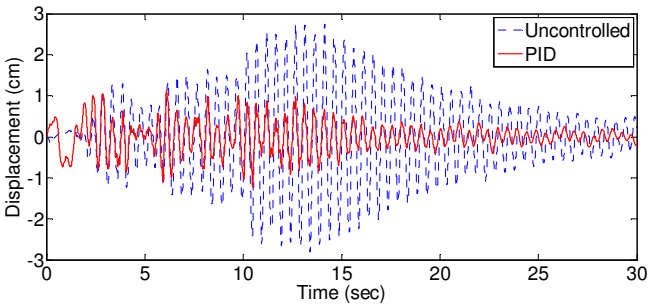

Figure 4.11: Uncontrolled and controlled displacements of the first floor using PID controller.

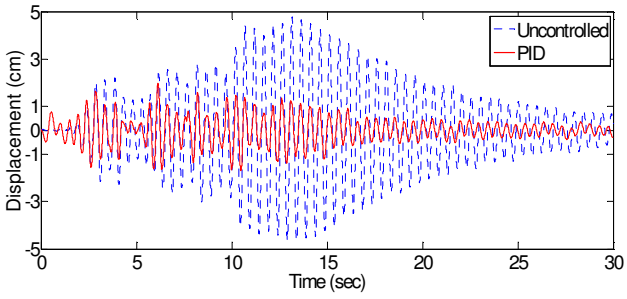

Figure 4.12: Uncontrolled and controlled displacements of the second floor using PID controller.

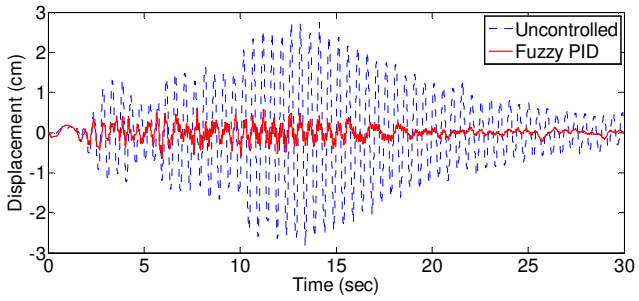

Figure 4.13: Uncontrolled and controlled displacements of the first floor using Fuzzy PID controller.

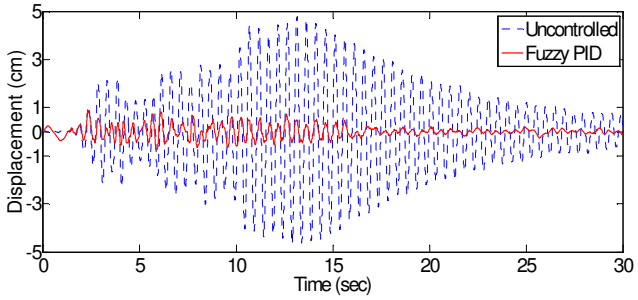

Figure 4.14: Uncontrolled and controlled displacements of the second floor using Fuzzy PID controller.

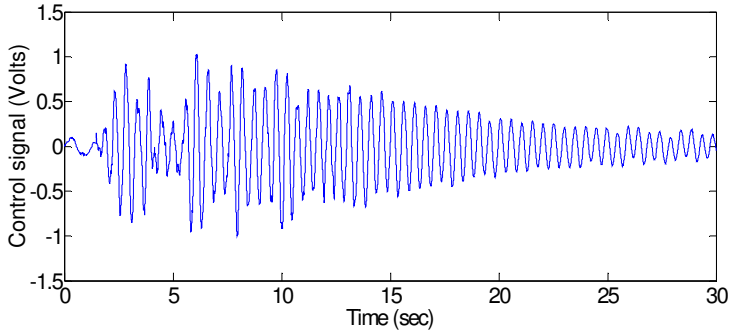

Figure 4.15: Control signal from PD controller.

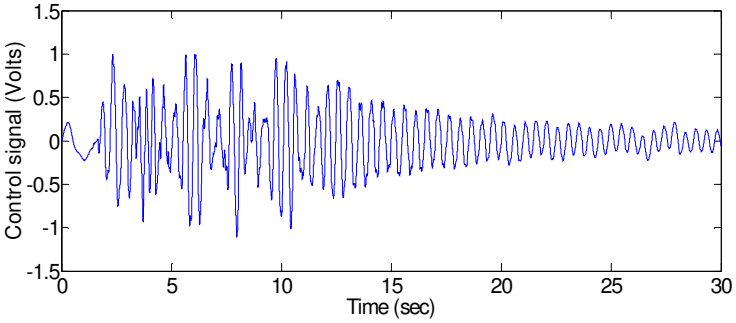

Figure 4.16: Control signal from Fuzzy controller.

maximized by the addition of fuzzy compensation to the standard PD/PID control. The performance improvement is based on the fact that this adaptive fuzzy algorithm estimates the control force and also compensate the nonlinear and uncertain forces. From Table 4.1 we can conclude that the fuzzy PID achieves the maximum attenuation.

The fuzzy weights adaptation of the fuzzy PD and fuzzy PID control are shown in Figures 4.20 and 4.21, respectively. In structural vibration control case, the weight matrix does not necessarily converge to a constant value. If there exists a position or a velocity error due to an excitation, then the weights keep changing, see (4.28) and (4.68). The adaptation of the fuzzy weights of the fuzzy PID control is less than fuzzy PD, due to the integral action.

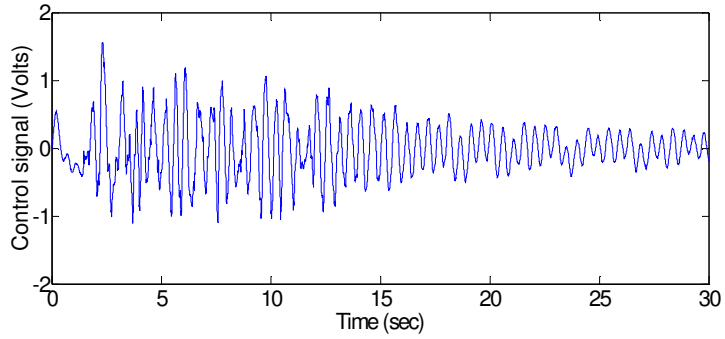

Figure 4.17: Control signal from Fuzzy PD controller.

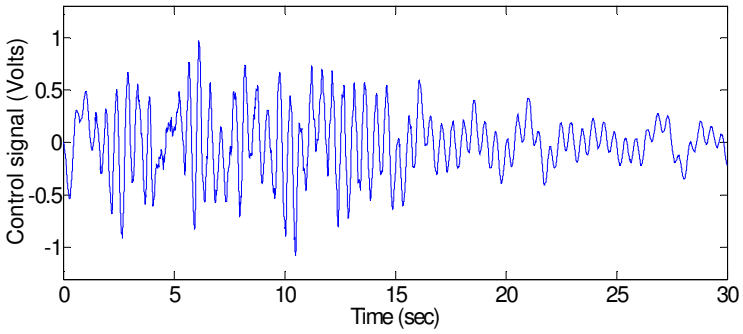

Figure 4.18: Control signal from PID controller.

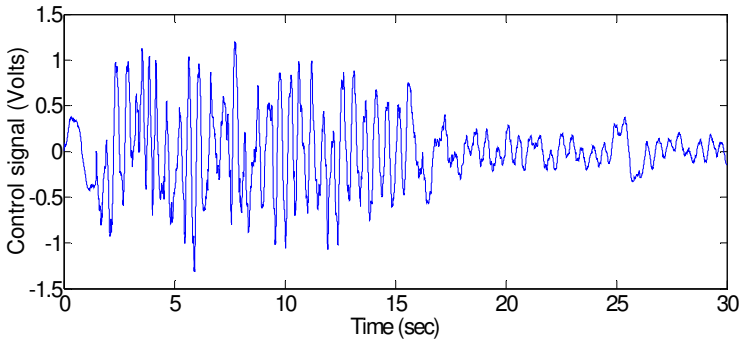

Figure 4.19: Control signal from Fuzzy PID controller.

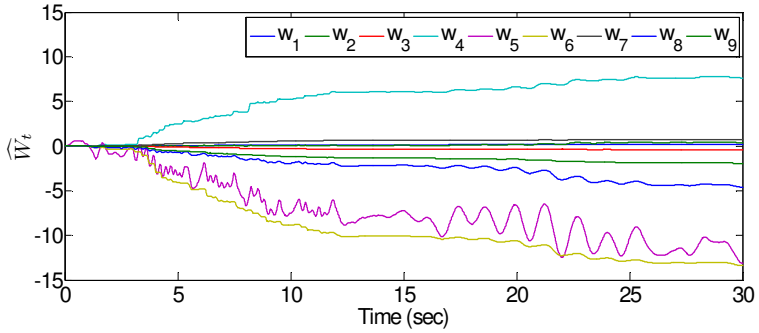

Figure 4.20: Adaptation of fuzzy weights in fuzzy PD control.

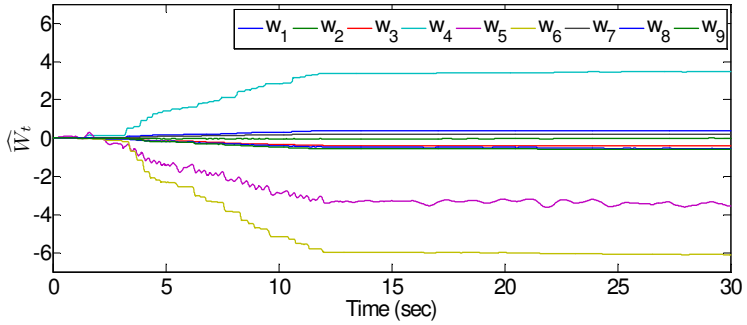

Figure 4.21: Adaptation of fuzzy weights in fuzzy PID control.

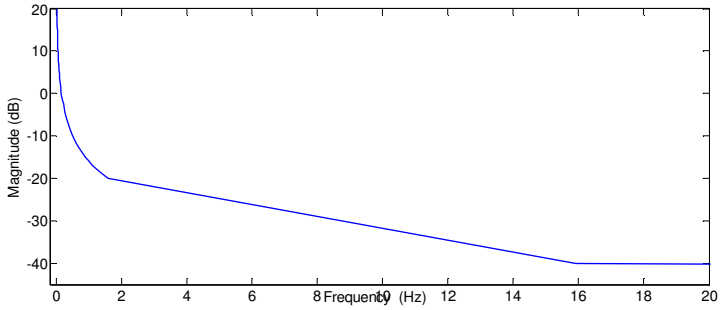

Figure 4.22: Bode magnitude plot of an ideal integrator.

Remark 4.3 *It is worth to note the frequency characteristics of an integrator. An ideal integrator acts like a low-pass filter. The bode magnitude plot of an ideal integrator is shown in Figure 4.22. At* 1.6 Hz *the integrator attenuates the input power by* 20 dB *and at* 16 Hz *it reaches to* 40 dB*. During earthquakes, the structure oscillates at its natural frequencies. If the natural frequency is very small then the integrator produces a larger output. The structure prototype we used for the experiments have natural frequencies* 2.1 Hz *and* 8.9 Hz*. Since these frequencies have an attenuation more than* 20 dB *a larger value can be used for* K_i*. On the other hand, if the building has a natural frequency less than* 1.6 Hz*, then the integral gain should be reduced accordingly. The error input to the integrator is the position data. From Figures 4.5–4.14 we can see that the position data for the most part takes successive positive and negative values. Hence, the integrator output for high-frequency input signal is small due to the rapid cancellation between these positive and negative values.*

Figure 4.23 shows the magnitude spectrum of control signals of the simple PID and fuzzy PID controllers. As the building structure is excited mainly in its natural frequency (2.1 Hz), the major control action occurs in this zone. In this region the fuzzy PID controller produces less control effort than the normal PID controller, but still achieves a better vibration attenuation. Additionally from Table 4.1 one can see that, even a small increase in the control action (due to the fuzzy compensation) results in a remarkable vibration attenuation. Some-

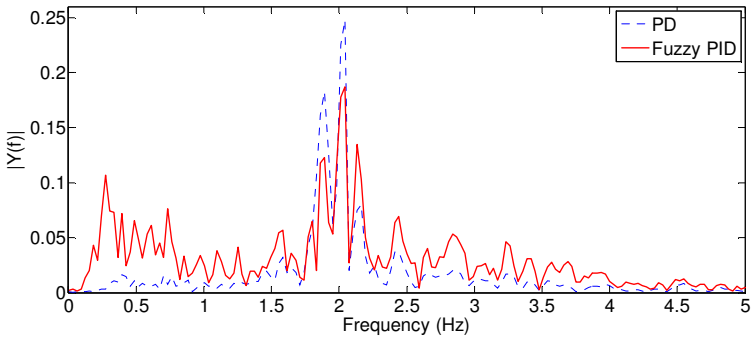

Figure 4.23: Fourier spectrum of control signals.

times, the integral control results in an actuator saturation. But as discussed in Remark 4.3, the output of the integrator is small in our case.

4.6 Summary

In this chapter, the model of building structures with an active vibration control has been analyzed. The theoretical contribution of this chapter is that the stability of the AMD-fuzzy PD/PID control for building structures has been proven. By using Lyapunov stability theory, sufficient conditions of stability are derived to tune the fuzzy and PD/PID gains. The above new approaches were successfully applied to a two-story building prototype. The experimental results show that even though the chosen gains are not optimal the controllers guarantee stable control performances.

Chapter 5

Fuzzy Sliding Mode Control of Building Structures Subjected to Wind-Induced Vibrations

5.1 Introduction

Active vibration control of building structures under wind and earthquake loadings is a popular field among civil and mechanical engineers. Different control devices and algorithms were proposed and implemented in the last few decades [46, 111]. One of the main challenges in the structural control design is the presence of uncertainties in the building structures, especially in parametric level. Robust control is a well established technique, which can deal with these uncertainties and disturbances present in the real systems like the building structures.

SMC is one of the most popular robust controllers, which is oftenly seen in the structural vibration control applications. A modal space SMC method is proposed in [2], where only the dominant frequency mode is considered in the design. Another SMC based on the modal analysis is presented in [9], which considers the first six modes. A decentralized system with SMC is presented in [79], where the reaching laws were derived, with and without considering

actuator saturations.

Although standard SMC is simple and robust, it does have some limitations. Due to the imperfection in the high-frequency discontinuous switching, the direct implementation of the SMC will result in chattering effect, which may cause damage to the mechanical components like the actuators. The switching gain is selected such that it can overcome the system uncertainties and disturbances. However, the proper gain selection is difficult in the presence of system uncertainty. Different modifications were brought into the standard SMC in the last few decades, which overcome many limitations of the SMC. Higher order sliding mode is one of the popular among them, which reduces chattering. But its design needs proper tuning of its gains, which requires the knowledge of the uncertainty bounds. In [114], different adaptation techniques were discussed, which are broadly classified into the gain adaptation (Sigma adaptation) and equivalent control (Dynamic adaptation) techniques. Since it is difficult to obtain building parameters, implementation of the equivalent control technique is challenging.

Intelligent control techniques like NN and FLC were also used to design SMC [135]. A NN based SMC for the active control of seismically excited building structures is proposed in [125]. Here the slope of the sliding surface is considered in the design, which moves in a stable region resulting in a moving sliding surface. To achieve a minimum performance index, this controller is optimized using a Genetic Algorithm (GA) during the training process. It is shown that a high performing controller is achieved by using the moving sliding surface. Another SMC based on Radial Basis Function (RBF) NN is reported in [66]. The chattering free SMC is obtained using a two-layered RBF-NN. The relative displacement of each floor is fed as the input to the NN and the switching gain is derived as the output.

Many research works were carried out in designing the SMC using fuzzy logic so called FSMC [10, 56, 116]. The SMC provides a stable and fast system, whereas the fuzzy logic provides the ability to handle a nonlinear system. The chattering problem is avoided in most of these FSMC systems. A FSMC based on GA is presented in [115], where the GA is used to find the optimal rules and membership functions for the fuzzy logic controller. Some other structural control strategies based on the non-chattering SMC were also reported

[1, 9, 42, 130].

The majority of the structural vibration control using SMC [1, 2, 10] uses equivalent control technique. The uncertainty in the building parameters will make them difficult during the implementation. In [42], a low-pass filter is used to estimate the equivalent control. But the filter parameters are difficult to tune and can add phase error to the closed-loop system [114]. SMC with gain adaptation have not yet been discussed in structural vibration control applications. Since the building structure response can be measured, gain adaptation will be a promising technique.

In this chapter, the fuzzy logic and gain adaptation technique were combined for an effective attenuation of the wind-induced vibrations in tall buildings. In order to avoid the chattering phenomenon with respect to the unknown building uncertainty bounds, the sliding mode structural control has been modified in two ways: 1) the sliding surface is approximated by using a fuzzy system; 2) the switching gain of SMC is adapted online. These modifications successfully overcome the problems of the other fuzzy/adaptive SMC, such as the necessity of the equivalent control and the knowledge of the upper bounds of the structure uncertainties. Moreover, the adaptation algorithm guarantees that the switching gain is not overestimated. Theoretically, it has been shown that the proposed controller guarantees a bounded system trajectory and the states can be driven to an arbitrarily small neighborhood of the sliding surface. An active vibration control system for a six-story building structure equipped with an AMD has been constructed for the experimental study. The controller performance was also verified under the seismic excitation. The experimental results were compared with the other controller results and the effectiveness of the proposed algorithms has been demonstrated.

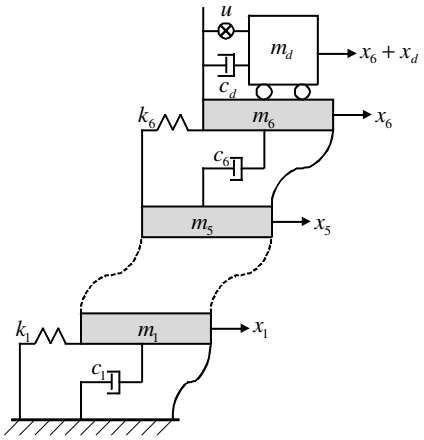

Figure 5.1: Building structure equipped with AMD.

5.2 Control of Wind-Induced Vibration of High-rise Buildings

If the wind-induced vibration exceeds more than $0.15\,\mathrm{m/s^2}$, humans may feel uncomfortable and the fragile items in the building may get damaged. In order to attenuate the vibrations caused by the external wind force, an AMD is installed on the top floor of the building structure, see Figure 5.1. Depending on the size of the building, the power requirements of these actuators may vary from kilowatts to several megawatts. So it is important to achieve a satisfying vibration attenuation by keeping the energy requirements as minimum as possible. Moreover, a larger input signal can result in a saturation of the actuator.

The structure model (4.2) can be rewritten in state-space form as

$$\begin{aligned} \dot{z}_1 &= z_2 \\ \dot{z}_2 &= f(z) + \widetilde{\Gamma} u \end{aligned} \tag{5.1}$$

where $z_1 = x$, $z_2 = \dot{x}$, $f(z) = -M^{-1}\left[Cz_2 + F_s(x, \dot{x}) + F_e\right]$, $\widetilde{\Gamma} = M^{-1}\Gamma$. The output can be defined as $y = Hz$, where H is a known matrix.

One of the most effective approach for dealing the model uncertainty is the robust control.

Equation (5.1) can be written as

$$\dot{z} = \tilde{A}z + \tilde{B}f_0(z) + \tilde{B}\Delta f + \tilde{B}\widetilde{\Gamma}u \tag{5.2}$$

where f_0 is the nominal structure dynamics, Δf is uncertainty part, $\tilde{A} = \begin{bmatrix} 0 & I_n \\ 0 & 0 \end{bmatrix} \in \Re^{2n\times 2n}$, $\tilde{B} = [0, I_n]^T \in \Re^{2n\times n}$, $z = \left[z_1^T, z_2^T\right]^T \in \Re^{2n}$. We assume that the uncertainty, $\Delta f = f(z) - f_0(z)$ is bounded as

$$\|\Delta f\| \leq \bar{f}_d \tag{5.3}$$

If the parameters of $f(z)$ is completely unknown, then we assume that $f(z)$ is also bounded.

$$\|f(z)\| \leq \bar{f} \tag{5.4}$$

This assumption is practically reasonable, because in the absence of external forces the building structure is stable and the big external excitation forces are also bounded, $\|F_e\| \leq \bar{F}_e$.

5.2.1 Sliding mode control with fuzzy sliding surface

In recent years, increasing attention has been given to the systems with discontinuous control actions. By intelligent selection of control actions, the state trajectories of the system under control could be modified correspondingly to give the desired properties. The control design problem in such systems with discontinuous control actions (SMC) can be reduced to the convergence problem to a special surface in the corresponding phase space (sliding surface).

A general class of discontinuous control is defined by the following relationships.

$$u = -\eta P^{-1}\text{sign}(s) = \begin{cases} -\eta P^{-1} & \text{if} \quad s > 0 \\ 0 & \text{if} \quad s = 0 \\ \eta P^{-1} & \text{if} \quad s < 0 \end{cases}, \quad P = P^T > 0 \tag{5.5}$$

where $\eta > 0$ is the switching gain, s is the sliding surface and $\text{sign}(s) = [\text{sign}(s_1), \ldots, \text{sign}(s_{2n})]^T$. The sliding surface can be a function of the the regulation error $e = z - z^d$, where z^d is the

desired state. If we use $s = e$, then the objective of the SMC is to drive the regulation error to zero in the presence of disturbance. In active vibration control of building structures, the references are defined as $z^d = \left[\left(x^d\right)^T, \left(\dot{x}^d\right)^T\right]^T = 0$, then $s = \left[x^T, \dot{x}^T\right]^T \in \Re^{2n}$ and $\dot{s} = \dot{z}$.

Consider the positive definite quadratic forms

$$V_1 = s^T P \Phi^\dagger s, \quad \Phi = \tilde{B}\widetilde{\Gamma} \tag{5.6}$$

where $\Phi^\dagger = \left(\Phi^T\Phi\right)^{-1}\Phi$ is the pseudo-inverse matrix of Φ. Finding the time derivative of function (5.6) on the trajectory of system (5.2), we get

$$\dot{V}_1 = z^T\left(\tilde{A}^T P\Phi^\dagger + P\Phi^\dagger\tilde{A}\right)z + 2z^T P\Phi^\dagger\tilde{B}f + 2z^T P\Phi^\dagger\tilde{B}\widetilde{\Gamma}u \tag{5.7}$$

Since $\tilde{A}$ is a stable matrix, there exits $Q = Q^T > 0$, such that $\tilde{A}^T P\Phi^\dagger + P\Phi^\dagger\tilde{A} = -Q$. Using the property $\Phi^\dagger = \Phi^{-1}$, (5.4), and (5.5), we can get

$$\dot{V}_1 \leq -\|z\|_Q^2 + 2\bar{f}\left\|P\Phi^\dagger\tilde{B}\right\|\|z\| - 2z^T P\eta P^{-1}\text{sign}(z) \tag{5.8}$$

Now using the property $z^T\text{sign}(z) = \|z\|$ we can write

$$\begin{aligned}\dot{V}_1 &\leq -\|z\|_Q^2 + 2\bar{f}\left\|P\Phi^\dagger\tilde{B}\right\|\|z\| - 2\eta\|z\| \\ &= -\|z\|_Q^2 + 2\|z\|\left(\bar{f}\left\|P\Phi^\dagger\tilde{B}\right\| - \eta\right) \\ &\leq 2\|z\|\left(\bar{f}\left\|P\Phi^\dagger\tilde{B}\right\| - \eta\right)\end{aligned} \tag{5.9}$$

Obviously, if the gain of the sliding mode control satisfies the following condition

$$\eta \geq \bar{f}\left\|P\Phi^\dagger\tilde{B}\right\|$$

then $\dot{V}_1 \leq 0$. From [91] we know that $s = e$ will converge to zero.

Generally, the civil engineers design the structural parameters such that it can withstand a given load [14]. From this design one can have an approximation about the upper bound of the structural uncertainty. In the case of robust control such as the classic SMC, the gain is selected to assure a robust performance by considering the worst situation. Hence by choosing a sufficiently high gain η in (5.5), the effect of any parameter variations can be

made negligible. However, this may amplify the chattering effect, where the control signal switches in a high-frequency within a tight neighborhood of the sliding surface. In structural control, this is also caused by the unmodeled parasitic dynamics present in the system. This high-frequency switching can damage mechanical systems like the actuators. Although, the huge AMD with big time constant in the structural vibration control can be regarded as a second order low-pass filter and does not respond to high-frequency commands, the chattering control signal may damage the damper's motor mechanism.

Many strategies were proposed to reduce the chattering phenomenon. The boundary layer method approximates the sign function in (5.5) by using a saturation function.

$$u = -\eta \text{sat}(s) = \begin{cases} -\eta & \text{if} \quad s > \delta \\ \frac{s}{\delta}\eta & \text{if} \quad \delta \geq s \geq -\delta \\ \eta & \text{if} \quad s < -\delta \end{cases}, \quad \eta > 0 \tag{5.10}$$

where δ is a positive constant and 2δ is the thickness of the boundary layer. In general, the bigger the boundary layer thickness, the smoother the control signal, and the bigger the residual set to which s will converge. The boundary layer method smooths the control signal with a loss of control accuracy.

In this chapter, we use a fuzzy system to smooth the sliding surface s. We use the following three fuzzy rules.

$$\begin{array}{llll} \text{R}^1\text{: IF } s \text{ is} & \text{“Positive” } P & \text{THEN } u \text{ is} & \text{“Negative” } -\eta \\ \text{R}^2\text{: IF } s \text{ is} & \text{“Zero” } Z & \text{THEN } u \text{ is} & \text{“Zero” } Z \\ \text{R}^3\text{: IF } s \text{ is} & \text{“Negative” } N & \text{THEN } u \text{ is} & \text{“Positive” } \eta \end{array}$$

The choice of membership functions decides how well a fuzzy system approximate a function. Here the goal is to select the membership functions such that it can approximated the sign function with a smooth switching near the zero vicinity, see Figure 5.2. The membership function of the input linguistic variable s is defined as μ_A and the membership function of the output linguistic variable u is defined as μ_B. It is straightforward to verify that the membership functions shown in Figure 5.3 can produce an output surface similar to Figure 5.2.

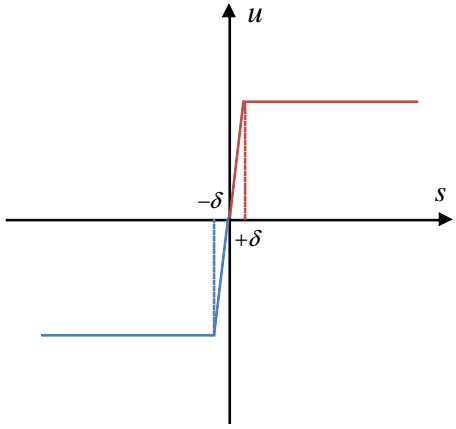

Figure 5.2: FSMC switching.

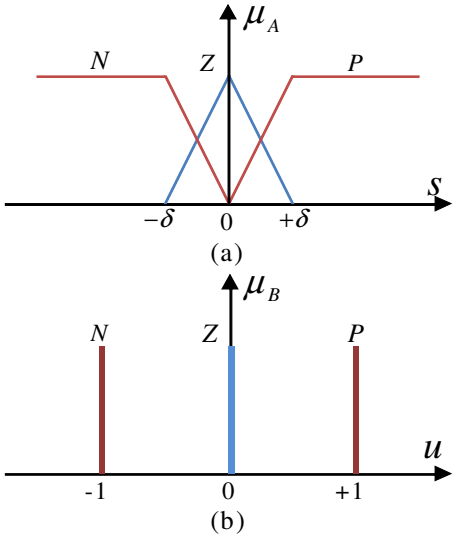

Figure 5.3: Membership functions: (a) input set (b) output set.

By using product inference, center-average, and singleton fuzzifier, the output of the fuzzy logic system can be expressed as

$$u = \eta \frac{w_1 \mu_{A_P}(s) + w_2 \mu_{A_Z}(s) + w_3 \mu_{A_N}(s)}{\mu_{A_P}(s) + \mu_{A_Z}(s) + \mu_{A_N}(s)} \tag{5.11}$$

where μ_{A_P}, μ_{A_Z}, and μ_{A_N} are the membership functions of "Positive", "Zero", and "Negative" of the input s, w_i, $i = 1, 2, 3$, are the points at which $\mu_B = 1$. From Figure 5.3 (b) $w_1 = -1$, $w_2 = 0$, $w_3 = 1$, then (5.11) becomes

$$u = \frac{\mu_{A_N}(s) - \mu_{A_P}(s)}{\mu_{A_P}(s) + \mu_{A_Z}(s) + \mu_{A_N}(s)} \tag{5.12}$$

We can see that, when $s > \delta$, $\mu_{A_P}(s) = 1$, $\mu_{A_Z}(s) = 0$, $\mu_{A_N}(s) = 0$, then $u = -\eta$; when $s < -\delta$, $\mu_{A_P}(s) = 0$, $\mu_{A_Z}(s) = 0$, $\mu_{A_N}(s) = 1$, then $u = \eta$. Finally, the sliding mode control with fuzzy sliding surface is

$$u = \begin{cases} -\eta P^{-1} \operatorname{sign}(s) & \text{if} \quad \|s\| > \delta \\ \eta \frac{\mu_{A_N}(s) - \mu_{A_P}(s)}{\mu_{A_P}(s) + \mu_{A_Z}(s) + \mu_{A_N}(s)} & \text{if} \quad \|s\| \leq \delta \end{cases}, \quad \eta > 0 \tag{5.13}$$

The stability of the fuzzy sliding mode control (5.13) is proved by using the same Lyapunov function (5.6). By substituting the FSMC control (5.13) into (5.7), the stability can be concluded using the following two cases:

1) When $\|s\| > \delta$, $u = -\eta P^{-1} \text{sign}(s)$. It is the same as (5.9), if $\eta \geq \bar{f} \left\| P \Phi^{\dagger} \tilde{B} \right\|$, then $\dot{V}_1 \leq 0$, hence s decreases.

2) When $\|s\| \leq \delta$, $u = \eta \frac{\mu_{A_N}(s) - \mu_{A_P}(s)}{\mu_{A_P}(s) + \mu_{A_Z}(s) + \mu_{A_N}(s)}$. Then s is bounded in the residual set δ.

From 1) and 2), we know that s is bounded and the total time during which $\|s\| > \delta$ is finite. Let T_j denotes the time interval during which $\|s\| > \delta$. (a) If only finite times that s stay outside the circle of radius δ (and then reenter), s will eventually stay inside this circle. (b) If s leave the circle infinite times, since the total time s leave the circle is finite,

$$\sum_{j=1}^{\infty} T_j < \infty, \quad \lim_{j \to \infty} T_j = 0 \tag{5.14}$$

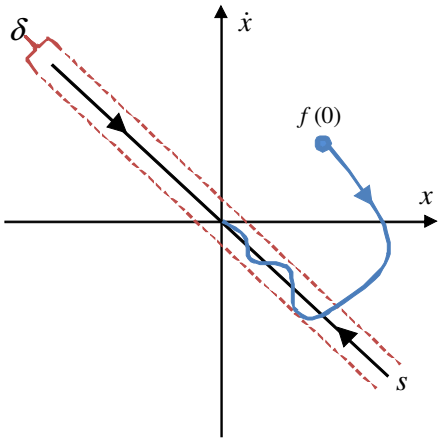

Figure 5.4: Concept of real sliding surface.

So s is bounded via an invariant set argument. Let $s(j)$ denotes the largest tracking error during the T_j interval. Then (5.14) and bounded $s(j)$ imply that

$$\lim_{j\to\infty} [-s(j) + \delta] = 0$$

So $s(j)$ will converge to δ. From these discussions, one can say that the implementation of (5.13) can only assures a "real sliding surface" [62], which guarantees that the state trajectories will slide within a domain (δ), see Figure 5.4.

5.2.2 Fuzzy sliding mode control with adaptive gain

Although the fuzzy sliding mode control (5.13) solves the chattering problem near the sliding surface, it requires a big gain $\eta \geq \bar{f} \left\| P\Phi^{\dagger}B \right\|$. This overestimation of the gain is not well advised. In the absence of system boundary knowledge, on-line gain adaptation can solve this problem. Here the switching gain η in (5.13) is replaced by the adaptive gain η_t, which uses the following adaptive law:

$$\dot{\eta}_t = \begin{cases} \bar{\eta} \left\| s \right\| \ \text{sign}\left(\left\| s \right\| - \delta \right) & \text{if} \quad \eta_t > \mu \\ 0 & \text{if} \quad \eta_t \leq \mu \end{cases}, \quad \bar{\eta}, \mu > 0 \tag{5.15}$$

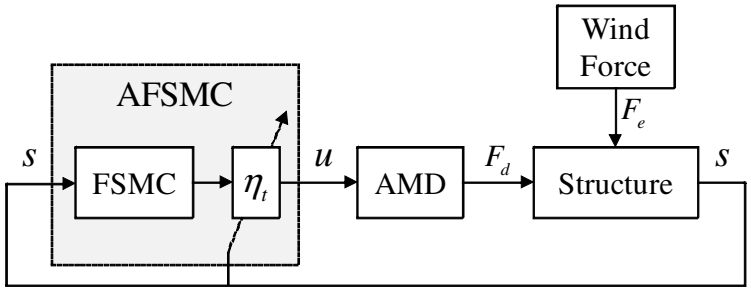

Figure 5.5: Block diagram of the AFSMC.

where μ is used to assure that the gain η_t is always positive and δ is the parameter defined in (5.13). When the state trajectory is outside the domain δ, the gain η_t will keep increasing until $\|s\| < \delta$; then the gain starts decreasing, once the state trajectory reaches inside the δ-domain. Thus the overestimation of the switching gain is avoided. Figure 5.5 shows the block diagram of the proposed fuzzy sliding mode control with adaptive gain.

We use the following Lyapunov-like candidate

$$V_2 = s^T P \Phi^\dagger s + \frac{1}{2\gamma}(\eta_t - \eta^*)^2 \tag{5.16}$$

where $\gamma, \eta^* > 0$. When the gain of the sliding mode is updated by a gradient algorithm as in (5.15), the gain is bounded [87]. We can assume that the upper bound of η_t is η^*.

The time derivative of (5.16) is

$$\dot{V}_2 = z^T \left(\tilde{A}^T P \Phi^\dagger + P \Phi^\dagger \tilde{A} \right) z + 2 z^T P \Phi^\dagger \tilde{B} f + 2 z^T P \Phi^\dagger \tilde{B} \widetilde{\Gamma} u + \frac{1}{\gamma}(\eta_t - \eta^*)\dot{\eta}_t \tag{5.17}$$

Once again using (5.4), (5.5), and $z^T \text{sign}(z) = \|z\|$, we can write (5.17) as

$$\begin{aligned} \dot{V}_2 &\leq - \|z\|_Q^2 + 2\bar{f} \left\| P \Phi^\dagger \tilde{B} \right\| \|z\| - 2 z^T P \Phi^\dagger \tilde{B} \widetilde{\Gamma} \eta_t P^{-1} \text{sign}(z) + \tfrac{1}{\gamma}(\eta_t - \eta^*)\dot{\eta}_t \\ &= - \|z\|_Q^2 + 2 \|z\| \left(\bar{f} \left\| P \Phi^\dagger \tilde{B} \right\| - \eta_t \right) + \tfrac{1}{\gamma}(\eta_t - \eta^*)\dot{\eta}_t \end{aligned} \tag{5.18}$$

By using the adaptive law (5.15), (5.18) becomes

$$\begin{aligned}\dot{V}_2 &\leq -\|z\|_Q^2 + 2\|z\|\left(\bar{f}\left\|P\Phi^\dagger\tilde{B}\right\| - \eta_t\right) + \tfrac{1}{\gamma}(\eta_t - \eta^*)\bar{\eta}\|z\| \ \text{sign}(\|z\| - \delta) \\ &\leq 2\|z\|\left(\bar{f}\left\|P\Phi^\dagger\tilde{B}\right\| - \eta_t\right) + \tfrac{1}{\gamma}(\eta_t - \eta^*)\bar{\eta}\|z\| \ \text{sign}(\|z\| - \delta) \\ &= 2\|z\|\left(\bar{f}\left\|P\Phi^\dagger\tilde{B}\right\| - \eta^*\right) + 2(\eta_t - \eta^*)\left(-\|z\| + \tfrac{\bar{\eta}}{2\gamma}\|z\| \ \text{sign}(\|z\| - \delta)\right)\end{aligned} \tag{5.19}$$

The above expression can be rewritten as

$$\begin{aligned}&\dot{V}_2 \leq 2\|z\|\left(\bar{f}\left\|P\Phi^\dagger\tilde{B}\right\| - \eta^*\right) + 2(\eta_t - \eta^*)\left(-\|z\| + \tfrac{\bar{\eta}}{2\gamma}\|z\| \ \text{sign}(\|z\| - \delta)\right) \\ &-2|\eta_t - \eta^*| + 2|\eta_t - \eta^*|\end{aligned} \tag{5.20}$$

Since η^* is the upper bound of η_t, $(\eta_t - \eta^*) = -|\eta_t - \eta^*|$, then (5.20) is

$$\begin{aligned}&\dot{V}_2 \leq -2\|z\|\left(\eta^* - \bar{f}\left\|P\Phi^\dagger\tilde{B}\right\|\right) - 2|\eta_t - \eta^*| \\ &-2|\eta_t - \eta^*|\left(-\|z\| + \tfrac{\bar{\eta}}{2\gamma}\|z\| \ \text{sign}(\|z\| - \delta) - 1\right)\end{aligned} \tag{5.21}$$

Let's define

$$\begin{aligned}\beta_z &= 2\left\|P\Phi^\dagger\right\|^{\frac{1}{2}}\left(\eta^* - \bar{f}\left\|P\Phi^\dagger\tilde{B}\right\|\right) \\ \Psi &= 2|\eta_t - \eta^*|\left(-\|z\| + \tfrac{\bar{\eta}}{2\gamma}\|z\| \ \text{sign}(\|z\| - \delta) - 1\right)\end{aligned} \tag{5.22}$$

Then (5.21) can be written as

$$\begin{aligned}\dot{V}_2 &\leq -\left\|P\Phi^\dagger\right\|^{\frac{1}{2}}\beta_z\|z\| - 2|\eta_t - \eta^*| - \Psi \\ &= -\left\|P\Phi^\dagger\right\|^{\frac{1}{2}}\beta_z\|z\| - \tfrac{2\sqrt{2\gamma}|\eta_t - \eta^*|}{\sqrt{2\gamma}} - \Psi \\ &\leq -\min\left\{\beta_z, \sqrt{8\gamma}\right\}\left(\left\|P\Phi^\dagger\right\|^{\frac{1}{2}}\|z\| + \tfrac{|\eta_t - \eta^*|}{\sqrt{2\gamma}}\right) - \Psi\end{aligned} \tag{5.23}$$

Finally, we have

$$\dot{V}_2 \leq -\beta_v V_2^{\frac{1}{2}} - \Psi \tag{5.24}$$

where $\beta_v = \min\left\{\beta_z, \sqrt{8\gamma}\right\}$. The stability of the system depends on the term Ψ. It is obvious that $\dot{V}_2 \leq 0$ when $\Psi = 0$. We consider the following two cases:

1) $\|s\| = \|z\| > \delta$. If we select γ in (5.16) such that it satisfies

$$0 < \gamma < \frac{\bar{\eta}\delta}{2(\delta + 1)} \tag{5.25}$$

then $\Psi > 0$, (5.24) is

$$\dot{V}_2 \leq -\beta_v V_2^{\frac{1}{2}} \leq 0 \tag{5.26}$$

2) $\|s\| = \|z\| \leq \delta$. From the definition (5.22), $\Psi < 0$. If $|\Psi| > \left|\beta_v V_2^{\frac{1}{2}}\right|$, then $u = \eta_t \frac{\mu_{A_N}(s) - \mu_{A_P}(s)}{\mu_{A_P}(s) + \mu_{A_Z}(s) + \mu_{A_N}(s)}$, the state trajectory may go unstable, i.e. $\|z\|$ will increase until $\|z\| > \delta$, which satisfies the condition 1). Now, $\dot{V}_2 \leq 0$, hence $\|z\|$ will decrease and falls inside the δ-domain. If $|\Psi| \leq \left|\beta_v V_2^{\frac{1}{2}}\right|$, then $\dot{V}_2 \leq 0$ which is same as the condition 1).

When $\|s\| > \delta$, the controller requires time for s to return to the δ-domain. Until then, s will remain in another domain δ_l, where $\delta_l > \delta$. From (5.15) we can see that the rate of change of η_t can be increased by selecting a big $\bar{\eta}$. Increasing the gain $\bar{\eta}$ means that δ_l will decrease towards δ.

5.3 Experimental Results

The experimental setup is similar to that of Chapter 4 with the following changes.

1. Here a six-story building is used instead of the two-story building, see Figure 5.6. The accelerometer and damper is placed on the top floor.

2. The linear servo actuator STB1104 is used instead of STB1108, hence the mass (2% of building mass) and the force constant (5.42 N/ A) has been changed.

The objective of the structural control system is to reduce the relative motion between the floors. In the case of wind excitation, the ground acceleration in (2.2), $x_g = 0$. The proposed controller needs the structure position and velocity data. Two accelerometers (Summit Instruments 13203B) are used to measure the ground and the top floor accelerations. The ground acceleration is then subtracted from the top floor acceleration to get the relative floor movement. The velocity and position data are then estimated using the numerical integrator proposed in Chapter 3.

The proposed AFSMC performance is compared with the classic PID controller and normal SMC. All of these controllers are designed to work within the normal operation

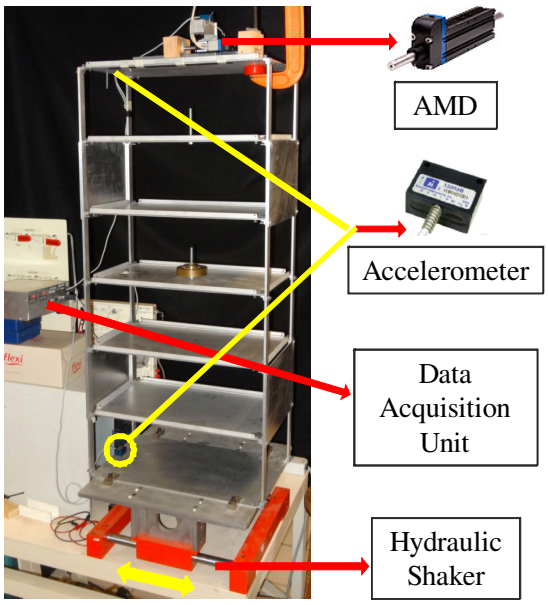

Figure 5.6: Six-story building prototype with the shaking table.

range of the AMD. The PID control given in (4.35) has been used here, with gains $k_p = 425$, $k_i = 50$, $k_d = 55$. The SMC has a fixed gain of $\eta = 0.8$. The AFSMC parameters are $\bar{\eta} = 50$, $\eta_{t=0} = 0.8$, and $\mu = 0.001$. These parameters are selected in such a way that a satisfactory chattering and vibration attenuation is achieved. In the case of structural vibration control, the parameter δ indicates the maximum acceptable vibration, which is $0.15\,\mathrm{m/s^2}$. In this experiment, the velocity and position are kept within an acceptable zone by choosing $\delta = 0.02$.

The control performance is evaluated in terms of their ability to reduce the relative displacement of each floor. The wind force signal shown in Figure 5.7 is used as the excitation signal for the building prototype. Figures 5.8–5.10 show the time responses of the sixth floor displacement for both the controlled and uncontrolled cases. The control algorithm outputs are shown in Figures 5.11–5.13. The gain adaptation of the AFSMC is shown in Figure 5.14.

From Figure 5.11, it can be noted that the PID controller generates peak control signals and moreover its response time is slower than that of the aggressive SMC. For normal SMC,

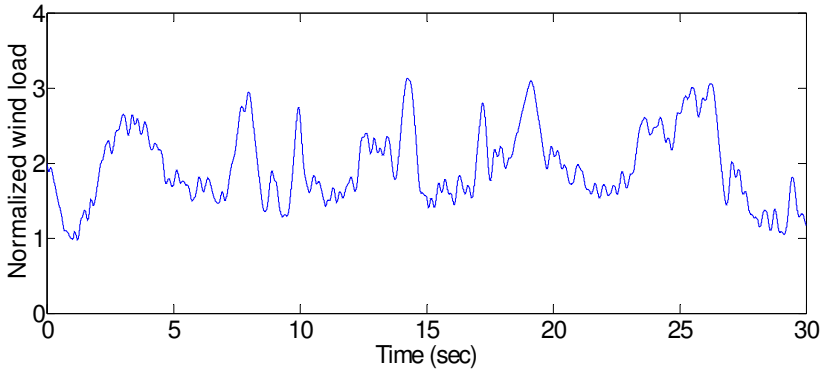

Figure 5.7: Wind excitation signal.

increasing η beyond 0.8 resulted in unwanted vibration in certain points, which is caused by the chattering effect. In order to avoid this problem, the switching gain is set to $\eta = 0.8$. Among these three controllers, AFSMC achieves the better vibration attenuation. The adaptive algorithm of AFSMC significantly reduces the switching gain when the vibration is within the acceptable range, see Figure 5.14. As a result, both the movement and power requirement of the AMD have been minimized, when compared to the non-adaptive case, see Figures 5.12 and 5.13.

It is worth verifying the control performance of the AFSMC for an earthquake excitation. Figures 5.15–5.18 show the time responses of the sixth floor displacement for the earthquake excitation. The control algorithm outputs are shown in Figures 5.19–5.22. A saturation of 1.5 V has been added to the PID controller output to avoid any excessive damper movement. Since the earthquake excitation frequency is higher than that of the wind, the AFSMC gain must adapt quickly. the gain adaptation speed is increased by selecting $\bar{\eta} = 65$. The gain adaptation of the AFSMC for the earthquake vibration attenuation is shown in Figure 5.23.

Figures 5.15–5.18 evidently indicates that the displacement has been reduced considerably by using the AFSMC. For normal SMC, increasing η beyond 0.8 resulted in unwanted vibration in certain points, which is caused by the chattering effect. For example, the classic SMC with $\eta = 1$ performs poor while x starts damping from a large to a small value. In

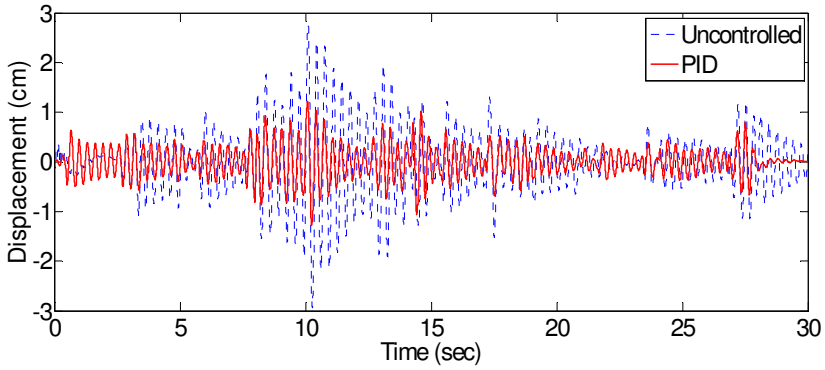

Figure 5.8: Uncontrolled and controlled displacements of the top floor using PID controller.

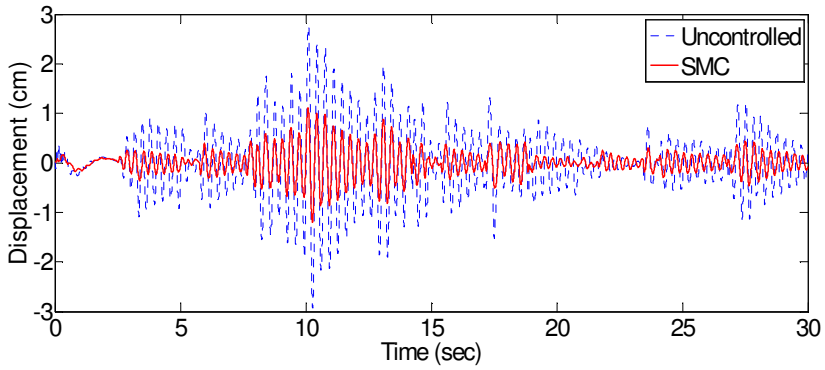

Figure 5.9: Uncontrolled and controlled displacements of the top floor using SMC.

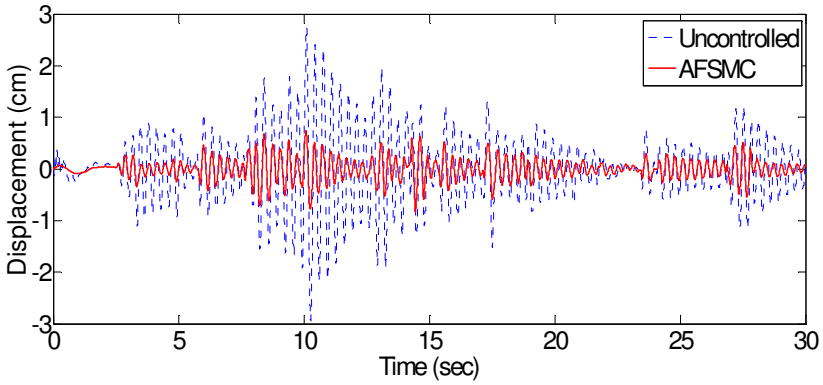

Figure 5.10: Uncontrolled and controlled displacements of the top floor using AFSMC.

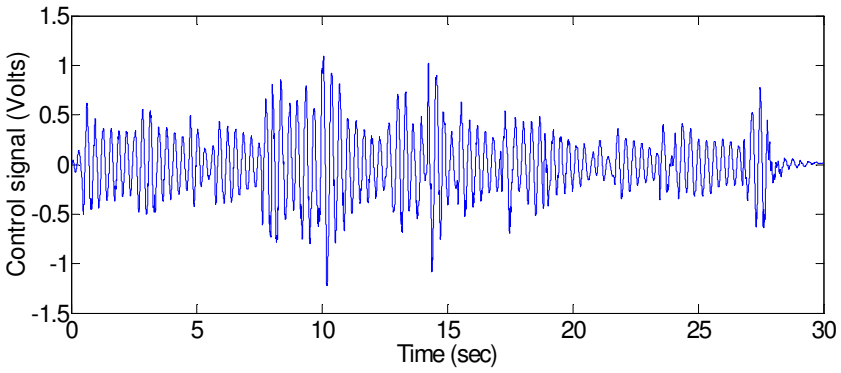

Figure 5.11: Control signal from PID controller.

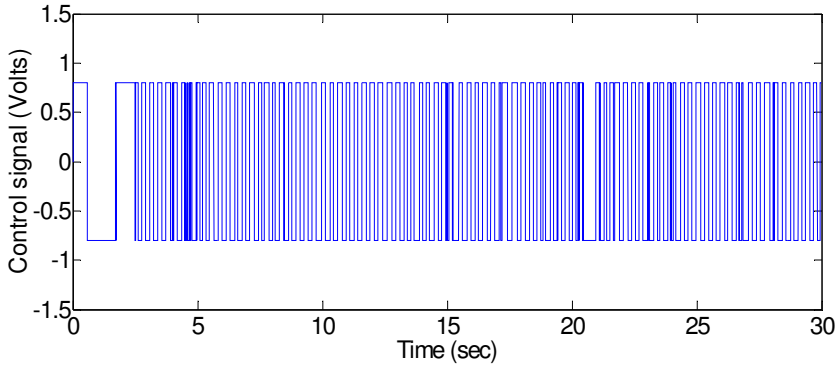

Figure 5.12: Control signal from SMC.

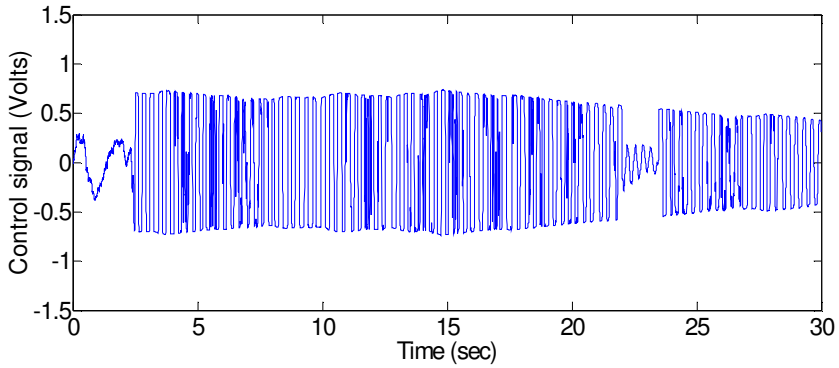

Figure 5.13: Control signal from AFSMC.

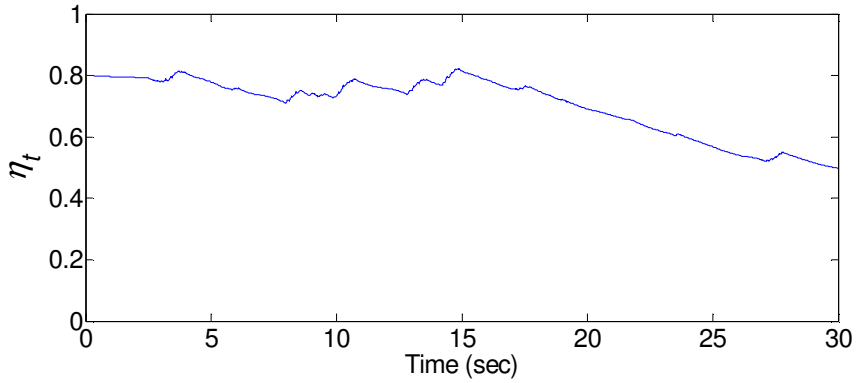

Figure 5.14: Switching gain adaptation.

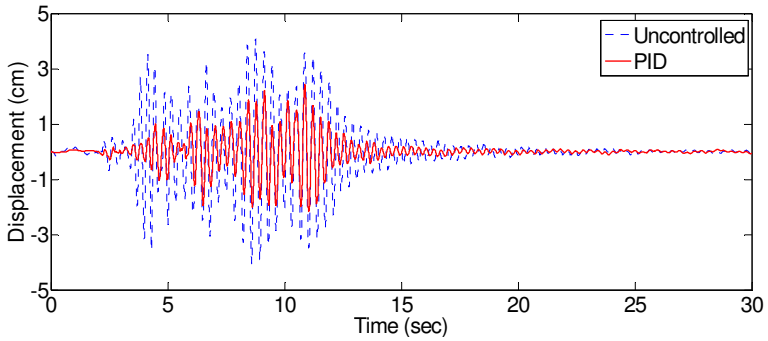

Figure 5.15: Uncontrolled and controlled displacements of the top floor using PID controller.

Figure 5.16, after 18 s we can notice an increase in the vibration level. This is due to the fact that SMC switches aggressively with a gain of η (Figure 5.20), even though the actual vibration is considerably small. This will cause the actuator to add excessive force on the structure. In order to avoid this problem, the switching gain is set to $\eta = 0.8$. Whereas Figure 5.18 proves that the gain of the AFSMC adapts in a suitable way, such that the control action is improved near the sliding surface.

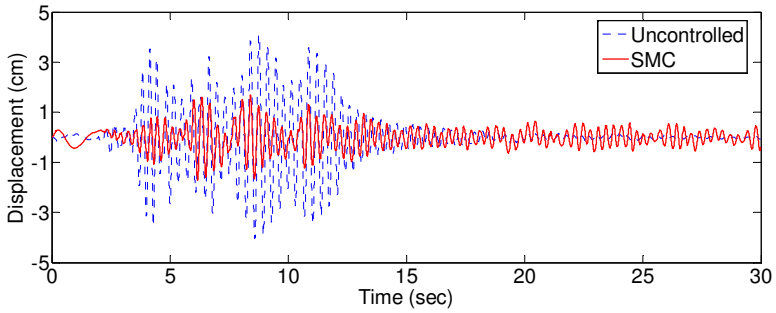

Figure 5.16: Uncontrolled and controlled displacements of the top floor using SMC with $\eta = 1$.

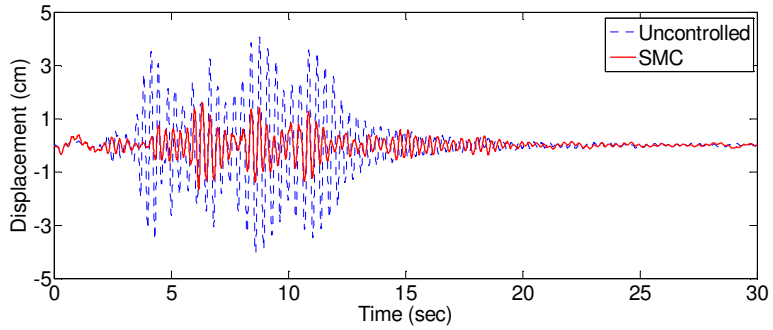

Figure 5.17: Uncontrolled and controlled displacements of the top floor using SMC with $\eta = 0.8$.

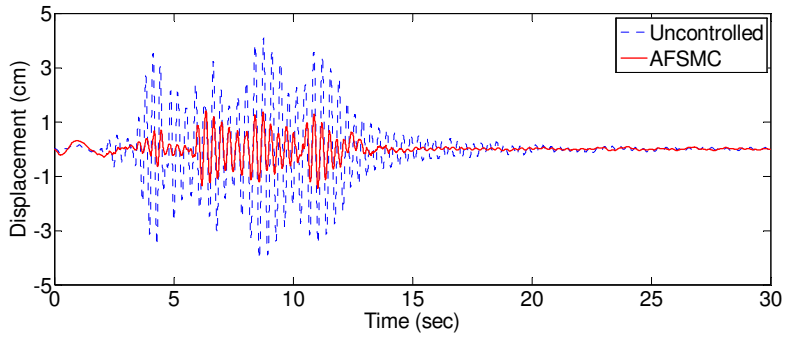

Figure 5.18: Uncontrolled and controlled displacements of the top floor using AFSMC.

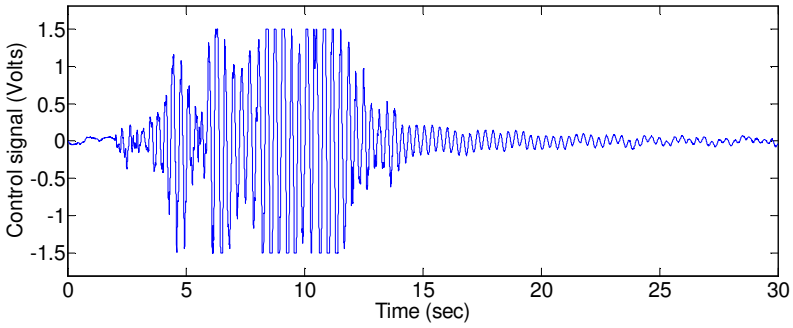

Figure 5.19: Control signal from PID controller.

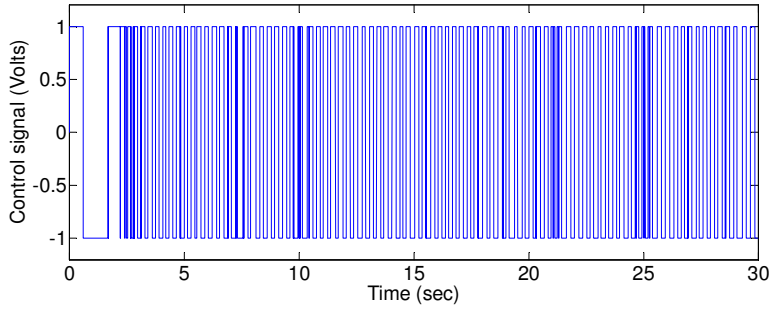

Figure 5.20: Control signal from SMC with $\eta = 1$.

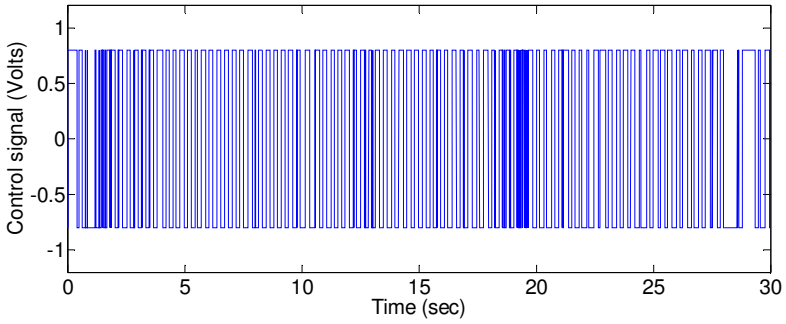

Figure 5.21: Control signal from SMC with $\eta = 0.8$.

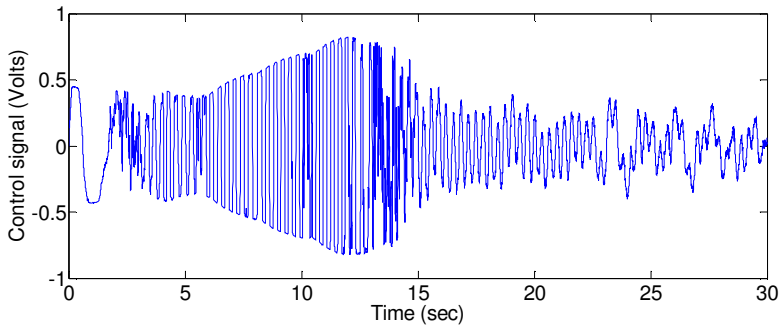

Figure 5.22: Control signal from AFSMC.

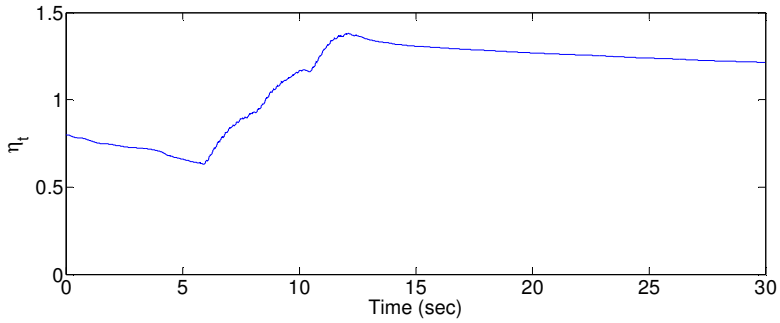

Figure 5.23: Switching gain adaptation.

5.4 Summary

In this chapter, adaptive and intelligent control techniques are combined to overcome the structural uncertainties, nonlinearities, and disturbance effects. A FSMC has been derived by fuzzyfying the conventional discontinuous switching function to offer a smooth operation near the sliding surface. Selection of the switching gain is crucial in the SMC design, which has been updated on-line. The proposed AFSMC stability is established using Lyapunov stability theory. Designed controllers have been tested on a lab prototype under both wind and earthquake excitations. The experimental results obtained using AFSMC have been compared with the results of the conventional PID controller and SMC and the performance has been found to be satisfactory, even in the presence of complete parametric uncertainty.

Chapter 6

Conclusions

There has been a large amount of increased research in structural vibration control in the past few decades. A number of control algorithms and devices have been applied to the structural control applications. Linear controllers were found to be simple and effective. More advanced controllers have improved the performance and robustness. Even though this field is well developed, there is still room for further research.

In this thesis, an active vibration control system for building structures was developed. The system uses accelerometers for measuring the building floor acceleration. But the accelerometer output signal is polluted with DC offset and other low-frequency noise signals. Direct integration of this signal will result in an inaccurate velocity and position estimation. A numerical integrator was developed, which has different filtering stages to attenuate the noise present in the measured acceleration signal. Experiments showed that the proposed integrator estimates the position and velocity with a good accuracy.

Two different control algorithms were developed for the structure vibration attenuation. In the first case, both the classic PID and fuzzy logic control techniques were used. The PID is used to generate the control signal to attenuate the vibration and the fuzzy logic is used to compensate the uncertain nonlinear effects present in the system. The PID gains are selected such that the system is stable in Lyapunov sense. An adaptive technique was developed for tuning the fuzzy weights to minimize the regulation error. This controller

shows very good vibration attenuation capability. However, its design needs some level of system knowledge. As a result another controller has been proposed, which can work with a parametrically uncertain system. Here the popular sliding mode controller has been used. The switching gain of the controller was tuned adaptively, without overestimating it. The discontinues switching function was fuzzified to assure a smooth operation near the sliding surface. The stability of both controllers were proved using Lyapunov stability theorem.

The proposed algorithms were experimentally verified in a lab prototype. The numerical integrator was used to estimate the velocity and position for the controller. Initially, the adaptive Fuzzy PD/PID controllers under seismic excitation were tested. The AFSMC was used to attenuate the wind induced vibrations in tall buildings. An AMD has been used to generate the force required to nullify the effects caused by the external excitations. The results of the experiments show that both the controllers can attenuate the vibrations considerably well. Moreover, the controllers, especially the AFSMC, can function with nonlinear and uncertain systems like the real building structures.

Bibliography

[1] R. Adhikari, H. Yamaguchi "Sliding mode control of buildings with ATMD", *Earthquake Engineering and Structural Dynamics*, Vol. 26, pp. 409-422, 1997.

[2] R. Adhikari, H. Yamaguchi, T. Yamazaki "Modal space sliding-mode control of structures", *Earthquake Engineering and Structural Dynamics*, Vol. 27, pp. 1303-1314, 1998.

[3] A.K. Agrawal, Y. Fujino, B.K. Bhartia "Instability due to time delay and its compensation in active control of structures", *Earthquake Engineering and Structural Dynamics*, Vol. 22, pp. 211-224, 1993.

[4] A.K. Agrawal, J.N. Yang "Effect of fixed time delay on stability and performance of actively controlled civil engineering structures", *Earthquake Engineering and Structural Dynamics*, Vol. 26, pp. 1169-1185, 1997.

[5] A.K. Agrawal, J.N. Yang "Compensation of time-delay for control of civil engineering structures", *Earthquake Engineering and Structural Dynamics*, Vol. 29, pp. 37-62, 2000.

[6] A. Alavinasab, H. Moharrami "Active control of structures using energy-based LQR method", *Computer-Aided Civil and Infrastructure Engineering,* Vol. 21, pp. 605-611, 2006.

[7] M. Aldawod, F. Naghdy, B. Samali, K.C.S. Kwok "Active control of wind excited structures using fuzzy logic", *IEEE International Fuzzy Systems Conference Proceedings*, pp. 72-77,1999.

[8] S.F. Ali, A. Ramaswamy "Optimal fuzzy logic control for MDOF structural systems using evolutionary algorithms", *Engineering Applications of Artificial Intelligence*, Vol. 22, pp. 407-419, 2009.

[9] M. Allen, F.B. Zazzera, R. Scattolini "Sliding mode control of a large flexible space structure", *Control Engineering Practice*, Vol. 8, pp. 861-871, 2000.

[10] H. Alli, O. Yakut "Fuzzy sliding-mode control of structures", *Engineering Structures*, Vol. 27, pp. 277-284, 2005.

[11] F. Amini, M.R. Tavassoli "Optimal structural active control force, number and placement of controllers", *Engineering Structures*, Vol. 27, pp. 1306-1316, 2005.

[12] K.J. Åström, T. Hägglund, C.C. Hang, W.K. Ho "Automatic tuning and adaptation for PID controllers-a survey", *Control Engineering Practice,* Vol. 1, pp. 699-714, 1993.

[13] K.J. Åström, T. Hagglund, "Revisiting the Ziegler–Nichols step response method for PID control", *Journal of Process Control,* Vol. 14, pp. 635-650, 2004.

[14] J.M. Angeles, L. Alvarez, "3D identification of buildings seismically excited", *Proceedings of the 2005 IFAC World Congress,* Prage, Czech Republic, 2005.

[15] T. Balendra, C.M. Wang, N. Yan "Control of wind-excited towers by active tuned liquid column damper", *Engineering Structures*, Vol. 23, pp. 1054-1067, 2001.

[16] D.M. Boore "Analog-to-digital conversion as a source of drifts in displacements derived from digital recordings of ground acceleration", *Bulletin of the Seismological Society of America*, Vol. 93, pp. 2017-2024, 2003.

[17] M. Brokate, A. Visintin "Properties of the Preisach model for hysteresis", *IJ. Reine und Angewandte Math,* Vol. 402, pp. 1-40, 1989.

[18] C.M. Chang, B.F. Spencer, "Active base isolation of buildings subjected to seismic excitations", *Earthquake Engineering and Structural Dynamics*, Vol. 39, pp. 1493-1512, 2010.

[19] J.C.H. Chang, T.T. Soong "Structural control using active tuned mass damper", *Journal of Engineering Mechanics,* ASCE, Vol. 106, pp. 1091-1098, 1980.

[20] A.G. Chassiakos, S.F. Masri "Identification of structural systems by neural networks", *Mathematics and Computers in Simulation*, Vol. 40, pp. 637-656, 1996.

[21] C.W. Chen, W.L. Chiang, F.H. Hsiao, C.H. Tsai "H_∞ fuzzy control of structural systems using Takagi-Sugeno fuzzy model", *Proceedings of the IEEE International Conference on Mechatronics*, pp. 340-345, 2004.

[22] C.W. Chen "Modeling and control for nonlinear structural systems via a NN-based approach", *Expert Systems with Applications,* Vol. 36, pp. 4765-4772, 2009.

[23] F.Y. Cheng, H. Jiang, K. Lou, *Smart Structures: Innovative Systems for Seismic Response Control*, CRC Press, 2008.

[24] H.C. Cho, M.S. Fadali, M.S. Saiidi, K.S. Lee "Neural network active control of structures with earthquake excitation", *International Journal of Control, Automation and Systems*, Vol. 2, pp. 202-210, 2005.

[25] K.M. Choi, S.W. Cho, D.O. Kim, I.W. Lee "Active control for seismic response reduction using modal-fuzzy approach", *International Journal of Solids and Structures*, Vol. 42, pp. 4779-4794, 2005.

[26] A.K. Chopra, *Dynamics of Structures: Theory and application to Earthquake engineering*, Second Edition, Prentice Hall, 2001.

[27] L.O. Chua, S.C. Bass "A generalized hysteresis model", *IEEE Transaction of Circuit Theory*, Vol. 19, pp. 36-48, 1972.

[28] D. Das, T.K. Datta, A. Madan "Semiactive fuzzy control of the seismic response of building frames with MR dampers", *Earthquake Engineering and Structural Dynamics*, Vol. 41, pp. 99-118, 2012.

[29] T.K. Datta "A state-of-the-art review on active control of structures", *ISET Journal of Earthquake Technology*, Vol. 40, pp. 1-17, 2003.

[30] S.L. Djajakesukma, B. Samali, H. Nguyen "Study of a semi-active stiffness damper under various earthquake inputs", *Earthquake Engineering and Structural Dynamics*, Vol. 31, pp. 1757-1776, 2002.

[31] H. Du, N. Zhang "H_∞ control for buildings with time delay in control via linear matrix inequalities and genetic algorithms", *Engineering Structures*, Vol. 30, pp. 81-92, 2008.

[32] N.D. Duc, N.L. Vu, D.T. Tran, H.L. Bui "A study on the application of hedge algebras to active fuzzy control of a seism-excited structure", *Journal of Vibration and Control*, Vol., pp. 1-15, 2011.

[33] T.S. Edwards "Effects of aliasing on numerical integration", *Mechanical Systems and Signal Processing*, Vol. 21, pp. 165-176, 2007

[34] N.R. Fisco, H. Adeli "Smart structures: Part I- Active and semi-active control", *Scientia Iranica*, Vol. 18, pp. 275-284, 2011.

[35] N.R. Fisco, H. Adeli "Smart structures: part II- Hybrid control systems and control strategies", *Scientia Iranica*, Vol. 18, pp. 285-295, 2011.

[36] P.J. Fleming, R.C. Purshouse "Evolutionary algorithms in control systems engineering: a survey", *Control Engineering Practic*e, Vol. 10, pp. 1223-1241, 2002.

[37] A. Forrai, S. Hashimoto, H. Funato, K. Kamiyama "Structural control technology: system identification and control of flexible structures", *Computing and control engineering Journal*, Vol. 402, pp. 1-40, 2001.

[38] Freescale Semiconductor. (2007) "Accelerometer Terminology Guide", Available: http://cache.freescale.com/files/sensors/doc/support_info/ SENSORTERMSPG.pdf

[39] H.P. Gavin, R. Morales, K. Reilly "Drift-free integrators", *Review of Scientific Instruments*, Vol. 69, pp. 2171-2175, 1998.

[40] W. Gawronski "Actuator and sensor placement for structural testing and control", *Journal of Sound and Vibration*, Vol. 208, pp. 101-109, 1997.

[41] Z.Q. Gu, S.O. Oyadiji "Application of MR damper in structural control using ANFIS method", *Computers and Structures*, Vol. 86, pp. 427-436, 2008.

[42] R. Guclu "Sliding mode and PID control of a structural system against earthquake", *Mathematical and Computer Modelling*, Vol. 44, pp. 210-217, 2006.

[43] R. Guclu, H. Yazici "Vibration control of a structure with ATMD against earthquake using fuzzy logic controllers", *Journal of Sound and Vibration*, Vol. 318, pp. 36-49, 2008.

[44] M. Guney, E. Eskinat "Optimal actuator and sensor placement in flexible structures using closed-loop criteria", *Journal of Sound and Vibration*, Vol. 312, pp. 210-233, 2008.

[45] K. Hiramoto, H. Doki, G. Obinata "Optimal sensor/actuator placements for active vibration control using explicit solution of algebraic Riccati equation", *Journal of Sound and vibration*, Vol. 229, pp. 1057-1075, 2000.

[46] G.W. Housner, L.A. Bergman, T.K. Caughey, A.G. Chassiakos, R.O. Claus, S.F. Masri, R.E. Skelton, T.T. Soong, B.F. Spencer, J.T.P. Yao "Structural control: Past, present and future", *Journal of Engineering Mechanics*, Vol. 123, pp. 897-974, 1997.

[47] G.W. Housner, T.T. Soong, S.F. Masri "Second generation of active structural control in civil engineering", *Computer-Aided Civil and Infrastructure Engineering*, Vol. 11, pp. 289-296, 1996.

[48] D. Hrovat, P. Barak, M. Rabins "Semi-active versus passive or active tuned mass dampers for structural control", *Journal of Engineering Mechanics*, Vol. 109, pp. 691-705, 1983.

[49] S.L. Hung, C.S. Huang, C.M. Wen, Y.C. Hsu "Nonparametric identification of a building structure from experimental data using wavelet neural network", *Computer-Aided Civil and Infrastructure Engineering*, Vol. 18, pp. 356-368, 2003.

[50] F. Ikhouane, V. Mañosa, J. Rodellar "Dynamic properties of the hysteretic Bouc-Wen model", *Systems & Control Letters,* Vol. 56, pp. 197-205, 2007.

[51] H. Imai, C.B. Yun, O. Maruyama, M. Shinozuka "Fundamentals of system identification in structural dynamics", *Probabilistic Engineering Mechanics,* Vol. 4, pp. 162-173, 1989.

[52] M.D. Iuliis, C. Faella "Effectiveness analysis of a semiactive base isolation strategy using information from an early-warning network", *Engineering Structures*, Vol. 52, pp. 518-535, 2013.

[53] B. Jiang, X. Wei, Y. Guo "Linear quadratic optimal control in active control of structural vibration systems", *Control and Decision Conference*, 2010 Chinese, Vol. 98, pp. 3546-3551, 2010.

[54] R. Kelly "A tuning procedure for stable PID control of robot manipulators", *Robotica*, Vol. 13, pp. 141-148, 1995.

[55] G. Kerschen, K. Worden, A.F. Vakakis, J.C. Golinva "Past, present and future of nonlinear system identification in structural dynamics", *Mechanical Systems and Signal Processing*, Vol. 20, pp. 505-592, 2006.

[56] S.B. Kim, C.B. Yun "Sliding mode fuzzy control: Theory and verification on a benchmark structure", *Earthquake Engineering and Structural Dynamics*, Vol. 29, pp. 1587-1608, 2000.

[57] D.H. Kim, D. Kimb, S. Chang, H.Y. Jung "Active control strategy of structures based on lattice type probabilistic neural network", *Probabilistic Engineering Mechanics*, Vol. 23, pp. 45-50, 2008.

[58] D.H. Kim "Neuro-control of fixed offshore structures under earthquake", *Engineering Structures*, Vol. 31, pp. 517-522, 2009.

[59] S. Korkmaz "A review of active structural control: challenges for engineering informatics", *Computers and Structures*, Vol. 89, pp. 2113-2132, 2011.

[60] M.A. Krasnoselskii, A.V. Pokrovskii, *Systems with Hysteresis*, New York: Springer-Verlag, 1989.

[61] K.C.S. Kwok, B. Samali "Performance of tuned mass dampers under wind loads", *Engineering Structures*, Vol. 17, pp. 655-667, 1995.

[62] A. Levant, "Sliding order and sliding accuracy in sliding mode control", *International Journal of Control*, Vol. 58, pp. 1247-1263, 1993.

[63] F.L. Lewis, D.M. Dawson, C.T. Abdallah, *Robot Manipulator Control: Theory and Practice,* Second Edition, Marcel Dekker, Inc, 2004.

[64] L.J. Li "MRF absorber damping control for building structural vibration response by means of genetic optimum algorithm", *Advanced Materials Research*, Vol. 219-220, pp. 1133-1137, 2011.

[65] Q.S. Li, D.K. Liu, J.Q. Fang, C.M. Tam "Multi-level optimal design of buildings with active control under winds using genetic algorithms", *Journal of Wind Engineering and Industrial Aerodynamics*, Vol. 86, pp. 65-86, 2000.

[66] Z. Li, Z. Deng, Z. Gu "New sliding mode control of building structure using RBF neural networks", *Chinese Control and Decision Conference*, pp. 2820-2825, 2010.

[67] Z. Liang, G.C. Lee, G.F. Dargush, J. Song, *Structural Damping: Applications in Seismic Response Modification*, CRC Press, 2011.

[68] A. Link, H.J. von Martens "Accelerometer identification using shock excitation", *Measurement*, Vol. 35, pp. 191-199, 2004

[69] D.K. Liu, Y.L. Yang, Q.S. Li "Optimum positioning of actuators in tall buildings using genetic algorithm", *Computers and Structures*, Vol. 81, pp. 2823-2827, 2003.

[70] J. Liu, K. Xia, C. Zhu "Structural vibration intelligent control based on magnetorheological damper", *International Conference on Computational Intelligence and Software Engineering*, pp. 1-4, 2009.

[71] W. Liu, Z. Hou, M.A. Demetriou "A computational scheme for the optimal sensor/actuator placement of flexible structures using spatial H_2 measures", *Mechanical Systems and Signal Processing*, Vol. 20, pp. 881-895, 2006.

[72] L. Ljung, *System Identification Theory for the Users,* Prentice-Hall, Inc, New Jersey, 1987.

[73] A. Madan "Vibration control of building structures using self-organizing and self-learning neural networks", *Journal of Sound and Vibration*, Vol. 287, pp. 759-784, 2005.

[74] E.H. Mamdani "Application of fuzzy algorithms for control of simple dynamic plant", *IEE Proceedings*, Vol. 121, pp. 1585-1588, 1974.

[75] D.P. Mandic, J.A. Chambers, *Recurrent neural networks for prediction: Learning algorithms, architectures and stability,* John Wiley and Sons, 2001.

[76] S F Masri, L.H Sheng, J P Caffrey, R L Nigbor, M Wahbeh, and A M Abdel-Ghaffar, "Application of a Web-enabled real-time structural health monitoring system for civil infrastructure systems", *Smart Materials and Structures*, Vol. 13, pp. 1269-1283, 2004.

[77] I.D. Mayergoyz, *Mathematical Models of Hysteresis*, New York: Springer-Verlag, 1991.

[78] A.C. Nerves, R. Krishnan "Active control strategies for tall civil structures", *Proceedings of IEEE, International Conference on Industrial Electronics, Control, and Instrumentation*, Vol. 2, pp. 962-967, 1995.

[79] S.M. Nezhad, F.R. Rofooei "Decentralized sliding mode control of multistory buildings", *The Structural Design of Tall and Special Buildings*, Vol. 16, pp. 181-204, 2007.

[80] O.I. Obe "Optimal actuators placements for the active control of flexible structures", *Journal of Mathematical Analysis and Applications*, Vol. 105, pp. 12-25, 1985.

[81] J. Pandya, Z. Akbay, M. Uras, H. Aktan "Experimental implementation of hybrid control", *Proceedings of Structures Congress XIV*, Chicago, pp. 1172-1179, 1996.

[82] K.S. Park, H.M. Koh "Preference-based optimum design of an integrated structural control system using genetic algorithms", *Advances in Engineering Software*, Vol. 35, pp. 85-94, 2004.

[83] K.S. Park, H.M. Koh, S.Y. Ok "Active control of earthquake excited structures using fuzzy supervisory technique", *Advances in Engineering Software*, Vol. 33, pp. 761-768, 2002.

[84] K.S. Park, H.M. Koh, C.W. Seo "Independent modal space fuzzy control of earthquake-excited structures", *Engineering Structures*, Vol. 26, pp. 279-289, 2004.

[85] W. Park, K.S. Park, H.M. Koh "Active control of large structures using a bilinear pole-shifting transform with H_∞ control method", *Engineering Structures*, Vol. 30, pp. 3336-3344, 2008.

[86] M.J. Perry, C.G. Koh, Y.S. Choo "Modified genetic algorithm strategy for structural identification", *Computers and Structures*, Vol. 84, pp. 529-540, 2006.

[87] F. Plestana, Y. Shtessel, V. Bregeaulta, A. Poznyak, "New methodologies for adaptive sliding mode control", *International Journal of Control*, Vol. 83, pp. 1907-1919, 2010.

[88] S. Pourzeynali, H.H. Lavasani, A.H. Modarayi "Active control of high rise building structures using fuzzy logic and genetic algorithms", *Engineering Structures,* Vol. 29, pp. 346-357, 2007.

[89] S.H. Razavi, A. Abolmaali, M. Ghassemieh "A weighted residual parabolic acceleration time integration method for problems in structural dynamics", *Journal of Computational Methods in Applied Mathematics*, Vol. 7, pp. 227-238, 2007.

[90] E. Reithmeier, G. Leitmann "Structural vibration control", *Journal of the Franklin Institute*, Vol. 338, pp. 203-223, 2001.

[91] J.Resendiz, W.Yu, L.Fridman, "Two-stage neural observer for mechanical systems", *IEEE Transactions on Circuits and Systems: Part II*, Vol.55, pp. 1076-1080, 2008.

[92] J.G.T. Ribeiro, J.T.P. de Castro, J.L.F. Freire "Using the FFT- DDI method to measure displacements with piezoelectric, resistive and ICP accelerometers", *Conference and Exposition on Structural Dynamics*, 2003.

[93] C. Roldán, F.J. Campa, O. Altuzarra, and E. Amezua "Automatic Identification of the Inertia and Friction of an Electromechanical Actuator", *New Advances in Mechanisms, Transmissions and Applications*, Springer Netherlands, Vol.17, pp. 409-416, 2014.

[94] P.M. Sain, M.K. Sain, B.F. Spencer "Models for hysteresis and application to structural control", *Proceedings of the American Control Conference,* pp. 16-20, 1997.

[95] R. Saragih "Designing active vibration control with minimum order for flexible structures", *IEEE International Conference on Control and Automation*, Vol., pp. 450-453, 2010.

[96] K. Seto "A structural control method of the vibration of flexible buildings in response to large earthquake and strong winds", *Proceedings of the 35th Conference on Decision and Control*, Kobe, Japan, 1996.

[97] D.A. Shook, P.N. Roschke, P.Y. Lin, C.H. Loh "GA-optimized fuzzy logic control of a large-scale building for seismic loads", *Engineering Structures*, Vol. 30, pp. 436-449, 2008.

[98] E.D. Sontag, Y. Wang "On characterizations of the input-to-state stability property", *Systems & Control Letters,* Vol. 24, pp. 351-359, 1995.

[99] T.T. Soong, *Active Structural Control: Theory and Practice*, Longman, New York, 1990.

[100] T.T. Soong, A.M. Reinhorn, Y.P. Wang, R.C. Lin "Full-scale implementation of active control-I: Design and simulation", *Journal of Structural Engineering*, Vol. 117, pp. 3516-3536, 1991.

[101] T.T. Soong, S.F. Masri, G.W. Housner "An overview of active structural control under seismic loads", *Earthquake Spectra*, Vol. 7, pp. 483-505, 1991.

[102] T.T. Soong, B.F. Spencer "Supplemental energy dissipation: state-of-the-art and state-of-the-practice", *Engineering Structures*, Vol. 24, pp. 243-259, 2002.

[103] B.F. Spencer, *Reliability of Randomly Excited Hysteretic Structures*, New York: Springer-Verlag, 1986.

[104] B.F. Spencer, M.K. Sain "Controlling buildings: A new frontier in feedback", *IEEE Control Systems Magazine on Emerging Technology*, Vol. 17, pp. 19-35, 1997.

[105] B.F. Spencer, S.J. Dyke, M.K. Sain, J.D. Carlson "Phenomenological model of a magnetorheological damper", *Journal of Engineering Mechanics, ASCE,* Vol. 123, pp. 230-238, 1997.

[106] B.F. Spencer, S. Nagarajaiah "State of the art of structural control", *Journal of Structural Engineering,* Vol. 129, pp. 845-856, 2003.

[107] M.D. Symans, M.C. Constantinou "Semi-active control systems for seismic protection of structures: a state-of-the-art review", *Engineering Structures*, Vol. 21, pp. 469-487, 1999.

[108] Y. Tang "Active control of SDF systems using artificial neural networks", *Computers and Structures*, Vol. 60, pp. 695-703, 1996.

[109] A. Tani, H. Kawamura, S. Ryu "Intelligent fuzzy optimal control of building structures", *Engineering Structures*, Vol. 20, pp. 184-192, 1998.

[110] T.L. Teng, C.P. Peng, C. Chuang "A study on the application of fuzzy theory to structural active control", *Computer Methods in Applied Mechanics and Engineering*, Vol. 189, pp. 439-448, 2000.

[111] S. Thenozhi, W. Yu "Advances in modeling and vibration control of building structures", *Annual Reviews in Control*, Vol. 37, No.2, pp. 346-364, 2013.

[112] Y.K. Thong, M.S. Woolfson, J.A. Crowe, B.R.H. Gill, D.A. Jones "Numerical double integration of acceleration measurements in noise", *Measurement,* Vol. 36, pp. 73-92, 2004.

[113] V.I. Utkin, *Sliding Modes in Control and Optimization*, Springer-Verlag, Berlin, 1990.

[114] V.I. Utkin, A.S. Poznyak "Adaptive sliding mode control", *Advances in Sliding Mode Control*, Springer Berlin Heidelberg, pp. 21-53, 2013.

[115] A.P. Wang, C.D. Lee "Fuzzy sliding mode control for a building structure based on genetic algorithms", *Earthquake Engineering and Structural Dynamics*, Vol. 31, pp. 881-895, 2002.

[116] A.P. Wang, Y.H. Lin "Vibration control of a tall building subjected to earthquake excitation", *Journal of Sound and Vibration*, Vol. 299, pp. 757-773, 2007.

[117] L.X. Wang, *Adaptive Fuzzy Systems and Control: Design and Stability Analysis,* PTR Prentice Hall, 1994.

[118] Y.K. Wen "Method for random vibration of hysteretic systems", *Journal of Engineering Mechanics*, Vol. 102, pp. 249-263, 1976.

[119] Y.K. Wen, J. Ghaboussi, P. Venini, K. Nikzad "Control of structures using neural networks", *Smart Materials and Structures*, Vol. 4, pp. 149-157, 1995.

[120] K. Worden "Data processing and experiment design for the restoring force surface method, Part I: integration and differentiation of measured time data", *Mechanical Systems and Signal Processing*, Vol. 4, pp. 295-319, 1990.

[121] B. Xu, Z. Wu, G. Chen, K. Yokoyama "Direct identification of structural parameters from dynamic responses with neural networks", *Engineering Applications of Artificial Intelligence,* Vol. 17, pp. 931-943, 2004.

[122] Y.L. Xu "Parametric study of active mass dampers for wind-excited tall buildings", *Engineering Structures*, Vol. 18, pp. 64-76, 1996.

[123] Y.L. Xu, B. Chen, "Integrated vibration control and health monitoring of building structures using semi-active friction dampers: Part I-methodology", *Engineering Structures,* Vol. 30, pp. 1789-1801, 2008.

[124] Z. Xu, A.K. Agrawal, J.N. Yang "Semi-active and passive control of the phase I linear base-isolated benchmark building model", *Structural Control and Health Monitoring*, Vol. 13, pp. 626-648, 2006.

[125] O. Yakut, H. Alli "Neural based sliding-mode control with moving sliding surface for the seismic isolation of structures", *Journal of Vibration and Control*, Vol. 17, pp. 2103-2116, 2011.

[126] S.K. Yalla, A. Kareem, J.C. Kantor "Semi-active tuned liquid column dampers for vibration control of structures", *Engineering Structures*, Vol. 23, pp. 1469-1479, 2001.

[127] G. Yan, L.L. Zhou "Integrated fuzzy logic and genetic algorithms for multi-objective control of structures using MR dampers", *Journal of Sound and Vibration*, Vol. 296, pp. 368-382, 2006.

[128] J. Yang, J.B. Li, G. Lin "A simple approach to integration of acceleration data for dynamic soil-structure interaction analysis", *Soil Dynamics and Earthquake Engineering, Vol.* 26, pp. 725-734, 2006.

[129] J.N. Yang, T.T. Soong "Recent advances in active control of civil engineering structures", *Probabilistic Engineering Mechanics*, Vol. 3, pp. 179-188, 1988.

[130] J.N. Yang, J.C. Wu, A.K. Agrawal, S.Y. Hsu "Sliding mode control with compensator for wind and seismic response control", *Earthquake Engineering and Structural Dynamic*s, Vol. 26, pp. 1137-1156, 1997.

[131] J.T.P Yao "Concept of structural control", *Journal of the Structural Division*, Vol. 98, pp. 1567-1574, 1972.

[132] K. Yeh, W.L. Chiang, D.S. Juang "Application of fuzzy control theory in active control of structures", *IEEE Proceeding NAFIPS/IFIS/NASA*, pp. 243-247, 1994.

[133] F. Yi, S.J. Dyke "Structural control systems: Performance assessment", *Proceedings of the American Control Conference*, Vol. 1, pp. 14-18, 2000.

[134] W. Yu, M.A. Moreno-Armendarizb, F.O. Rodrigueza "Stable adaptive compensation with fuzzy CMAC for an overhead crane", *Information Sciences*, Vol. 181, pp. 4895-4907, 2011.

[135] X. Yu, "Sliding-mode control with soft computing: A survey", *IEEE Transactions on Industrial Electronics*, Vol. 56, pp. 3275-3285, 2009.

[136] J. Zhang, P.N. Roschke "Active control of a tall structure excited by wind", *Journal of Wind Engineering and Industrial Aerodynamics*, Vol. 83, pp. 209-223, 1999.

[137] W.H. Zhu "Velocity estimation by using position and acceleration sensors", *IEEE Transactions on Industrial Electronics*, Vol. 54, pp. 2706-2715, 2007.